Final Report for AOARD Grant #114013 (FA2386-11-1-4013)

"Investigation and characterization of defects in epitaxial films for ultraviolet light emitting devices using FUV time-resolved photoluminescence, time-resolved cathodoluminescence, and spatio-time-resolved cathodoluminescence excited using femtosecond laser pulses"

5/22/2013

Principal Investigator:

Shigefusa F. Chichibu, Dr. Eng. (Professor)
Tohoku University
Institute of Multidisciplinary Research for Advanced Materials (IMRAM)
2-1-1 Katahira, Aoba, Sendai 980-8577, Japan
Area Code/Phone Number: +81-22-217-5360 Fax Number: +81-22-217-5360
E-mail: chichibu@tagen.tohoku.ac.jp

Co-Principal Investigator:

Kouji Hazu, Dr. Eng. (Assistant Professor, Chichibu Lab., Tohoku University, address the same as above)
E-mail: k_hazu@tagen.tohoku.ac.jp

Period of Performance: 03/08/2011 –03/07/2013

Abstract:

Impacts of structural and point defects on the carrier (exciton) recombination dynamics in wide bandgap semiconductors such as AlN, high AlN mole fraction $Al_xGa_{1-x}N$ alloys, and GaN were studied in this project. For this purpose, we quantified the radiative lifetimes (τ_R) and nonradiative lifetimes (τ_{NR}) for the near-band-edge (NBE) emission by measuring the luminescence lifetimes (τ) and equivalent values of internal quantum efficiencies (η_{int}) as a function of temperature by means of deep ultraviolet (DUV) time-resolved photoluminescence (TRPL) and time-resolved cathodoluminescence (TRCL) measurements using a frequency-quadrupled (4ω) femtosecond Al_2O_3:Ti laser and pulsed electron beams generated using an in-house pulsed photoelectron- (PE-) gun driven by the a frequency-tripled (3ω) femtosecond laser, respectively. By comparing these lifetime data with the results of structural characterizations and positron annihilation spectroscopy (PAS) measurement, we correlated the lifetimes and cation vacancy concentrations. We also developed a spatio-time-resolved cathodoluminescence (STRCL) measurement system first equipped with a rear-excitation configuration pulsed PE-gun and later replaced by a front-excitation configuration one for probing local carrier dynamics in wide bandgap semiconductors. This technique enabled to measure spatially- and time-resolved luminescence signals even at DUV wavelengths. For demonstrating the improved PE-gun performances, spatially-resolved cathodoluminescence (SRCL) and local TRCL measurements were carried out on GaN, AlGaN, AlN, and hexagonal BN powders using the new STRCL system.

Introduction:

Aluminium nitride (AlN) and high AlN mole fraction $Al_xGa_{1-x}N$ alloys have attracted considerable interest for applications in UV-C (200~280 nm) DUV LEDs, because the bandgap energy (E_g) of AlN is 6.01 eV at 300 K [1,2]. Taniyasu *et al.* have demonstrated [3] the shortest wavelength electroluminescence peak at 210 nm from an AlN *p-i-n* homojunction LED. However, its external quantum efficiency (η_{ext}) was as low as 10^{-8} [3], and the highest η_{ext} for the state-of-the-art AlGaN DUV LEDs is limited to be approximately 10% for the emission

Report Documentation Page

Form Approved
OMB No. 0704-0188

Public reporting burden for the collection of information is estimated to average 1 hour per response, including the time for reviewing instructions, searching existing data sources, gathering and maintaining the data needed, and completing and reviewing the collection of information. Send comments regarding this burden estimate or any other aspect of this collection of information, including suggestions for reducing this burden, to Washington Headquarters Services, Directorate for Information Operations and Reports, 1215 Jefferson Davis Highway, Suite 1204, Arlington VA 22202-4302. Respondents should be aware that notwithstanding any other provision of law, no person shall be subject to a penalty for failing to comply with a collection of information if it does not display a currently valid OMB control number.

1. REPORT DATE	2. REPORT TYPE	3. DATES COVERED
23 JUL 2013	**Final**	**08-03-2011 to 07-03-2013**

4. TITLE AND SUBTITLE
Investigation and characterization of defects in epitaxial films for ultraviolet light emitting devices using FUV time-resolved photoluminescence, time-resolved cathodoluminescence, and spatio-time-resolved cathodoluminescence excited using femtosecond laser pulses

5a. CONTRACT NUMBER
FA2386-11-1-4013

5b. GRANT NUMBER

5c. PROGRAM ELEMENT NUMBER

6. AUTHOR(S)
Shigehisa Chichibu

5d. PROJECT NUMBER

5e. TASK NUMBER

5f. WORK UNIT NUMBER

7. PERFORMING ORGANIZATION NAME(S) AND ADDRESS(ES)
Tohoku University,Institute of Multidisciplinary Research for Advanced Materials,2-1-1 Katahira,Aoba, Sendai, 980-8577 Japan,NA,NA

8. PERFORMING ORGANIZATION REPORT NUMBER
N/A

9. SPONSORING/MONITORING AGENCY NAME(S) AND ADDRESS(ES)
AOARD, UNIT 45002, APO, AP, 96338-5002

10. SPONSOR/MONITOR'S ACRONYM(S)
AOARD

11. SPONSOR/MONITOR'S REPORT NUMBER(S)
AOARD-114013

12. DISTRIBUTION/AVAILABILITY STATEMENT
Approved for public release; distribution unlimited

13. SUPPLEMENTARY NOTES

14. ABSTRACT

Impacts of structural and point defects on the carrier (exciton) recombination dynamics in wide bandgap semiconductors such as AlN, high AlN mole fraction AlxGa1-xN alloys, and GaN were studied in this project. For this purpose, we quantified the radiative lifetimes (R) and nonradiative lifetimes (NR) for the near-band-edge (NBE) emission by measuring the luminescence lifetimes () and equivalent values of internal quantum efficiencies (int) as a function of temperature by means of deep ultraviolet (DUV) time-resolved photoluminescence (TRPL) and time-resolved cathodoluminescence (TRCL) measurements using a frequency-quadrupled (4) femtosecond Al2O3:Ti laser and pulsed electron beams generated using an in-house pulsed photoelectron- (PE-) gun driven by the a frequency-tripled (3) femtosecond laser, respectively. By comparing these lifetime data with the results of structural characterizations and positron annihilation spectroscopy (PAS) measurement, we correlated the lifetimes and cation vacancy concentrations. We also developed a spatio-time-resolved cathodoluminescence (STRCL) measurement system first equipped with a rear-excitation configuration pulsed PE-gun and later replaced by a front-excitation configuration one for probing local carrier dynamics in wide bandgap semiconductors. This technique enabled to measure spatially- and time-resolved luminescence signals even at DUV wavelengths. For demonstrating the improved PE-gun performances, spatially-resolved cathodoluminescence (SRCL) and local TRCL measurements were carried out on GaN, AlGaN, AlN, and hexagonal BN powders using the new STRCL system.

15. SUBJECT TERMS **Aluminum Gallium Nitride, Spectroscopic Techniques, Time Resolved Cathodoluminescence Spectroscopy**					
16. SECURITY CLASSIFICATION OF:			17. LIMITATION OF ABSTRACT	18. NUMBER OF PAGES	19a. NAME OF RESPONSIBLE PERSON
a. REPORT **unclassified**	b. ABSTRACT **unclassified**	c. THIS PAGE **unclassified**	**Same as Report (SAR)**	**53**	

Standard Form 298 (Rev. 8-98)
Prescribed by ANSI Std Z39-18

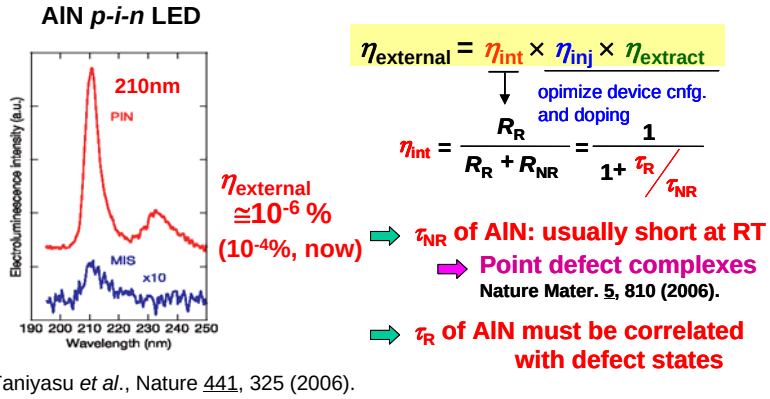

Taniyasu *et al*., Nature 441, 325 (2006).

Fig. 1 Needs for quantifying lifetimes in FUV-emitting wide bandgap semiconductors.

wavelength of 275 nm [4].

As known, η_{ext} is a product of internal quantum efficiency (η_{int}), injection efficiency, and light extraction efficiency. The latter two components should be increased by optimizing device configurations and doping. Meanwhile, η_{int} is a material talent that is a fraction of radiative rate over the sum of radiative and nonradiative rates; *i. e.* $\eta_{int}=(1+\tau_R/\tau_{NR})^{-1}$. To improve η_{int} of practical devices, τ_R and τ_{NR} must be quantitatively understood as functions of structural / point defect and impurity concentrations (crystal imperfections), which are influenced by growth conditions, growth environments, substrates, and so on (see Fig. 1).

However, only few papers [5-8] including our two reports have dealt with the recombination dynamics of AlN and high-*x* $Al_xGa_{1-x}N$, because of the lack of a desirable DUV femtosecond excitation source. Here we note that the intensity of 4ω beams of a Al_2O_3:Ti laser is usually so weak that TRPL measurement cannot be carried out especially at elevated temperatures, where nonradiative defects are activated. Therefore, in most cases only high quality films had been examined. Also, it is rather challenging to guide 4ω-Al_2O_3:Ti beams in scanning near-field optical microscopy (SNOM) system, due to the absorption of DUV lights by optics. These limitations have given us an idea to use femtosecond electron beams (*e*-beams) for both wide-area and spatially-resolved TRCL measurements. In reality, we have developed a novel rear-excitation configuration PE-gun [9] for constructing TRCL measurement system [10] to investigate the emission dynamics in AlN [7] and high AlN mole fraction $Al_xGa_{1-x}N$ alloys [8]. A schematic representation of our wide-area TRPL/TRCL measurement system [7,8,10] is shown in Fig. 2.

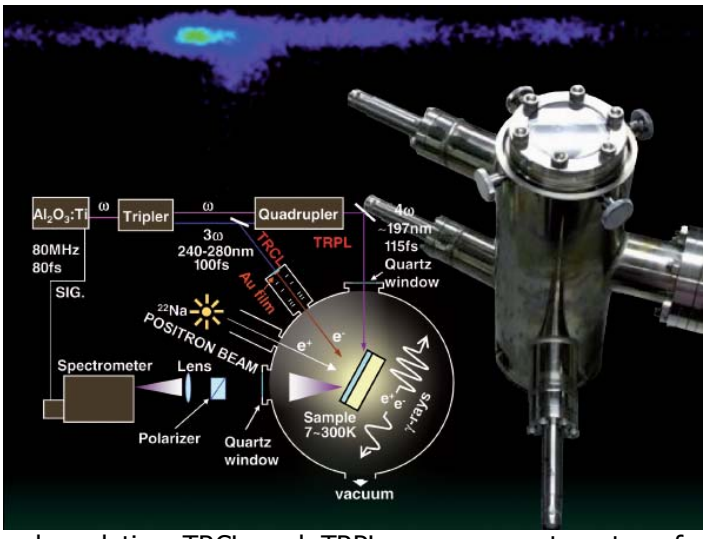

Fig. 2 Picosecond-resolution TRCL and TRPL measurement system for DUV-emitting semiconductors. A positron beam line is also added. [Cover page for Phys. Status Solidi C **10** (2013)].

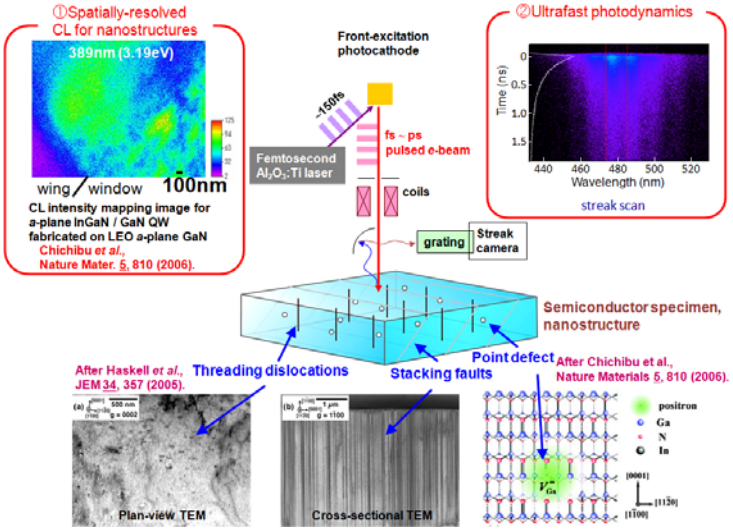

Fig. 3 Concept of the STRCL system equipped with a high emission efficiency front-excitation pulsed PE-gun. We are able to investigate how structural defects influence the local CL lifetime, intensity, and wavelength.

In order to probe local carrier dynamics in wide E_g semiconductors, SNOM with a short-pulsed laser is widely used. On the other hand, the use of a scanning electron microscopy (SEM) equipped with a femtosecond PE-gun [7-16], namely STRCL technique [12-16], makes it possible to measure local TRCL signals at the positions defined precisely by the secondary electron (SE) image. Indeed, STRCL takes full advantage of such a pulsed PE-beam, which enables high spatial resolution beyond the diffraction limit of light owing to the focused electronic excitation and thus makes it possible to interrogate local carrier/exciton dynamics. Unique opportunities offered by the STRCL demonstrated so far includes the investigations of the exciton dynamics around BSFs in an *a*-plane GaN [13], exciton dynamics around the trapezoidal dimple in a *c*-plane freestanding (FS-) GaN substrate [15], and the slight local variations of In incorporation in the $In_{0.05}Ga_{0.95}N$ epilayer [14] grown on an *m*-plane FS-GaN.

We first used a rear-excitation configuration PE-gun [9], which was similar to that invented by EPFL group of Switzerland [11-14], for measuring STRCL data. However, there remained several practical issues. One was the limited brightness of the photocathodes compared with conventional field-emission (FE) sources, which made it difficult to acquire high magnification SEM images. The other was the decrease in PE intensity with time due to the driving damage of a 20-nm-thick *thin* Au film. Therefore, we developed a new PE-gun during the period of current project (AOARD Grant #114013, FA2386-11-1-4013); in the final report of AOARD Grant #114108 (FA2386-11-1-4108), we reported on significant improvement in the emission efficiency of our new front-excitation configuration PE-gun, which enabled to measure high S/N ratio local CL spectra and TRCL signals. Eventually, measurements of slower emission decay and intensity mapping of the NBE emission of AlN became possible. The concept of STRCL is shown schematically in Fig. 3.

In this final report, we describe the results obtained throughout this two-year project. We grew AlN and high AlN mole fraction $Al_xGa_{1-x}N$ films by MOVPE, and also we prepared some freestanding (FS-) GaN (Mitsubishi Chemical Corporation) and AlN (NCSU/HexaTech) bulk crystals as well as Si-doped $Al_{0.6}Ga_{0.4}N$ films (Mie Univ.) and hexagonal (h-) BN powders (Shizuoka Univ.). They were looked at by means of temperature-variable DUV TRPL and/or TRCL measurements excited with a frequency-quadrupled (4ω) femtosecond Al_2O_3:Ti laser and a femtosecond-laser-driven pulsed *e*-beam, respectively. By comparing these lifetime data with the results of structural characterizations and positron annihilation spectroscopy (PAS) measurement, we correlated the lifetimes and cation vacancy concentrations. In addition, in order to obtain better spatial resolution for a SEM image and STRCL mapping image, we

developed a front-excitation PE-gun to generate higher density photoelectrons per pulse. For demonstrating the improved performances, spatially-resolved cathodoluminescence (SRCL) and local TRCL measurements were carried out on GaN, AlGaN, AlN, and hexagonal BN powders.

[1] B. Gil, Phys. Rev. B **81**, 205201 (2010).
[2] H. Ikeda, T. Okamura, K. Matsukawa, T. Sota, M. Sugawara, T. Hoshi, P. Cantu, R. Sharma, J. F. Kaeding, S. Keller, U. K. Mishra, K. Kosaka, K. Asai, S. Sumiya, T. Shibata, M. Tanaka, J. S. Speck, S. P. DenBaars, S. Nakamura, T. Koyama, T. Onuma, and S. F. Chichibu, J. Appl. Phys. **102**, 123707 (2007); erratum in J. Appl. Phys. **103**, 089901 (2008).
[3] Y. Taniyasu, M. Kasu, and T. Makimoto, Nature **441**, 325 (2006).
[4] M. Shatalov, W. Sun, A. Lunev, X. Hu, A. Dobrinsky, Y. Bilenko, J. Yang, M. Shur, R. Gaska, C. Moe, G. Garrett, and M. Wraback, Appl. Phys. Express **5**, 082101 (2012).
[5] K. B. Nam, J. Li, M. L. Nakarmi, J. Y. Lin, and H. X. Jiang, Appl. Phys. Lett. **82**, 1694 (2003).
[6] T. Onuma, K. Hazu, A. Uedono, T. Sota, and S. F. Chichibu, Appl. Phys. Lett. **96**, 061906 (2010).
[7] S. F. Chichibu, T. Onuma, K. Hazu, and A. Uedono, Appl. Phys. Lett. **97**, 201904 (2010).
[8] S. F. Chichibu, K. Hazu, T. Onuma, and A. Uedono, Appl. Phys. Lett. **99**, 051902 (2011).
[9] T. Onuma, Y. Kagamitani, K. Hazu, T. Ishiguro, T. Fukuda, and S. F. Chichibu, Rev. Sci. Instrum. **83**, 043905 (2012).
[10] S. F. Chichibu, T. Onuma, K. Hazu, and A. Uedono, Phys. Status Solidi C **10**, 501 (2013).
[11] M. Merano, S. Collin, P. Renucci, M. Gatri, S. Sonderegger, A. Crottini, J. D. Ganière, and B. Deveaud, Rev. Sci. Instrum. **76**, 085108 (2005).
[12] M. Merano, S. Sonderegger, A. Crottini, S. Collin, P. Renucci, E. Pelucchi, A. Malko, M. H. Baier, E. Kapon, B. Deveaud, J. D. Ganière, Nature **438**, 479 (2005).
[13] P. Corfdir, P. Lefebvre, J. Levrat, A. Dussaigne, J. -D. Ganière, D Martin, J. Ristić, T. Zhu, N. Grandjean, and B. Deveaud-Plèdran, J. Appl. Phys. **105**, 043102 (2009).
[14] M. Kagaya, P. Corfdir, J. -D. Ganière, B. Deveaud-Plèdran, N. Grandjean, and S. F. Chichibu, Jpn. J. Appl. Phys. **50**, 111002 (2011).
[15] Y. Ishikawa, M. Tashiro, K. Hazu, K. Furusawa, H. Namita, S. Nagao, K. Fujito, and S. F. Chichibu, Appl. Phys. Lett. **101**, 212106 (2012).
[16] S. F. Chichibu, Y. Ishikawa, M. Tashiro, K. Hazu, K. Furusawa, H. Namita, S. Nagao, K. Fujito, and A. Uedono, Electrochem. Soc. Trans. **50** (42), 1-8 (2013).

Results and discussions:

(1) Collateral evidence for an excellent radiative performance of $Al_xGa_{1-x}N$ alloy films of high AlN mole fractions

Single layers of AlN and high AlN mole fraction $Al_xGa_{1-x}N$ films were grown by MOVPE. By comparing the TRPL/TRCL data for the NBE emission of the films with the results of structural characterizations and PAS measurement, we correlated the values of τ_R and τ_{NR} with the *S* parameter, which represents the size/concentration of cation vacancies and their complexes. Their low-temperature τ_R was longer than that for the epilayers of low-*x* $Al_xGa_{1-x}N$ alloys, AlN, or GaN due to the contribution of bound and localized band-tail states. However, τ_R showed little change with temperature rise, and the value was a few ns at 300 K. The results essentially indicate an excellent radiative performance of $Al_xGa_{1-x}N$ alloys of high *x*, although the luminescence efficiency of $Al_xGa_{1-x}N$ DUV light-emitting-diodes reported so far is limited by the short τ_{NR}.

Details are described in attachment a)-1), Applied Physics Letters **99**, 051902 (2011) and b)-1), Phys. Status Solidi C **10**, 501 (2013).

(2) Impacts of Si-doping and resultant cation vacancy formation on the luminescence dynamics for the near-band-edge emission of $Al_{0.6}Ga_{0.4}N$ films grown on AlN templates by metalorganic vapor phase epitaxy

Luminescence dynamics for the NBE emission peak at around 250 nm of *c*-plane Si-doped $Al_{0.6}Ga_{0.4}N$ films grown on AlN templates by low-pressure metalorganic vapor phase epitaxy were studied using DUV TRPL and TRCL spectroscopies. For the films with the Si-doping concentration, [Si], lower than 1.9×10^{17} cm^{-3}, the doping lessened the concentration of cation vacancies, [V_{III}], through the surfactant effect or the aid of the reactant doping in a form of H_3SiNH_2. The room-temperature τ_{NR} and consequently the equivalent value of η_{int} (η_{int}^{eq}) in the weak excitation regime steeply decreased when [Si] exceeded 10^{18} cm^{-3}. Simultaneously the intensity ratio of the deep-state emission band to the NBE emission abruptly increased. Because the increase in [Si] essentially gives rise to the increase in [V_{III}] (for [Si] > 1.9×10^{17} cm^{-3}) and the overcompensation of Si is eventually observed for the film with [Si]=4.0×10^{18} cm^{-3}, the formation of acceptor-type native-defect complexes containing Si such as V_{III}-Si_{III} is suggested.

Details are described in attachment e)-1), Journal of Applied Physics **113** (2013), which has been accepted for publication and in press (ID#031321JAP).

(3) DUV TRPL of annealed hexagonal BN powders

In order to gain fundamental information on hexagonal (h-) BN, which is a layered compound and expected to emit UV-C and UV-B lights, we measured energy-resolved TRPL signals and cw CL spectra of h-BN powders by using the system shown in Fig. 2.

The white BN powders of more than 99%-purity were purchased. Their size and appearance are shown in Fig. 4. The powder was annealed at 900°C in O_2 ambient for 2 hours.

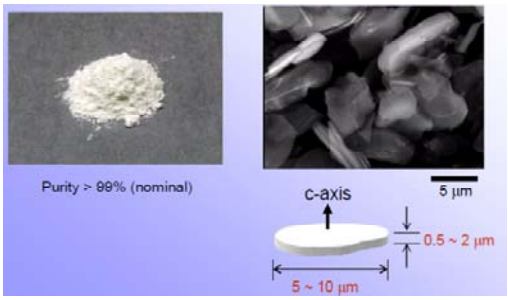

Fig. 4 Appearance of the BN powders.

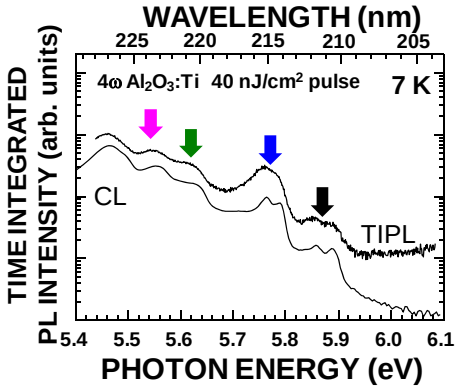

Fig. 5 Steady-state CL and time-integrated PL spectra for the h-BN powder measured at 7 K.

Steady-state CL and time-integrated PL (TIPL) spectra for the h-BN powder measured at 7 K are shown in Fig. 5. Both the spectra exhibit distinct NBE excitonic emissions in the energies higher than 5.7 eV. The energy-resolved TRPL signals for the four luminescence bands pointed by arrows in Fig. 5 are shown in Fig. 6. As shown,

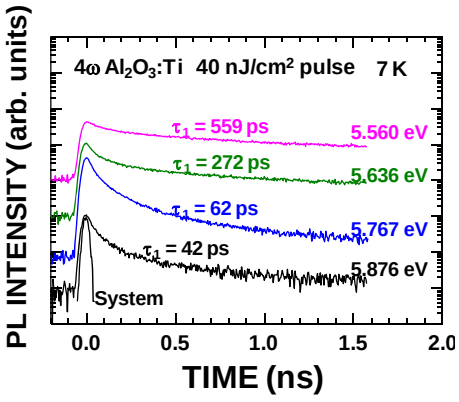

Fig. 6 Energy-resolved TRPL signals measured for the NBE excitonic emissions of the h-BN powder measured at 7 K.

reasonably short τ_R is quantified for the peaks at around 210-215 nm. The values of 42 to 62 ps seem to be consistent with the trend between τ_R and the energy gap (E_g), as shown in Fig. 7. Although precise emission mechanisms of this material is unclear at present, the data obtained herein will give us a chance to consider what

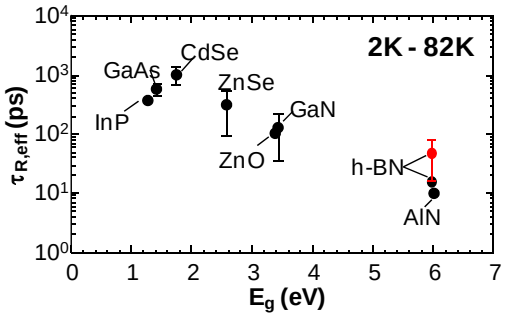

T. Onuma, S. F. Chichibu *et al.*, APL **96**, 061906 (2010).

Fig. 7 Low-temperature effective τ_R for the NBE emissions in III–V and II–VI compound semiconductors as a function of E_g.

happens in h-BN powders.

(4) Preparation of STRCL equipment

In order to construct STRCL system, we installed our rear-excitation PE-gun on a home-made uniquely designed SEM/CL equipment. Details of the PE-gun itself have been described in Review of Scientific Instruments **83**, 043905 (2012), which has been attached in our previous one-year report for AOARD Grant #114013 (FA2386-11-1-4013). Schematic representation of our first STRCL equipment is shown in Fig. 8. The system consists of an SEM equipped with an in-house PE-gun, which was driven by a 3ω of mode-locked Al_2O_3:Ti laser pulses. The beam was focused using a fused silica lens (f=300 mm) with a spot diameter of 50 μm to a rear-side of a photocathode. The average power of 80 mW was used at a repetition rate of 80 MHz, corresponding to laser fluence of 32 μJ/cm^2. This value was limited by the onset of optical damage of the photocathode. The output e-beam was launched to the SEM by focusing it to its filament position. The probe current was calibrated using a Faraday cup placed just above the temperature-controlled stage, and was typically 20 nA at an acceleration voltage (V_{acc}) of 10 kV. Although this is smaller than what can be achieved with a conventional W filament, reasonable quality of SEM images can be obtained. The luminescence from a sample was collected using an off-axis parabolic mirror (R=12 mm) placed above the sample and then analyzed using a grating spectrometer equipped with an electronically-cooled charged-coupled device and a streak camera with a temporal resolution of approximately 10 ps.

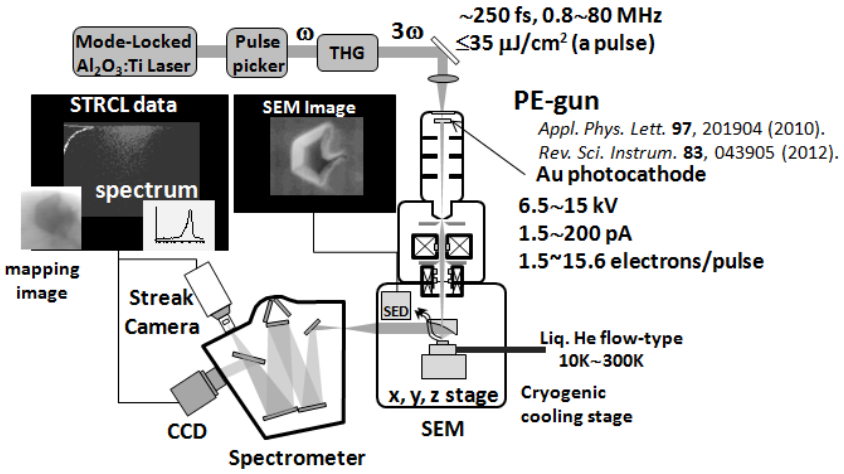

Fig. 8 Schematic diagram of the rear-excitation configuration STRCL measurement system. The wavelength and repetition rate of the frequency-tripled (3ω) femtosecond Al_2O_3:Ti laser are adjusted according to the purpose of the measurement.

(5) Local lifetime and luminescence efficiency for the NBE emission of FS-GaN substrates determined using STRCL

By using the system described in (4), STRCL measurements were carried out on low TD density FS-GaN substrates grown by HVPE. High-resolution CL imaging allows for visualization of nonradiative recombination channels in the vicinity of an accidentally formed surface dimple. Local CL lifetimes (τ_{CL}) for the NBE emission are shown to be sensitively position dependent. A linear relation between η_{int}^{eq} and τ_{CL} for the NBE emission was observed at room temperature under a weak excitation condition, and spatially resolved excitation led to the observation of the highest η_{int}^{eq} of 20 % with τ_{CL} of 3.3 ns.

Details are described in attachment a)-2), Appl. Phys. Lett. **101** (21), pp. 212106 1-4 (2012) and b)-2), Electrochem. Soc. Trans. **50** (42), pp. 1-8 (2013).

(6) Preparation of STRCL system with high-brightness front-excitation configuration pulsed PE-gun

Schematic diagram of the STRCL system equipped with the front-excitation configuration in-house PE-gun is shown in Fig. 9. It is principally the same as that used in attachments a)-2) and b)-2) except for the PE-gun, which is driven by a frequency-tripled mode-locked Al_2O_3:Ti laser pulses. The beam was focused using a fused silica lens with a spot diameter of 50 μm to a front-side of a photocathode. The output *e*-beam was launched to the SEM by focusing it to its filament position. The probe current was calibrated using a Faraday cup placed just above the temperature-controlled stage, and was controllable between 0.1 and 200 nA at an acceleration voltage (V_{acc}) of 12 kV by changing the average power of the excitation laser fluence. The luminescence from a sample was collected using an off-axis parabolic mirror (R=12 mm) placed above the sample and then analyzed using a grating spectrometer equipped with an electronically-cooled charged-coupled device and a streak camera with a temporal resolution of approximately 10 ps.

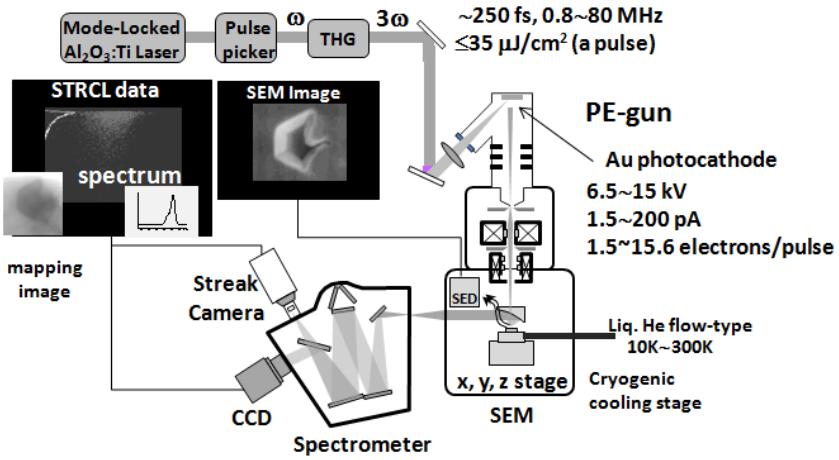

Fig. 9. Schematic diagram of the STRCL measurement system equipped with a front-excitation configuration PE-gun. Rest part is similar to that in Fig. 8.

(7) STRCL studies on local exciton dynamics of a freestanding GaN substrate grown by hydride vapor phase epitaxy

By using the PE-gun described in (6), high spatial-resolution STRCL measurements became possible. Its increased PE-emission efficiency enabled to vary the acceleration voltage (mean implantation depth of electrons) over a wide range. As a result, more surface-sensitive detection became possible, allowing us to clearly visualize the area containing a basal-plane stacking fault (BSF) in a FS-GaN substrate grown by HVPE. Local dynamics of excitons around

the BSF is discussed.

Details are described in an abstract for attachment d)-7), Extended abstracts of the 40th International Symposium on Compound Semiconductors (ISCS2013), May 19 - 23, 2013, Kobe, Japan, TuA1-4.

(8) Local TICL and TRCL signals of a high-quality AlN epitaxial film measured using the STRCL system equipped with the front-excitation configuration PE-gun

As a demonstration of our STRCL system, local exciton dynamics in AlN were examined. The measured sample was an approximately 2-μm-thick high quality (HQ) *c*-plane AlN epilayer grown on *c*-plane Al_2O_3 by low-pressure MOVPE [17,18]. The TD density (TDD) was 2×10^8 cm^{-2}, and it exhibited an atomically smooth surface with 0.25-nm-high monolayer atomic steps [17]. Fig. 10(a) shows a local TICL spectrum measured at 15 K. The spectral lineshape is very similar to that measured with a wide-area cw excitation using the blanking technique, as shown in Fig. 10(b) (after Ref. [18]), although several weak peaks/shoulders are absent probably due to the spatial inhomogeneity of the sample. We note that the peaks FX_A, $FX_{A(n=2)}$, D^0X^1, D^0X^2, 1LO, and 2LO represent the emissions originating from the recombination of free A-excitons, recombination of the first excited state of free A-excitons, recombination of excitons bound to a neutral donor, recombination of excitons bound to another neutral donor, their 1-phonon replicas, and 2-phonon replicas, respectively. In Ref. [7], D^0X^1 and D^0X^2 are written as I_2^1 and I_2^2, respectively.

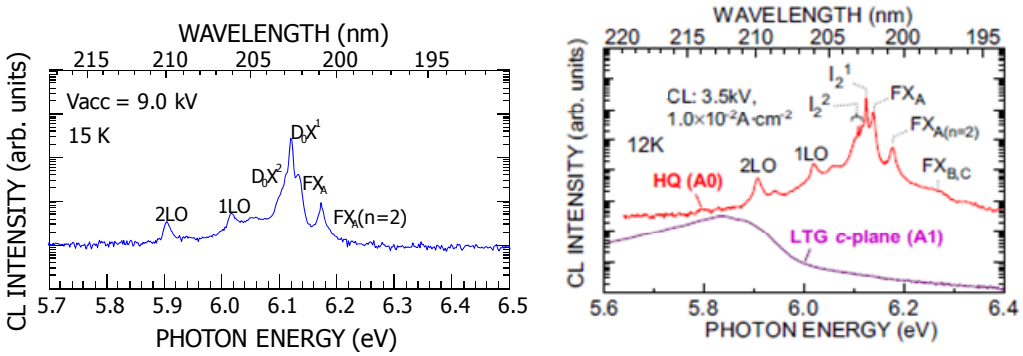

Fig. 10 (a) Very local TICL spectrum of a 2-μm-thick *c*-plane AlN epilayer measured at 15 K. (b) Steady-state wide-area CL spectrum of the same HQ AlN epilayer (sample ID#A0) at 12 K (after Ref. [7]).

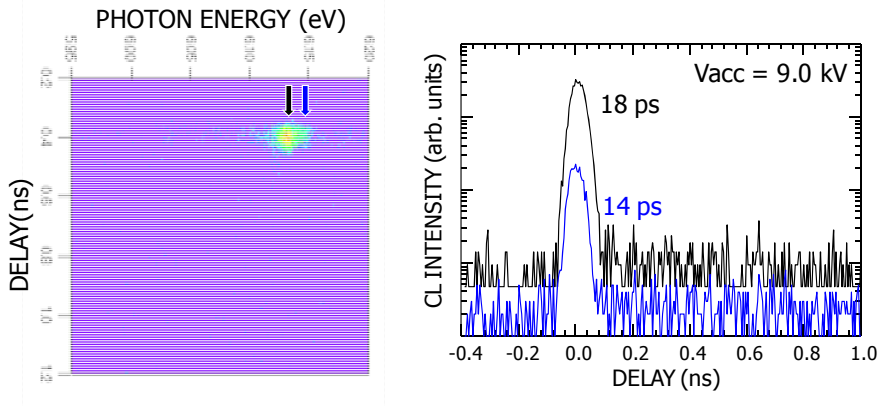

Fig. 11. (a) Very local streak-scope image showing the TRCL signal at 15 K for the *c*-plane AlN epilayer. (b) STRCL signals for D_0X^1 (upper) and FX_A (lower) peaks measured for the photon energies marked in panel (a). We note that time-resolution of our STRCL system using the front-excitation configuration PE-gun is approximately 10 ps.

In Fig. 11(a), local TRCL signal for the same *c*-plane AlN sample measured at 15 K is shown using a streak-scope image. As shown in Figs. 10(a) and 11(a), it is evident that we could monitor decay signals for D_0X^1 and FX_A, as pointed by the arrows. Their emission wavelengths are approximately 203 and 202 nm, respectively. In the next stage we will use this STRCL system to correlate the radiative and nonradiative lifetimes with structural irregularities in AlN and $Al_xGa_{1-x}N$ alloys of high x.

[17] T. Shibata, K. Asai, S. Sumiya, M. Mouri, M. Tanaka, O. Oda, H. Katsukawa, H. Miyake, and K. Hiramatsu, Phys. Status Solidi C **0**, 2023 (2003).
[18] T. Onuma, T. Shibata, K. Kosaka, K. Asai, S. Sumiya, M. Tanaka, T. Sota, A. Uedono, and S. F. Chichibu, J. Appl. Phys. **105**, 023529 (2009).

Summary and Prospects:

Impacts of structural and point defects on the carrier (exciton) recombination dynamics in wide bandgap semiconductors such as AlN, high AlN mole fraction $Al_xGa_{1-x}N$ alloys, and GaN were studied in this project. For this purpose, we used DUV TRPL and TRCL measurements using a 4ω femtosecond Al_2O_3:Ti laser and pulsed electron beams generated using an in-house PE-gun driven by the a 3ω femtosecond laser, respectively. By comparing these lifetime data with the results of structural characterizations and positron annihilation spectroscopy (PAS) measurement, we correlated the lifetimes and cation vacancy concentrations. The effects of Si-doping in AlGaN were also examined. We also developed a STRCL measurement system equipped with a front-excitation configuration pulsed PE-gun for probing local carrier dynamics in wide bandgap semiconductors. This technique enabled to measure spatially- and time-resolved luminescence signals even at DUV wavelengths. For demonstrating the improved PE-gun performances, spatially-resolved cathodoluminescence (SRCL) and local TRCL measurements were carried out on GaN, AlGaN, AlN, and hexagonal BN powders using the new STRCL system.

List of Publications and Significant Collaborations that resulted from your AOARD supported project:

a) papers published in peer-reviewed journals,

1) S. F. Chichibu, K. Hazu, T. Onuma, and A. Uedono, "Collateral evidence for an excellent radiative performance of $Al_xGa_{1-x}N$ alloy films of high AlN mole fractions", Appl. Phys. Lett. **99** (5), pp.051902 1-3 (2011).
2) Y. Ishikawa, M. Tashiro, K. Hazu, K. Furusawa, H. Namita, S. Nagao, K. Fujito, and S. F. Chichibu, "Local lifetime and luminescence efficiency for the near-band-edge emission of freestanding GaN substrates determined using spatio-time-resolved cathodoluminescence", Appl. Phys. Lett. **101** (21), pp. 212106 1-4 (2012).

b) papers published in peer-reviewed conference proceedings,

1) S. F. Chichibu and A. Uedono, "Time-resolved luminescence studies on AlN and high AlN mole fraction AlGaN alloys", The Fourth International Symposium on Growth of III-Nitrides (ISGN-4), St. Petersburg, Russia, Jul.16-19 (2012), No. Th-1i (Invited); S. F. Chichibu, T. Onuma, K. Hazu, and A. Uedono, "Time-resolved luminescence studies on AlN and high AlN mole fraction AlGaN alloys", Phys. Status Solidi C **10** (3), pp. 501-506 (2013).
2) S. F. Chichibu, Y. Ishikawa, K. Hazu, M. Tashiro, K. Furusawa, H. Namita, S. Nagao, K. Fujito, and A. Uedono, "Spatio-time-resolved cathodoluminescence studies on freestanding GaN substrates grown by hydride vapor phase epitaxy", Pacific Rim Meeting on Electrochemical and Solid-State Science (PRiME 2012), Joint international meeting: 222nd Meeting of ECS, The Electrochemical Society and 2012 Fall Meeting of The Electrochemical Society of Japan, Session J3: Materials for Solid State Lighting,

Honolulu, Hawaii, USA, Oct. 7-12 (2012), No.J3-3956 (Invited); S. F. Chichibu, Y. Ishikawa, M. Tashiro, K. Hazu, K. Furusawa, H. Namita, S. Nagao, K. Fujito, and A. Uedono, "Spatio-time-resolved cathodoluminescence studies on freestanding GaN substrates grown by hydride vapor phase epitaxy", Electrochemical Society Transactions **50** (42), pp. 1-8 (2013).

c) papers published in non-peer-reviewed journals and conference proceedings,
none.

d) conference presentations without papers,

1) S. F. Chichibu, T. Onuma, K. Hazu, T. Sota, and A. Uedono, "Time-resolved photoluminescence and time-resolved cathodoluminescence studies on AlN and high AlN mole fraction AlGaN alloys", European Materials Research Society, 2011 Spring Meeting, Session F: Group III nitrides and their heterostructures for electronics and photonics, Congress Center, Nice, France, May.9-13 (2011), No. F-53 (Invited).
2) Y. Ishikawa, K. Hazu, H. Matsumoto, K. Suzaki, K. Fujito, S. Nagao, M. Shigeiwa, and S. F. Chichibu, "Spatio-time-resolved cathodoluminescence study on a freestanding GaN substrate grown by halide vapor phase epitaxy", The 9th International Conference on Nitride Semiconductors (ICNS-9), Glasgow, UK, Jul.10-15 (2011), No. A2.5 (oral).
3) S. F. Chichibu, T. Onuma, K. Hazu, T. Sota, and A. Uedono, "Time-resolved photoluminescence and time-resolved cathodoluminescence studies on AlN and high AlN mole fraction AlGaN alloys", The 9th International Conference on Nitride Semiconductors (ICNS-9), Glasgow, UK, Jul.10-15 (2011), No. E3.4 (oral).
4) S. F. Chichibu, Y. Ishikawa, M. Tashiro, K. Hazu, K. Furusawa, S. Nagao, K. Fujito, and A. Uedono, "Spatio-time-resolved cathodoluminescence study using a femtosecond focused electron beam on freestanding GaN substrates grown by hydride vapor phase epitaxy", The 39th International Symposium on Compound Semiconductors (ISCS 2012), Santa Barbara, CA, USA, Aug.27-30 (2012), No. We-2B.2 (oral).
5) S. F. Chichibu, K. Hazu, Y. Ishikawa, M. Tashiro, H. Miyake, K. Hiramatsu, and A. Uedono, "Impacts of point defects on the photoluminescence lifetime of Si-doped $Al_{0.6}Ga_{0.4}N$ epilayers grown on an AlN template", International Workshop on Nitride Semiconductors 2012 (IWN2012), Sapporo, Japan, Oct.14-19 (2012), Session PR6 (Defects), No. PR6-2 (oral).
6) K. Furusawa, Y. Ishikawa, M. Tashiro, K. Hazu, S. Nagao, K. Fujito, A. Uedono, and S. F. Chichibu, "Local carrier dynamics in freestanding GaN substrates grown by hydride vapor phase epitaxy studied using the spatio-time-resolved cathodoluminescence technique", International Workshop on Nitride Semiconductors 2012 (IWN2012), Sapporo, Japan, Oct.14-19 (2012), No. MoP-GR-54 (poster).
7) K. Furusawa, Y. Ishikawa, M. Tashiro, K. Hazu, S. Nagao, H. Ikeda, K. Fujito, and S. F. Chichibu, "Spatio-time-resolved cathodoluminescence studies on local exciton dynamics of a freestanding GaN substrate grown by hydride vapor phase epitaxy", The 40th International Symposium on Compound Semiconductors (ISCS 2013), Kobe, Japan, May 21 (2013), No. TuA1-4 (oral).
8) S. F. Chichibu, H. Miyake, Y. Ishikawa, M. Tashiro, T. Ohtomo, K. Hazu, K. Furusawa, K. Hiramatsu, and A. Uedono, "Effects of Si-doping on the recombination dynamics of excitons in AlGaN alloys studied by time-resolved cathodoluminescence", European Materials Research Society, 2013 Spring Meeting, Session L: Group III nitrides, Strasbourg, France, May.27-31 (2013), No. L-91 (Invited).
9) S. F. Chichibu, Y. Ishikawa, M. Tashiro, K. Hazu, and K. Furusawa, "Spatio-time-resolved cathodoluminescence studies on group-III-nitride semiconductors", The 2nd International Conference on Advanced Electromaterials (ICAE2013), Jeju, Korea, Nov. 12-15 (2013), Symposium 4: Advanced LED and Lighting Technology (Invited).

In addition, we had 17 presentations in intra-Japan domestic conferences.

e) manuscripts submitted but not yet published,

1) S. F. Chichibu, H. Miyake, Y. Ishikawa, M. Tashiro, T. Ohtomo, K. Furusawa, K. Hazu, K. Hiramatsu, and A. Uedono, "Impacts of Si-doping and resultant cation vacancy formation on the luminescence dynamics for the near-band-edge emission of $Al_{0.6}Ga_{0.4}N$ films grown on AlN templates by metalorganic vapor phase epitaxy", Journal of Applied Physics **113** (2013). (accepted for publication and in press, ID#031321JAP)

f) provide a list any interactions with industry or with Air Force Research Laboratory scientists or significant collaborations that resulted from this work.

1) The concept and the results of STRCL studies on AlN and high AlN mole fraction AlGaN alloys have been selected by the editor of Physica Status Solidi (c) as a cover page of the Proceedings of The Fourth International Symposium on Growth of III-Nitrides (ISGN-4) .
2) Get started a collaboration with NCSU / HexaTech, Prof. Z. Sitar on AlN research.
3) There is no proper categories to list up within a) to e) above, but we submitted two abstracts to ICNS10, which will be held in Washington D.C. in Aug. 2013.

Attachments: Publications a), b), e), d)-7), and f)-1). **DD882** is also attached.

Collateral evidence for an excellent radiative performance of $Al_xGa_{1-x}N$ alloy films of high AlN mole fractions

S. F. Chichibu,[1,a)] K. Hazu,[1] T. Onuma,[1] and A. Uedono[2]
[1]*Center for Advanced Nitride Technology, Institute of Multidisciplinary Research for Advanced Materials, Tohoku University, 2-1-1 Katahira, Aoba, Sendai 980-8577, Japan*
[2]*Institute of Applied Physics, Graduate School of Pure and Applied Sciences, University of Tsukuba, 1-1-1 Tennodai, Tsukuba 305-8573, Japan*

(Received 22 June 2011; accepted 4 July 2011; published online 1 August 2011)

Recombination dynamics for the deep-ultraviolet (DUV) near-band-edge emission of $Al_xGa_{1-x}N$ epilayers of high AlN mole fractions (x) are studied using time-resolved spectroscopy. Their low-temperature radiative lifetime (τ_R) is longer than that for the epilayers of low-x $Al_xGa_{1-x}N$, AlN, or GaN due to the contribution of bound and localized tail-states. However, τ_R shows little change with temperature rise, and the value is a few ns at 300 K. The results essentially indicate an excellent radiative performance of $Al_xGa_{1-x}N$ alloys of high x, although the luminescence efficiency of $Al_xGa_{1-x}N$ DUV light-emitting-diodes reported so far is limited by the short nonradiative lifetime. © *2011 American Institute of Physics*. [doi:10.1063/1.3615681]

Aluminium nitride and $Al_xGa_{1-x}N$ alloys of high AlN mole fractions (x) have attracted considerable interest for applications in UV-C (200–280 nm) deep-ultraviolet (DUV) light emitting diodes (LEDs). However, the external quantum efficiency (EQE) for the shortest-wavelength near-band-edge (NBE) electroluminescence peak at 210 nm of an AlN *p-i-n* LED (Ref. 1) was as low as 10^{-8} and typical EQE for the state-of-the-art AlGaN DUV LEDs are approximately 3%.[2]

To improve EQE, internal quantum efficiency (η_{int}), carrier injection efficiency, and light extraction efficiency must be increased. The latter two should be increased by optimizing device configurations and doping. Meanwhile, η_{int} is a material talent that is a fraction of radiative rate over the sum of radiative and nonradiative rates; i.e., $\eta_{int} = (1 + \tau_R/\tau_{NR})^{-1}$, where τ_R and τ_{NR} are the radiative and nonradiative lifetimes, respectively. To improve η_{int}, τ_R, and τ_{NR} must be quantitatively understood. However, only a few papers[3,4] have dealt with the recombination dynamics in UV-C range because of the lack of a desirable far UV femtosecond excitation source.

In this letter, the results of time-resolved photoluminescence (TRPL), time-resolved cathodoluminescence (TRCL), and positron annihilation spectroscopy (PAS) measurements on $Al_xGa_{1-x}N$ epilayers of high x values are reported. We show that the material essentially has an excellent radiative performance, in comparison with GaN and even InGaN. The slight decrease in τ_R with temperature rise from 80 K to 220 K is explained in terms of the wavefunction-overlap recovery.

Approximately 1.3-μm-thick (0001) $Al_xGa_{1-x}N$ epilayers ($x = 0.65$, 0.89, 0.97, and 1) were grown at 2.0×10^4 Pa by metalorganic vapor phase epitaxy (MOVPE) on an 1-μm-thick AlN epitaxial template,[5] which was grown on a (0001) Al_2O_3 substrate. Trimethylgallium, trimethylaluminium, and NH_3 were used as the precursors. The growth temperature was 1500 °C for one of the AlN epilayers and 1120–1200 °C for the rest. The former is classified as high-temperature-grown (HTG) AlN sample, which is the sample "A1" in Ref. 4. Other samples are classified as low-temperature-grown (LTG) ones. The LTG AlN sample is "A4" in Ref. 4. The threading dislocation (TD) densities having edge components (N_E) are 2×10^8 cm^{-2} for HTG AlN and 3×10^9 cm^{-2} for LTG AlN.[4] For the $Al_xGa_{1-x}N$ epilayers, N_E values are estimated from the full-width at half-maximum (FWHM) for the $\{10\bar{1}2\}$ x-ray rocking curve (1200–1500 arcsec) using the relation given in Ref. 6 to be 2–3×10^9 cm^{-2}. The TD densities having pure screw components are estimated[6] to be lower than 2–6×10^7 cm^{-2}. They were characterized using the x-ray reciprocal space mapping method to be partially relaxed against the AlN template. The x values were calculated from the in-plane and out-of-plane lattice parameters and the degree of relaxation using the relation similar to that given in Ref. 7.

Steady-state cathodoluminescence (CL) was excited using an electron beam (e-beam) operated at 3.5 kV acceleration voltage and 1.0×10^{-2} A/cm^2 probe current density.[4,5] Approximately 115 fs pulses of a frequency-quadrupled (4ω) mode-locked Al_2O_3:Ti laser were used for the TRPL measurement.[4] The wavelength (λ), repetition rate, and power density were 200 nm, 80 MHz, and 40 nJ/cm^2 a pulse, respectively. The maximum electron-hole (e-h) pair density is estimated to be 4×10^{15} cm^{-3} during the pulse, assuming the absorption coefficient of AlN as 10^5 cm^{-1}. We also used a home-made[4] fs-excitation photoelectron gun similar to Ref. 8 for the TRCL measurement. It was composed of a 15-nm-thick transmission-configuration Au film, extraction electrodes, and acceleration electrodes to give V_{acc}. The Au film was excited using the frequency-tripled (3ω) pulses of the Al_2O_3:Ti laser (240–280 nm, 100 fs, ~1μJ/cm^2 a pulse). The e-beam current density was 1.8 pA/cm^2 during each pulse, and the corresponding excitation density calibrated to our TRPL is approximately 10 nJ/cm^2. The excitation intensities for TRPL and TRCL were low enough to underline τ_{NR} at 300 K. The energy-resolved TRPL/TRCL signals were acquired using a streak-camera, and the time resolution was approximately 7 ps.

In order to crrelate τ_R and τ_{NR} with concentrations of cation vacancies (V_{III}) and V_{III}-complexes, PAS measurement[9,10]

a)Author to whom correspondence should be addressed. Electronic mail: chichibulab@yahoo.co.jp.

 © 2011 American Institute of Physics

was carried out using the monoenergetic positron (e^+) beam line.[10–12] Here, S parameter[9,10] for the Doppler-broadening spectrum of e^+-e^- annihilation γ-rays is used as the measure of concentration or size of negatively charged V_{III}-defects.[9,10] Details of the measurement and analysis are given in Refs. 10 and 12.

Steady-state PL or CL spectra for the $Al_xGa_{1-x}N$ epilayers measured at low temperature are shown in Fig. 1. The spectra for good quality end-point compounds, namely, GaN and HTG AlN, are characterized by the NBE excitonic lines such as neutral-donor bound exciton lines (I_2), a free A-exciton line (FX_A), and their LO phonon replicas. The spectra for the alloys exhibit a broader but reasonablly intense NBE emission peak. The peak energies are lower by approximately 200 meV than the bandgap energies, similar to the previous reports.[11,13,14] Peak intensities for the broad, deep emission bands below 4.4 eV are two or three orders of magnitude weaker than the NBE peak.

In order to confirm if TRCL gives similar data as TRPL, temperature variations of both the signals for the NBE emission of the $Al_{0.97}Ga_{0.03}N$ epilayer are shown in Fig. 2. In the case of TRCL, unwanted surface recombination effects may be reduced because e-beams can be implanted into the bulk region. For example, the implantation depth profile peak for the case of Fig. 2(b) is approximately 250 nm ($V_{acc} = 10$ kV). As shown, however, the data are reasonably similar, as is the case with AlN.[4] We note that the signals are vertically shifted for better looking. To systematically compare τ_R and τ_{NR} for various quality samples, the effective PL (CL) lifetime $\tau_{PL(CL),eff}$ is defined[12] as the time after excitation when $\int_0^{\tau_{PL(CL),eff}} I(t)dt / \int_0^{t_{lim}} I(t)dt$ becomes 1−1/e, where $I(t)$ is the intensity at time t and t_{lim} is defined as the time when $I(t_{lim})$ becomes $0.01I(0)$. The effective lifetimes $\tau_{R,eff}$ and $\tau_{NR,eff}$ are deduced from $\eta_{int} = (1 + \tau_{R,eff}/\tau_{NR,eff})^{-1}$ and $\tau_{PL(CL),eff}^{-1} = \tau_{R,eff}^{-1} + \tau_{NR,eff}^{-1}$, where η_{int} is approximated[12] as the spectrally integrated PL (CL) intensity at given temperature T over that at around 8−10 K (I_{TK}/I_{8K}).

As a typical example, temperature variations of I_{TK}/I_{8K} and $\tau_{CL,eff}$ for the NBE emission of the $Al_{0.97}Ga_{0.03}N$ epilayer are shown in Figs. 3(a) and 3(b), respectively. The calculated $\tau_{R,eff}$ and $\tau_{NR,eff}$ values are also plotted in Fig. 3(b). As T increases, η_{int} decreases to 0.8% at 300 K, which is responsible for the corresponding rapid decrease in $\tau_{NR,eff}$. The $\tau_{R,eff}$ value first increases for $T < 80$ K, then decreases between 80 K and 220 K and shows the second increase for

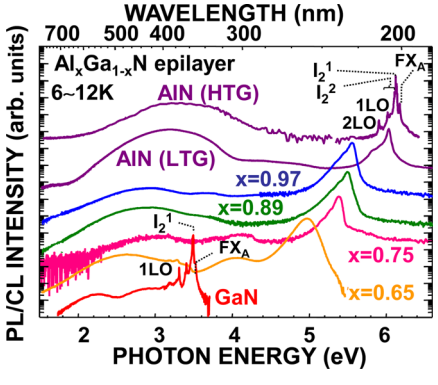

FIG. 1. (Color online) Steady-state PL and CL spectra at 6–12 K for the $Al_xGa_{1-x}N$ alloy epilayers grown by MOVPE.

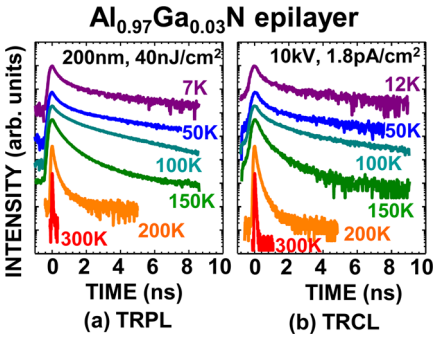

FIG. 2. (Color online) Comparison of (a) TRPL and (b) TRCL signals for the NBE emission of $Al_{0.97}Ga_{0.03}N$ epilayer grown on an AlN epitaxial template (Ref. 5).

$T > 220$ K. The result may reflect complex carrier recombination dynamics. For the case of quantum particles in three-dimensional (3D) space,[15] τ_R increases according to $T^{1.5}$ due to the increase in kinetic energy. The increase of τ_R for $T > 220$ K is attributed to this process. One of the possible reasons for the decrease in τ_R for 80 K $< T <$ 220 K is recovery of the oscillator strength (f) of $e-h$ pairs in a band-tail, as follows. At low temperature, e and h are spatially separated in the conduction band minima and valence band maxima, respectively, that are formed due to charged impurities and counter-charged point defects.[4] As T increases, e-h pairs may be released from the band-tail to 3D space gaining the wavefunction overlap. Here, we note that τ_R for LTG (inferior) AlN, which contains high concentration Si, C, and O up to 2×10^{19} cm^{-3} and high concentration Al vacancies (V_{Al}), also decreased with the temperature rise up to 230 K.[4] The increase in τ_R at very low temperature (<50 K) has often been attributed to particle delocalization from bound or localized states, especially in the case of alloys and quantum wells.[15] Because our $Al_xGa_{1-x}N$ epilayers were grown at lower temperature (≤1200 °C) than that required for better quality high-x $Al_xGa_{1-x}N$ film growth,[16] band-tail formation and compositional inhomogeneity were hard to avoid. In any case, shorter τ_R is preferred to obtain higher η_{int}.

As low-temperature $\tau_{R,eff}$ in AlN has been revealed to increase with increasing V_{Al} concentration,[4] we compare in Fig. 4 the variations of the (a) FWHM value for the NBE emission at 10 K, (b) S parameter, and (c) $\tau_{R,eff}$ (8 K), $\tau_{R,eff}$

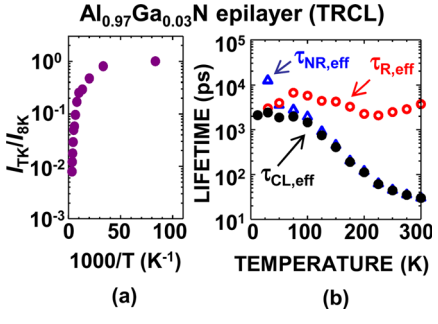

FIG. 3. (Color online) (a) Temperature variation of the equivalent η_{int} value for the NBE emission of $Al_{0.97}Ga_{0.03}N$ epilayer, which is approximated as the spectrally integrated CL intensity at given temperature (T) divided by that at around 8–10 K (I_{TK}/I_{8K}). (b) Temperature variations of measured $\tau_{CL,eff}$ (closed circles) and calculated $\tau_{R,eff}$ (open circles) and $\tau_{NR,eff}$ (open triangles) for the NBE emission of the $Al_{0.97}Ga_{0.03}N$ epilayer.

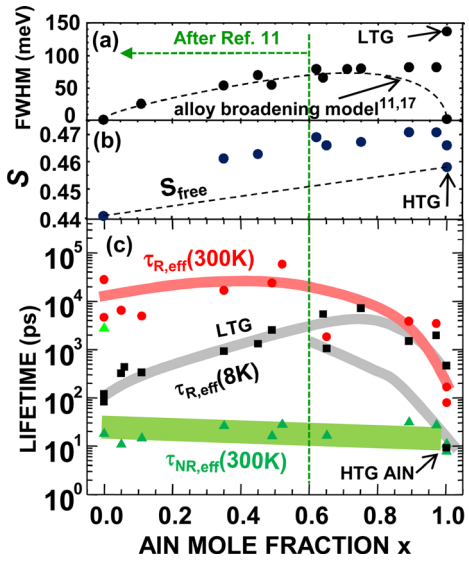

FIG. 4. (Color online) (a) FWHM value for the NBE emission at 8 K, (b) S parameter obtained by the PAS measurement, and (c) $\tau_{R,eff}$ at 8 K (closed squares), $\tau_{R,eff}$ at 300 K (closed circles), and $\tau_{NR,eff}$ at 300 K (closed triangles) for the NBE emission of $Al_xGa_{1-x}N$ epilayers. The samples of $x < 0.64$ were grown at 1150 °C on a (0001) Al_2O_3 substrate (Ref. 11). In panel (a), FWHM value calculated using the alloy broadening model (Refs. 11 and 17) is shown by dashed curve. The dashed line in (b) connects the S values for high quality GaN and AlN (Refs. 4, 10 and 12), which is expected to be close to the defect-free S value for AlxGa1-xN (S_{free}).

(300 K), and $\tau_{NR,eff}$ (300 K) for the $Al_xGa_{1-x}N$ epilayers. The samples of $x < 0.64$ were grown at 1150 °C on a (0001) Al_2O_3 substrate.[11] The dashed curve in Fig. 4(a) shows the calculated FWHM value[11] for the NBE emission of statistically homogeneous $Al_xGa_{1-x}N$ according to alloy-broadening model.[17] The dashed line in Fig. 4(b) connects the S values for high quality GaN and AlN (Refs. 4, 10 and 12), which is expected to be close to the defect-free S value for $Al_xGa_{1-x}N$ (S_{free}). From Fig. 4, following tendency can be extracted. Because the growth temperature was insufficient, the FWHM values for the present epilayers are larger than the ideal values. In addition, S of all the LTG $Al_xGa_{1-x}N$ epilayers are larger than S_{free}. The results mean that present samples contain high concentration V_{III}-defects. As the formation energy of V_{Al} in AlN is far lower than that of Ga vacancies in GaN and even negative for n-type sample,[18] major V_{III}-defect in $Al_xGa_{1-x}N$ is assigned to V_{Al}. The simultaneous increase in $\tau_{R,eff}$ (8 K) and S for LTG $Al_xGa_{1-x}N$, therefore, means that certain point-defect complexes involving V_{Al} produce the band-tail to elongate $\tau_{R,eff}$(8 K), as is the case with AlN.[4] Conversely, however, $\tau_{R,eff}$(300 K) decreases with increasing x, at least for $x > 0.4$. This is consistent with the fact that f for 3D e-h pairs (excitons) in AlN is approximately 4–10 times that of GaN.[4,19] As a matter of fact, $\tau_{R,eff}$ values for the HTG AlN are as short as 10 ps at 8 K and 180 ps at 300 K.[4] Therefore, although $\tau_{R,eff}$ values at 8 K are longer than the expected ones, room temperature $\tau_{R,eff}$ being in the order of a few ns for the $Al_xGa_{1-x}N$ alloys of high x are reasonably short, being comparable to or even shorter than that of GaN and InGaN films.[12]

In summary, TRPL and TRCL studies on LTG $Al_xGa_{1-x}N$ epilayers of high x revealed that their low-temperature τ_R is elongated due to the contribution of a band-tail formed through point-defect (V_{Al}-complex) incorporation. However, τ_R showed little change with temperature rise, and the value is a few ns at 300 K. The results indicate that high-x $Al_xGa_{1-x}N$ essentially has an excellent radiative performance. Because τ_{NR} at 300 K are as short as 10–30 ps, high-temperature growth and appropriate defect management [20] are mandatory in extracting their excellent radiative talent.

The authors thank Professor T. Sota and Dr. M. Tanaka for fruitful discussions. This work was supported in part by NEDO programs under METI, Grant-in-Aids for Scientific Research Nos. 23656206 and 18069001 under MEXT, Japan and AFOSR/AOARD Grant No. FA2386-11-1-4013 monitored by Dr. G. Jessen.

[1]Y. Taniyasu, M. Kasu, and T. Makimoto, Nature **441**, 325 (2006).
[2]Quantum efficiencies of state-of-the-art UV LEDs are described in C. Pernot, M. Kim, S. Fukahori, T. Inazu, T. Fujita, Y. Nagasawa, A. Hirano, M. Ippommatsu, M. Iwaya, S. Kamiyama, I. Akasaki, and H. Amano, Appl. Phys. Express **3**, 061004 (2010), and references cited therein.
[3]K. B. Nam, J. Li, M. L. Nakarmi, J. Y. Lin, and H. X. Jiang, Appl. Phys. Lett. **82**, 1694 (2003).
[4]S. F. Chichibu, T. Onuma, K. Hazu, and A. Uedono, Appl. Phys. Lett. **97**, 201904 (2010); T. Onuma, K. Hazu, A. Uedono, T. Sota, and S. F. Chichibu, ibid. **96**, 061906 (2010).
[5]T. Onuma, T. Shibata, K. Kosaka, K. Asai, S. Sumiya, M. Tanaka, T. Sota, A. Uedono, and S. F. Chichibu, J. Appl. Phys. **105**, 023529 (2009).
[6]C. G. Dunn and E. F. Koch, Acta Metall. **5**, 548 (1957).
[7]K. Hazu, M. Kagaya, T. Hoshi, T. Onuma, and S. F. Chichibu, J. Vac. Sci. Technol. B **29**, 021208 (2011).
[8]M. Merano, S. Collin, P. Renucci, M. Gatri, S. Sonderegger, A. Crottini, J. D. Ganiere, and B. Deveaud, Rev. Sci. Instrum. **76**, 085108 (2005).
[9]R. Krause-Rehberg and H. S. Leipner, *Positron Annihilation in Semiconductors, Solid-State Sciences* (Springer, Berlin, 1999), Vol. 127; P. G. Coleman, *Positron Beams and Their Application* (World Scientific, Singapore, 2000).
[10]A. Uedono, S. Ishibashi, S. Keller, C. Moe, P. Cantu, T. M. Katona, D. S. Kamber, Y. Wu, E. Letts, S. A. Newman, S. Nakamura, J. S. Speck, U. K. Mishra, S. P. DenBaars, T. Onuma, and S. F. Chichibu, J. Appl. Phys. **105**, 054501 (2009).
[11]T. Onuma, S. F. Chichibu, A. Uedono, T. Sota, P. Cantu, T. M. Katona, J. F. Keading, S. Keller, U. K. Mishra, S. Nakamura, and S. P. DenBaars, J. Appl. Phys. **95**, 2495 (2004).
[12]S. F. Chichibu, A. Uedono, T. Onuma, B. A. Haskell, A. Chakraborty, T. Koyama, P. T. Fini, S. Keller, S. P. DenBaars, J. S. Speck, U. K. Mishra, S. Nakamura, S. Yamaguchi, S. Kamiyama, H. Amano, I. Akasaki, J. Han, and T. Sota, Nature Mater. **5**, 810 (2006); Philos. Mag. **87**, 2019 (2007).
[13]N. Teofilov, K. Thonke, R. Sauer, L. Kirste, D. G. Ebling, K. W. Benz, Diamond Relat. Mater. **11**, 892 (2002).
[14]H. Murotani, Y. Yamada, H. Miyake, and K. Hiramatsu, Appl. Phys. Lett. **98**, 021910 (2011).
[15]J. Feldmann, G. Peter, E. O. Göbel, P. Dawson, K. Moore, C. Foxon, and R. J. Elliot, Phys. Rev. Lett. **59**, 2337 (1987).
[16]Y. Ohba, H. Yoshida, and R. Sato, Jpn. J. Appl. Phys., Part 2 **36**, L1565 (1997); N. Kato, S. Sato, T. Sumii, N. Fujimoto, N. Okada, M. Imura, K. Balakrishnan, M. Iwaya, S. Kamiyama, H. Amano, I. Akasaki, H. Maruyama, T. Noro, T. Takagi, and A. Bandoh, J. Cryst. Growth **298**, 215 (2007); C. Moe, T. Onuma, K. Vampola, N. Fellows, H. Masui, S. Newman, S. Keller, S. F. Chichibu, S. P. DenBaars, and D. Emerson, J. Cryst. Growth **298**, 710 (2007).
[17]E. F. Schubert, E. O. Göbel, Y. Horikoshi, K. H. Ploog, and H. J. Queisser, Phys. Rev. B **30**, 813 (1984).
[18]J. Neugebauer and C. G. Van de Walle, Phys. Rev. B **50**, 8067 (1994); Appl. Phys. Lett. **69**, 503 (1996); C. Stampfl and C. G. Van de Walle, Appl. Phys. Lett. **72**, 459 (1998); Phys. Rev. B **65**, 155212 (2002); C. G. Van de Walle and J. Neugebauer, J. Appl. Phys. **95**, 3851 (2004); A. F. Wright and U. Grossner, Appl. Phys. Lett. **73**, 2751 (1998); K. Leung, A. F. Wright, and E. B. Stechel, Appl. Phys. Lett. **74**, 2495 (1999); A. F. Wright, J. Appl. Phys. **90**, 1164 (2001).
[19]H. Murotani, T. Kuronaka, Y. Yamada, T. Taguchi, N. Okada, and H. Amano, J. Appl. Phys. **105**, 083533 (2009).
[20]S. F. Chichibu, T. Onuma, M. Kubota, A. Uedono, T. Sota, A. Tsukazaki, A. Ohtomo, and M. Kawasaki, J. Appl. Phys. **99**, 093505 (2006).

Local lifetime and luminescence efficiency for the near-band-edge emission of freestanding GaN substrates determined using spatio-time-resolved cathodoluminescence

Y. Ishikawa,[1] M. Tashiro,[1] K. Hazu,[1] K. Furusawa,[1] H. Namita,[2] S. Nagao,[2] K. Fujito,[2] and S. F. Chichibu[1,a)]
[1]*Optoelectronics Laboratory, Institute of Multidisciplinary Research for Advanced Materials, Tohoku University, 2-1-1 Katahira, Aoba, Sendai 980-8577, Japan*
[2]*Gallium Nitride Department, Mitsubishi Chemicals Co., 1000, Higashi-mamiana, Ushiku, Ibaraki 300-1295, Japan*

(Received 10 October 2012; accepted 29 October 2012; published online 21 November 2012)

Spatio-time-resolved cathodoluminescence measurements were carried out on low threading dislocation density freestanding GaN substrates grown by hydride vapor phase epitaxy. High-resolution cathodoluminescence imaging allows for visualization of nonradiative recombination channels in the vicinity of accidentally formed inversion domain boundaries. Local cathodoluminescence lifetimes (τ_{CL}) for the near-band-edge (NBE) emission are shown to be sensitively position dependent. A linear relation between the equivalent internal quantum efficiency (η_{int}^{eq}) and τ_{CL} for the NBE emission was observed at room temperature under a weak excitation condition, and spatially resolved excitation led to the observation of the highest η_{int}^{eq} of 20% with τ_{CL} of 3.3 ns. © *2012 American Institute of Physics*. [http://dx.doi.org/10.1063/1.4767357]

Wurtzite group-III nitride semiconductors have intensively been studied for the past few decades, and near-ultraviolet (UV) to green light emitting diodes (LEDs) as well as purple to blue laser diodes (LDs) based on InGaN active regions are now in common place.[1,2] Whilst InGaN LEDs fabricated on defective GaN templates grown on (0001) sapphire substrates, which have high density threading dislocations (TDs) typically $10^8 \sim 10^9\,cm^{-2}$, are commercially available owing to the defect-insensitive emission probability of InGaN alloys,[3–6] it becomes evident that high-quality GaN substrates are necessary not only for achieving ultimate performance and/or excellent reliabilities of optical devices but also for realizing AlGaN/GaN power-switching transistors. For fabricating such substrates, hydride vapor phase epitaxy (HVPE) is one of the most commonly accepted techniques[7] despite cumulative bowing of the crystal plane that arises from the mismatch of the thermal expansion coefficients between GaN and the substrate used. Indeed, both *c*-plane and off-polar plane FS-GaN wafers with significantly reduced TD density ($<10^7\,cm^{-2}$) and low basal-plane stacking fault (BSF) density ($<10^3\,cm^{-1}$) are distributed.[7,8]

The internal quantum efficiency (η_{int}^{eq}) for the near-band-edge (NBE) emission is determined by the balance between the radiative and the nonradiative recombination rates; $\eta_{int}^{eq} = (1 + \tau_R/\tau_{NR})^{-1}$, where τ_R and τ_{NR} are the radiative and nonradiative lifetimes, respectively. As τ_{NR} for the NBE emission of GaN has been correlated with the gross concentration of point defects and complexes[9] rather than TD density, understanding local carrier (exciton) dynamics within low structural defect density areas of a GaN substrate is of paramount importance.

In order to probe local carrier dynamics in wide bandgap (E_g) semiconductors, scanning near-field optical microscopy with a short-pulsed laser is widely used. However, use of a short-pulsed electron-beam (*e*-beam) (Refs. 10–15) becomes attractive when characterizing wide E_g materials such as AlN (Ref. 11). Spatio-time-resolved cathodoluminescence (STRCL) (Refs. 13–15) takes full advantage of such a pulsed *e*-beam, which enables high spatial resolution beyond the diffraction limit of light owing to the focused electronic excitation and thus makes it possible to interrogate local carrier/exciton dynamics. Unique opportunities offered by the STRCL demonstrated so far includes the investigations of the exciton dynamics around BSF in an *a*-plane GaN (Ref. 14) and the slight local variations of In incorporation in the $In_{0.05}Ga_{0.95}N$ epilayer[15] grown on an *m*-plane FS-GaN.

In this letter, the correlation between the local cathodoluminescence (CL) intensities and lifetimes for the NBE emission is demonstrated using the STRCL technique in low TD density FS-GaN substrates grown by HVPE.[7] In the vicinity of an accidentally formed trapezoidal dimple surrounded by inversion domain boundaries (IDBs), the spatial variations of τ_{CL} and carrier/exciton diffusion length (L_d) are clearly visualized.

Approximately 0.5-mm-thick unintentionally doped *c*-plane FS-GaN substrates grown at 1050 °C using the vertical flow HVPE apparatus[7] were studied. The residual electron concentrations were 3×10^{18} and $2 \times 10^{17}\,cm^{-3}$ for samples A1 and A2, respectively. The TD densities were estimated from the full-width at half-maximum (FWHM) values of the x-ray rocking curves (XRCs) using the relation given in Ref. 16. Those containing edge components (N_E) were estimated to be 6.6×10^6 and $6.3 \times 10^6\,cm^{-2}$ for A1 and A2, respectively.

Prior to STRCL measurement, macroarea steady-state photoluminescence (PL) and time-resolved photoluminescence (TRPL) measurements were carried out using the

a)Author to whom correspondence should be addressed. Electronic mail: chichibulab@yahoo.co.jp.

 © 2012 American Institute of Physics

325 nm line of a cw He-Cd laser with an excitation intensity of 20 W/cm^2 and a frequency-tripled mode-locked Al_2O_3 : Ti laser operating at a wavelength of 267 nm (200 nJ/cm^2), respectively. Note that for both cases, weak excitation conditions were maintained, meaning that the excited carrier concentration was lower than that of the residual carriers. Our STRCL system consists of a scanning electron microscope (SEM) equipped with an in-house photoelectron gun (PE-gun),[12] which was driven by a frequency-tripled mode-locked Al_2O_3 : Ti laser pulses. The beam was focused using a fused silica lens ($f = 300$ mm) with a spot diameter of 50 μm to a photocathode. The average power of 80 mW was used at a repetition rate of 80 MHz, corresponding to laser fluence of 32 $\mu J/cm^2$. This value was limited by the onset of optical damage of the photocathode. The output *e*-beam was launched to the SEM by focusing it to its filament position. The probe current was calibrated by using a Faraday cup placed just above the temperature-controlled stage, and was typically 20 nA at an acceleration voltage (V_{acc}) of 10 kV. Although this is smaller than what can be achieved with a conventional W filament, reasonable quality of SEM images can be obtained. The luminescence from a sample was collected using an off-axis parabolic mirror ($R = 12$ mm) placed above the sample and then analyzed by using a grating spectrometer equipped with an electronically cooled charged-coupled device and a streak camera with a temporal resolution of approximately 10 ps.

Figure 1(a) shows a representative macroarea PL spectrum of A1 at 293 K. The sample exhibited a predominant NBE peak at 3.373 eV with the FWHM value of 73 meV and its LO phonon replica (a shoulder peak) at around 3.28 eV. The peak intensity of the broad emission band at around 2.2 eV (so-called yellow luminescence band) was more than three orders of magnitude lower than that of the NBE emission. The sample A2 showed an essentially same spectrum, indicating that both samples are of excellent quality. Figure 1(b) shows room temperature TRPL decay signals for the NBE emission in A1, measured at three different positions. It is found that characteristic lifetimes of the fast decay components (τ_1) were strongly position dependent, varying from 0.47 to 1.24 ns, although the overall PL spectra were almost unchanged (data not shown). The result implies that room temperature τ_{NR} varies depending on the positions.

In order to visualize spatial variations of the luminescence intensity and to evaluate local τ_{NR} for the NBE emission, STRCL measurement was conducted near the region surrounded by the IDBs in A1. We note that IDBs are occasionally formed by some growth perturbations. Figures 2(a)–2(c), respectively, illustrate SEM image and CL intensity images recorded for the NBE emission at 293 K and 20 K. These CL images were taken with a probe current of 100 pA and a dwell time of 200 ms, corresponding to 30 min per image. The SEM image showed a trapezoidal dimple surrounded by the IDBs. Also, several dark spots were found although their contrasts were rather faint. These spots were also observed as the dark spots in the CL image at 293 K, as shown in Fig. 2(b). The CL image at 293 K showed complex structures since its contrast reflects spatial distribution of nonradiative recombination centers (NRCs), while its spatial resolution is limited by $L_d = \sqrt{D \cdot \tau}$ of minority carriers,[17] where D and τ are their diffusivity and lifetime, respectively. The sharpness of the CL image taken at 20 K was greatly

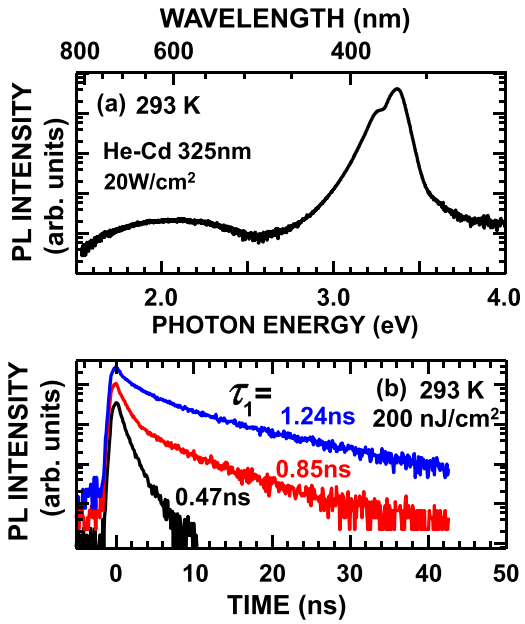

FIG. 1. (a) A macroarea steady-state PL spectrum at 293 K and (b) macroarea TRPL decay signals taken at 293 K for the NBE emission of the FS-GaN substrate grown by HVPE (A1). The TRPL signals were taken from three different positions, and vertical offsets are given for better looking.

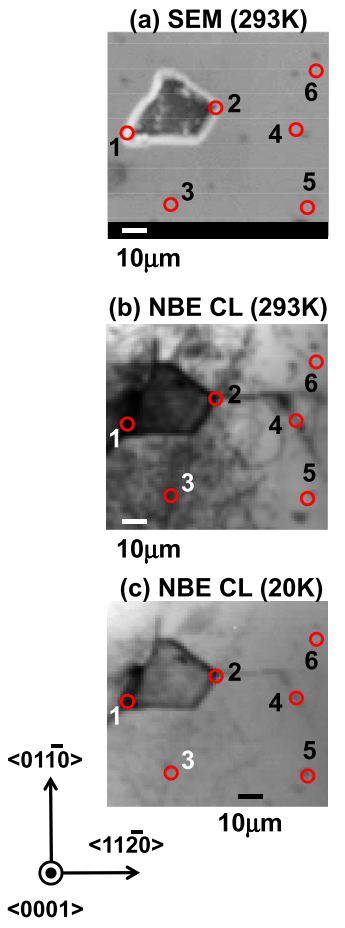

FIG. 2. (a) SEM image, (b) NBE CL intensity image taken at 293 K, and (c) NBE CL intensity image taken at 20 K for the FS-GaN sample A1.

improved because D approaches to zero towards 0 K according to Einstein's relation $D = k_B T\mu/q$, where k_B is the Boltzmann constant, T the temperature, q the electric charge, and μ the mobility. Furthermore, since the NRCs are essentially frozen out at low temperatures, contributions from pure NRCs are excluded in Fig. 2(c). Therefore, the dark areas and lines that remain in Fig. 2(c) are possibly due to the absence of the material itself or the presence of extremely strong NRCs. In both Figs. 2(b) and 2(c), it can be seen that some straight line structures run from the corners of the trapezoid parallel to m-planes. This implies that the tensile stress accumulated around the IDBs is relaxed by introducing cracks. Since there are no corresponding structures in the SEM image, it is likely that these cracks run under the surface, and which can specifically be detected in the CL images due to the finite implantation depth of the e-beam and the longitudinal diffusion of the minority carriers.

The virtue of STRCL is that it is readily accessible to the local recombination dynamics for a particular emission peak. Local time-integrated cathodoluminescence (TICL) and time-resolved cathodoluminescence (TRCL) decay signals for the NBE emission of A1 measured at room temperature at the positions encircled in Fig. 2 are shown in Figs. 3(a) and 3(b), respectively. In this instance, the probe current was decreased to 25 pA, which amounts to 2 electrons per pulse, in order to prevent any degradation in temporal resolution.[12] The resultant number of excited electron-hole pairs in GaN is deduced to be less than 2000 from the empirical relation given in Ref. 18. We note that this excitation density gives the τ_1 value for the TRPL decay constant of a GaN template when excited with the laser fluence of 2 μJ/cm^2 (Ref. 12). This value is an order of magnitude higher than that used for the TRPL measurement. However, weak excitation conditions are still maintained. The nominal NBE peak energy was approximately 3.38 eV, while the FWHM values were 90 meV, both of which are in reasonable agreement with Fig. 1(a). In these spectra, we found subtle redshifts of the NBE emission peak inside and on the peripheries of the trapezoid. This can be attributed to the local strain or increased residual electron concentration. We fit the decay curves by a double exponential function to extract τ_1, and found that τ_1 significantly varied depending on

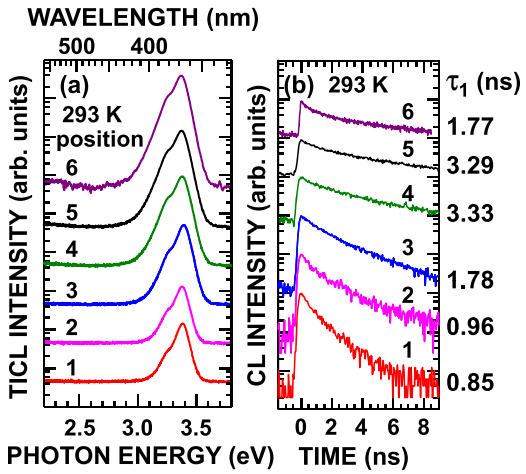

FIG. 3. Position dependent TICL spectra (a) and TRCL decay signals (b) for the NBE emission of FS-GaN sample A1 measured at 293 K. The number corresponds to the position encircled in Fig. 2.

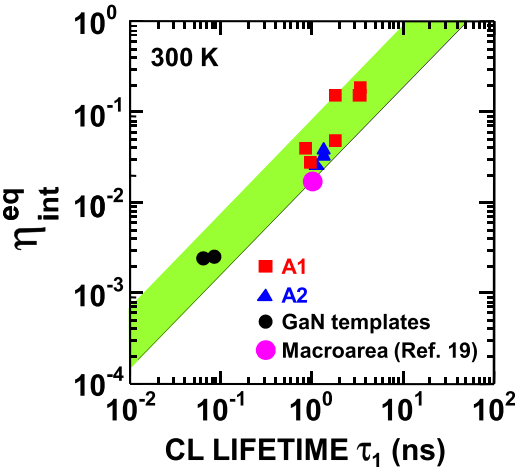

FIG. 4. The values of η_{int}^{eq} for the NBE emission peak of FS-GaN samples at room temperature as a function of the fast decay constant (τ_1) obtained from the STRCL measurement. The results for the macroarea measurement for both the HVPE FS-GaN (sample C0 in Ref. 19) that exhibited the longest positron diffusion length ($L_+ = 116$ nm) and GaN templates are also included for reference.

the positions. The decrease of τ_1 near the visual defects in the CL image at 293 K [see Fig. 2(b)] can be understood as enhanced recombination at NRCs because τ_1 at room temperature is generally dominated by τ_{NR}. By contrast, local τ_1 values measured at 10 K were almost independent of the positions being 180 ps. This is reasonable since τ_R dominates τ_{CL} at low temperature.

We also evaluated the local equivalent internal quantum efficiencies (η_{int}^{eq}) for the NBE emission by simply taking the ratio of the integrated spectral intensities at 293 K to that at 20 K. The results for A1 and A2 are summarized as a function of τ_1 in Fig. 4. The best data for the macroarea PL measurement on similar HVPE FS-GaN (Ref. 19) and typical values observed for GaN templates are also plotted for reference. As shown, η_{int}^{eq} linearly increases with the increase in τ_1 according to $\eta_{int}^{eq} = (1 + \tau_R/\tau_{NR})^{-1}$, where we assume that τ_R is an intrinsic value to a particular material[20] and that τ_{CL} is generally dominated by τ_{NR} at room temperature under the relation $\tau_{CL}^{-1} = \tau_R^{-1} + \tau_{NR}^{-1}$. Although the overall trend of higher η_{int}^{eq} in the local measurement may indicate somewhat higher excitation density used, the spatially focused excitation in STRCL can selectively probe highly luminescent regions that are less affected by NRCs. As a result, a record high η_{int}^{eq} of up to 20% was obtained for position 4 in Fig. 2, where τ_1 was as long as 3.33 ns.

In summary, local carrier recombination dynamics in the low TD density FS-GaN substrates grown by HVPE were studied by STRCL measurement. In addition to the visualization of defect networks originating from the IDBs in the CL intensity images, the spatially resolved TICL and TRCL measurements revealed a linear correlation between η_{int}^{eq} and τ_{CL} at room temperature. The spatially focused excitation led us to observe the highest η_{int}^{eq} of 20% and the longest τ_{CL} of 3.33 ns at 293 K. We believe that our results demonstrate the potential of FS-GaN grown by HVPE and serves as a benchmark for future development.

This work was supported in part by NEDO programs by METI and a Grant-in-Aids for Scientific Research Nos.

23645206 and 24760250 from MEXT, Japan, and AOARD/AFOSR monitored by Dr. G. Jessen.

[1]S. Nakamura and G. Fasol, *The Blue Laser Diode: GaN Based Light Emitters and Lasers* (Springer, Berlin, 1997).
[2]I. Akasaki and H. Amano, Jpn. J. Appl. Phys., **36**, 5395 (1997).
[3]S. F. Chichibu, T. Azuhata, T. Sota, and S. Nakamura, Appl. Phys. Lett. **69**, 4188 (1996); S. F. Chichibu, A. C. Abare, M. P. Mack, M. S. Minsky, T. Deguchi, D. Cohen, P. Kozodoy, S. B. Fleischer, S. Keller, J. S. Speck, J. E. Bowers, E. Hu, U. K. Mishra, L. A. Coldren, S. P. DenBaars, K. Wada, T. Sota, and S. Nakamura, Mater. Sci. Eng., B **59**, 298 (1999).
[4]Y. Narukawa, Y. Kawakami, S. Fujita, S. Fujita, and S. Nakamura, Phys. Rev. B **55**, R1938 (1997).
[5]L. Bellaiche, T. Mattila, L.-W. Wang, S.-H. Wei, and A. Zunger, Appl. Phys. Lett. **74**, 1842 (1999); P. R. C. Kent and A. Zunger, *ibid.* **79**, 1977 (2001).
[6]S. F. Chichibu, A. Uedono, T. Onuma, B. A. Haskell, A. Chakraborty, T. Koyama, P. T. Fini, S. Keller, S. P. DenBaars, J. S. Speck, U. K. Mishra, S. Nakamura, S. Yamaguchi, S. Kamiyama, H. Amano, I. Akasaki, J. Han, and T. Sota, Nature Mater. **5**, 810 (2006).
[7]K. Fujito, S. Kubo, H. Nagaoka, T. Mochizuki, H. Namita, and S. Nagao, J. Cryst. Growth **311**, 3011 (2009).
[8]K. Fujito, K. Kiyomi, T. Mochizuki, H. Oota, H. Namita, S. Nagao, and I. Fujimura, Phys. Status Solidi A **205**, 1056 (2008).
[9]S. F. Chichibu, A. Uedono, T. Onuma, T. Sota, B. A. Haskell, S. P. DenBaars, J. S. Speck, and S. Nakamura, Appl. Phys. Lett. **86**, 021914 (2005).
[10]M. Merano, S. Collin, P. Renucci, M. Gatri, S. Sonderegger, A. Crottini, J. D. Ganière, and B. Deveaud, Rev. Sci. Instrum. **76**, 085108 (2005).
[11]S. F. Chichibu, T. Onuma, K. Hazu, and A. Uedono, Appl. Phys. Lett. **97**, 201904 (2010).
[12]T. Onuma, Y. Kagamitani, K. Hazu, T. Ishiguro, T. Fukuda, and S. F. Chichibu, Rev. Sci. Instrum. **83**, 043905 (2012).
[13]M. Merano, S. Sonderegger, A. Crottini, S. Collin, P. Renucci, E. Pelucchi, A. Malko, M. H. Baier, E. Kapon, B. Deveaud, and J. D. Ganière, Nature **438**, 479 (2005).
[14]P. Corfdir, P. Lefebvre, J. Levrat, A. Dussaigne, J.-D. Ganière, D. Martin, J. Ristić, T. Zhu, N. Grandjean, and B. Deveaud-Plédran, J. Appl. Phys. **105**, 043102 (2009).
[15]M. Kagaya, P. Corfdir, J.-D. Ganière, B. Deveaud-Plédran, N. Grandjean, and S. F. Chichibu, Jpn. J. Appl. Phys., Part 1 **50**, 111002 (2011).
[16]C. G. Dunn and E. F. Koch, Acta Metall. **5**, 548 (1957).
[17]K. Kumakura, T. Makimoto, N. Kobayashi, T. Hashizume, T. Fukui, and H. Hasegawa, Appl. Phys. Lett. **86**, 052105 (2005).
[18]C. A. Klein, J. Appl. Phys. **39**, 2029 (1968).
[19]S. F. Chichibu, K. Hazu, Y. Ishikawa, M. Tashiro, H. Namita, S. Nagao, K. Fujito, and A. Uedono, J. Appl. Phys. **111**, 103518 (2012).
[20]D. Takamizu, Y. Nishimoto, S. Akasaka, H. Yuji, K. Tamura, K. Nakahara, T. Onuma, T. Tanabe, H. Takasu, M. Kawasaki, and S. F. Chichibu, J. Appl. Phys. **103**, 063502 (2008).

Phys. Status Solidi C **10**, No. 3, 501–506 (2013) / **DOI** 10.1002/pssc.201200676

physica status solidi c
www.pss-c.com
current topics in solid state physics

Time-resolved luminescence studies on AlN and high AlN mole fraction AlGaN alloys

Shigefusa F. Chichibu[*,1], Takeyoshi Onuma[1], Kouji Hazu[1], and Akira Uedono[2]

[1] Institute of Multidisciplinary Research for Advanced Materials, Tohoku University, 2-1-1 Katahira, Aoba, Sendai 980-8577, Japan
[2] Division of Applied Physics, University of Tsukuba, 1-1-1 Tennodai, Tsukuba 305-8573, Japan

Received 11 September 2012, accepted 16 November 2012
Published online 17 January 2013

Keywords deep ultraviolet, AlN, AlGaN, carrier dynamics, point defects, positron annihilation

[*] Corresponding author: e-mail chichibulab@yahoo.co.jp, Phone: +81 22 217 5363, Fax: +81 22 217 5363

Impacts of point defects and impurities on the recombination dynamics for the near-band-edge (NBE) emission in AlN and high AlN mole fraction $Al_xGa_{1-x}N$ epilayers are revealed by means of deep ultraviolet (DUV) time-resolved luminescence and positron annihilation measurements. Extremely radiative nature of AlN is identified, as the radiative lifetime (τ_R) for a free excitonic polariton emission is as short as 10 ps at 7 K and 180 ps at 300 K, which are the shortest ever reported for spontaneous emission of bulk semiconductors. However, τ_R increases with the increase in impurity and Al-vacancy (V_{Al}) concentrations up to 530 ps at 7 K, irrespective of the threading dislocation (TD) density. Continuous decrease in τ_R with temperature rise up to 200 K for heavily-doped samples may reflect the carrier release from band-tail states. Similar to these AlN, low-temperature τ_R for low-temperature-grown high-x $Al_xGa_{1-x}N$ are longer than that for low-x $Al_xGa_{1-x}N$, AlN, or GaN due to the contribution of bound and localized tail-states. However, τ_R shows little change with temperature rise, and is still a few ns at 300 K. The results essentially indicate an excellent radiative performance, although the luminescence efficiency of AlN and $Al_xGa_{1-x}N$ DUV light-emitting-diodes (LEDs) reported so far is limited by short nonradiative lifetimes (τ_{NR}). To increase τ_{NR}, high temperature growth with appropriate defect management is preferable.

© 2012 WILEY-VCH Verlag GmbH & Co. KGaA, Weinheim

1 Introduction Aluminium nitride (AlN) and high AlN mole fraction (x) $Al_xGa_{1-x}N$ alloys have attracted considerable interest for applications in UV-C (200~280 nm) DUV LEDs, because the bandgap energy (E_g) of AlN is 6.01 eV at 300 K [1, 2]. Taniyasu *et al*. [3] have demonstrated the shortest wavelength electroluminescence peak at 210 nm from an AlN *p-i-n* homojunction LED. However, its external quantum efficiency (η_{ext}) was as low as 10^{-8} [3], and typical η_{ext} for the state-of-the-art AlGaN DUV LEDs is approximately 3% [4].

As known, η_{ext} is a product of internal quantum efficiency (η_{int}), injection efficiency, and light extraction efficiency. The latter two components should be increased by optimizing device configurations and doping. Meanwhile, η_{int} is a material talent that is a fraction of radiative rate over the sum of radiative and nonradiative rates; *i. e.* $\eta_{int}=(1+\tau_R/\tau_{NR})^{-1}$. To improve η_{int}, τ_R and τ_{NR} must be quantitatively understood as functions of structural / point defect and impurity concentrations (crystal imperfections). However, only few papers [5-8] have dealt with the recombination dynamics of AlN and high-x $Al_xGa_{1-x}N$, because of the lack of a desirable DUV femtosecond excitation source.

In this article, the results of time-resolved luminescence and positron annihilation spectroscopy (PAS) measurements on AlN and high-x $Al_xGa_{1-x}N$ alloys are reported [6-8]. We first introduce two femtosecond excitation sources for time-resolved photoluminescence (TRPL) and time-resolved cathodoluminescence (TRCL) measurements. Then we quantify gross intrinsic τ_R for a free excitonic polariton emission of high-quality AlN to identify its extremely radiative nature. Next we show the results for various quality AlN to reveal that point defects and impurities, rather than TDs, play the major role in limiting τ_R and τ_{NR} for the NBE emission. Finally, we show that $Al_xGa_{1-x}N$ epilayers of high x essentially have an excellent radiative performance.

© 2012 WILEY-VCH Verlag GmbH & Co. KGaA, Weinheim

2 Experimental procedures

2.1 Analytical techniques Steady-state cathodoluminescence (CL) was excited using an electron beam (*e*-beam) operated at 3.5 kV acceleration voltage and 1.0×10^{-2} A·cm^{-2} probe current density [6-9].

As E_g of AlN is as large as 6.01 eV [1,2], a frequency-quadrupled (4ω) mode-locked Al_2O_3:Ti laser [5-8] was used for the TRPL measurement. Approximately 115 fs pulses of the laser light (197~200 nm) were generated by mixing the fundamental (ω) and frequency-tripled (3ω) beams using a barium borate crystal, as shown in Fig. 1. The repetition rate and power density were 80 MHz and 40 nJ·cm^{-2} (per pulse), respectively. The maximum electron-hole (*e*-*h*) pair concentration is estimated to be 4×10^{15} cm^{-3} during the pulse, assuming the absorption coefficient of AlN as 10^5 cm^{-1} at 198 nm. In order to excite semiconductors having E_g larger than the photon energy of the 4ω beam, we constructed a femtosecond-laser-driven photoelectron gun (PE-gun) [7, 8, 10] similar to Ref. [11] for TRCL measurements. It consisted of a 15-nm-thick Au film, extraction electrodes, and acceleration electrodes to give V_{acc}, as shown in Fig. 1. The Au film was excited from the rear surface using the 3ω pulses of the Al_2O_3:Ti laser (240~280 nm, 100 fs, ~1 μJ·cm^{-2} a pulse). The distance between the PE-gun and the sample was 52.5 mm. The quantum efficiency of the PE-gun was approximately 2.5×10^{-6} electrons per photon for V_{acc}=10 kV, and the *e*-beam current density was 1.8 pA·cm^{-2} during each pulse. The corresponding excitation density calibrated to our TRPL is approximately 10 nJ·cm^{-2}. Therefore, excitation intensities for TRPL and TRCL were low enough to satisfy a weak-excitation regime, which underlines the nonradiative processes at 300 K.

Energy-resolved TRPL and TRCL signals were acquired using a streak-camera, which limits the overall minimum time resolution approximately 7 ps. In case of TRCL, because *e*-beams can be implanted into far below the surface, unwanted surface recombination effects may be minimized. For example, the implantation depth profile peak is approximately 250 nm for V_{acc}=10 kV. To systematically compare τ_R and τ_{NR} for various quality samples, the effective PL (CL) lifetime $\tau_{PL(CL),eff}$ is defined [12] as the time after excitation when $\int_0^{\tau_{PL(CL),eff}} I(t)\,dt \Big/ \int_0^{t_{lim}} I(t)\,dt$ becomes 1-1/*e*, where $I(t)$ is the intensity at time t and t_{lim} is defined as the time when $I(t_{lim})$ becomes $0.01I(0)$. The effective radiative and nonradiative lifetimes ($\tau_{R,eff}$ and $\tau_{NR,eff}$, respectively) are deduced from $\eta_{int}=(1+\tau_{R,eff}/\tau_{NR,eff})^{-1}$ and $\tau_{PL(CL),eff}^{-1}=\tau_{R,eff}^{-1}+\tau_{NR,eff}^{-1}$, where η_{int} is approximated [12] as the spectrally-integrated weakly-excited PL (CL) intensity at given temperature T over that at around 8~10 K (I_{TK}/I_{8K}). Here, the relaxation efficiency toward the radiative NBE states is assumed to be nearly independent of T.

In order to correlate τ_R and τ_{NR} with concentrations of cation vacancies (V_{III}) and V_{III}-complexes, PAS measurement [13-15] was carried out using the monoenergetic positron (e^+) beam line [12,15,16]. Here, *S* parameter [13-15] for the Doppler-broadening spectrum of e^+-e^- annihilation γ-rays is used as the measure of concentration or size of negatively charged V_{III}-defects [13-15]. Details of the measurement and analysis are given in Refs. [12, 15, 16].

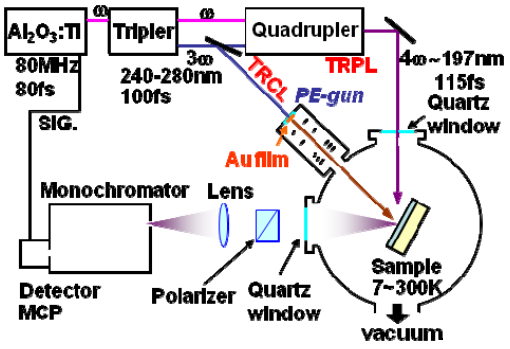

Figure 1 Schematic drawing of TRPL and TRCL measurement system. (Reproduced from Ref. [7]).

2.2 Samples Various quality AlN and $Al_xGa_{1-x}N$ epilayers [6-9] were grown by low-pressure metalorganic vapor phase epitaxy (MOVPE). In most cases, the reactor pressure was 2.0×10^4 Pa.

Approximately 2-μm-thick *c*-plane AlN films (sample numbers A1~A5) were grown on *c*-plane Al_2O_3 substrates, and an *m*-plane AlN film (A6) was grown on an *m*-plane freestanding GaN substrate [17]. The mole flow ratio of NH_3 to trimethylaluminium (TMAl) was varied between 32 to 3160. The TD densities having edge components (N_E) were 2×10^8 cm^{-2} for A1, 1×10^9 cm^{-2} for A2 and A6, 3×10^9 cm^{-2} for A4 and A5, and 1×10^{10} cm^{-2} for A3 (the values are shown in Fig. 2). The growth temperatures (T_g) were 1500 °C for A1 and 1350 °C for A2 and A3. These samples are classified as high-temperature grown (HTG) samples. Their Si, C, and O concentrations were below the detection limit of secondary-ion-mass spectrometry (below 5×10^{17} cm^{-3}, 10^{17} cm^{-3}, and 5×10^{17} cm^{-3}, respectively). The low-temperature grown (LTG) AlN samples A4 and A5 were grown at 1200 °C, and A6 was grown at 1120 °C to prevent GaN substrate from decomposing. Among these, A5 contained high concentration impurities ([Si]≅[C]=4×10^{19} cm^{-3} and [O]=2×10^{19} cm^{-3}). Those concentrations in A4 and A6 were an order of magnitude lower than A5. All the epilayers exhibited smooth surface morphology with 0.25-nm-high monolayer or 0.50-nm-high bilayer atomic steps.

We also grew approximately 1.3-μm-thick (0001) $Al_xGa_{1-x}N$ epilayers (x=0.65, 0.75, 0.89, and 0.97) on an 1-μm-thick AlN epitaxial template [9], which was grown on a (0001) Al_2O_3 substrate. Trimethylgallium (TMGa), TMAl, and NH_3 were used as the precursors, and the mole flow ratio of NH_3 to sum of TMGa and TMAl was varied between 32 to 3160. The value of T_g was varied between 1120 and 1200 °C. These samples are classified as LTG AlGaN. The N_E values were estimated from the full-width at half-maximum (FWHM) for the {10-12} X-ray rocking curve (1200~1500 arcsec) using the relation given in Ref.

© 2012 WILEY-VCH Verlag GmbH & Co. KGaA, Weinheim

[18] to be 2~3×10^9 cm^{-2}. The TD densities having pure screw components are estimated [18] to be lower than 2~6×10^7 cm^{-2}. They were characterized using the X-ray reciprocal space mapping method to be partially relaxed. The x values were calculated from the in-plane and out-of-plane lattice parameters and the degree of relaxation using the relation similar to that given in Ref. [19].

3 Results and discussion

3.1 AlN Room-temperature (RT) and low-temperature (LT) CL spectra for the AlN samples are shown in Fig. 2. As shown, the LT CL spectra for HTG samples are characterized by the predominant sharp excitonic NBE peaks and weak broad emission bands between 4.2 and 2.5 eV. Precisely [6, 9], the spectrum of A1 exhibited four bound exciton peaks (6.1040~6.1243 eV), ground state and the first excited state free A-excitonic peaks at FX_A=6.1383 and $FX_{A(n=2)}$=6.1768 eV, respectively, their longitudinal optical (LO) phonon replicas energetically lower than 6.058 eV, and B- and C-excitonic shoulder at $FX_{B,C}$=6.27 eV. These energies are higher by 95 meV than the strain-free values due to the in-plane compressive strain [2]. The strongest neutral donor bound exciton peak at 6.1243 eV (I_2^1) exhibited the narrowest FWHM being 2.9 meV, indicating reasonable crystal homogeneity. The crystal perfection of A1 is also confirmed by the small S being 0.458, which is close to the characteristic S for nearly V_{Al}-free ([V_{Al}]<10^{15} cm^{-3}) AlN (S_{free}) [15].

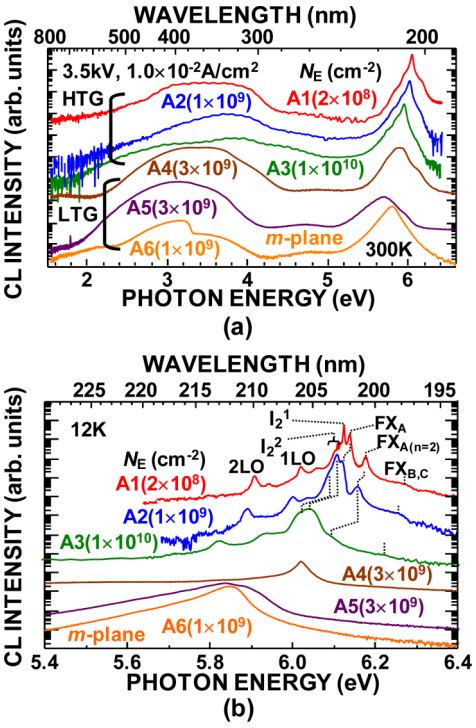

Figure 2 Steady-state CL spectra of AlN epilayers measured at (a) 300 K and (b) 12 K. The N_E values are shown in parentheses. FX, I_2, and LO mean free exciton, neutral donor bound exciton, and LO phonon replica, respectively (Reproduced from Ref. [7]).

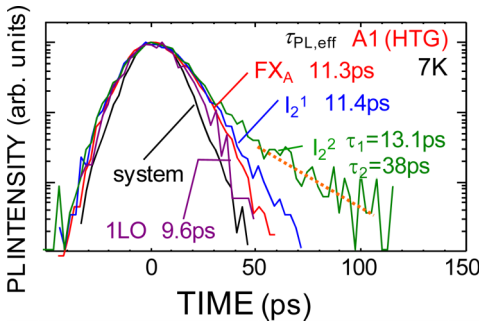

Figure 3 Energy-resolved TRPL signals for FX_A, I_2^1, I_2^2, and a LO phonon replica of FX_A (1LO) peaks in the AlN sample A1 at 7 K. (Reproduced from Ref. [6]).

The CL spectra for LTG ones, in contrast, are characterized by stronger deep-state emission bands and a broad NBE emission band at around 5.7~5.8 eV. For A5 and A6, the NBE CL peak energies were approximately 200 meV lower than E_g and the FWHM values were as large as 160 meV at 12 K, indicating that the emission originates from certain bound states. Because the deep-state emission bands at 3.1, 3.8, and 4.5 eV have been assigned to originate from point defect complexes involving V_{Al}-O [20-23], V_{Al}-Si [22], and V_{Al} [23], respectively, the results suggest a formation of band-tail due to the residual impurities incorporated during LTG. As shown, the spectral feature is not really influenced by N_E.

Energy-resolved TRPL signals for A1 at 7 K are shown in Fig. 3. The spectra exhibited a single or a double exponential decay shape with very fast lifetime (τ_1). The $\tau_{PL,eff}$ value for FX_A was as short as 11.3 ps. However, because $\tau_{PL,eff}$ for the neutral donor bound excitons I_2^1 and I_2^2 were 11.4~13.1 ps and τ_R of free excitons should be shorter than bound excitons, $\tau_{PL,eff}$ of FX_A may be shorter than 11 ps. It is well-known that measuring lifetime of an LO phonon replica is preferable to determine reliable τ_{PL} in the bulk region. This is because the energies of LO phonon replicas are lower than E_g and they can come out from the bulk, where any possible effects due to surface recombination can be excluded. As shown in Fig. 3, $\tau_{PL,eff}$ of FX_A-1LO peak at 6.016 eV was 9.6 ps.

In general, τ_{PL} at LT is governed by τ_R, because nonradiative recombination centres (NRCs) are frozen and ideal diffusion lengths of carriers approach nearly zero. Obviously, $\tau_{PL,eff}$ of FX_A approximately 10 ps is much shorter than general τ_{PL} values reported for GaN (35~220 ps) [24] and ZnO (106 ps) [25]. The $\tau_{R,eff}$ value for the NBE emission at LT in III-V and II-VI semiconductors are plotted as a function of E_g in Fig. 4 [6]. The value of τ_R is described [26] as $\tau_R = 2\pi\varepsilon_0 m_0 c^3/(ne^2\omega^2 f)$, where f is the oscillator strength, n the refractive index, ε_0 the dielectric constant in vacuum, and m_0 the electron mass in vacuum. As described in Ref. [6], τ_R of FX_A in AlN is calculated to be 8.4 ns, which is shorter by a factor of 14 than GaN (120 ns).

© 2012 WILEY-VCH Verlag GmbH & Co. KGaA, Weinheim

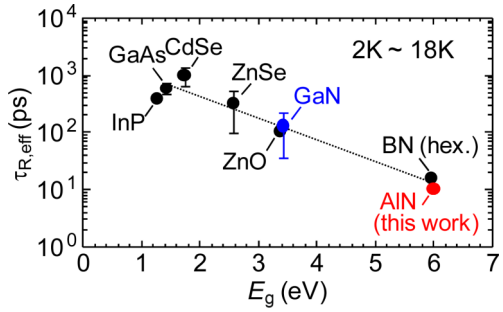

Figure 4 Low-temperature $\tau_{R,eff}$ for the NBE emissions in III-V and II-VI compound semiconductors as a function of E_g. (Reproduced from Ref. [6]).

This trend is consistent with Fig. 4. However, absolute values are 3 orders of magnitude longer than the measured ones. The discrepancy can be partially explained considering the formation of exciton-polaritons [27, 28]. Right after excitation, electrons and holes loose their excess energy and momentum within the bands, which usually take sub ps [29]. Subsequently excitons are formed and relax to an exciton-polariton bottleneck, especially at LT. An exciton-polariton is a manifold of an exciton and a light wave that can propagate in a material, and thereby the *polariton lifetime* is the time-of-flight to the surface [28]. This is dependent on energy, in particular around the bottleneck, due to the strong variation of the group velocity. It also depends strongly where the polariton has been created. Then, what one measures could be space-averaged time-of-flight. This is only true if polaritons propagate without collisions. As we have thick samples, elastic collisions may dominate the *polariton lifetime*. Assuming that the *polariton lifetime* near the bottleneck in AlN is close to that calculated for GaN being a few ps [30], the measured lifetime of 10 ps may reflect *whole* processes. Nevertheless, the shortest intrinsic $\tau_{R,eff}$ at LT in Fig. 4 indicates that the material itself is quite radiative.

Different from HTG samples, TRPL and TRCL signals for LTG AlN (and $Al_xGa_{1-x}N$) samples exhibited a

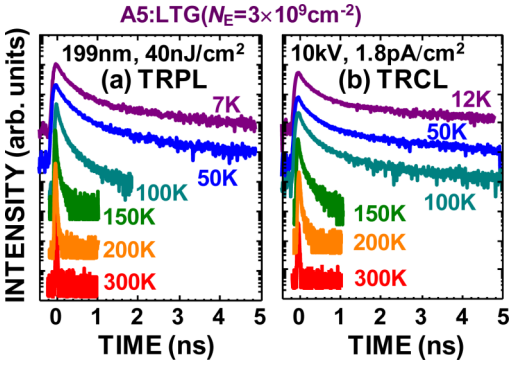

Figure 5 Temperature variations of (a) TRPL and (b) TRCL signals for the NBE emission of heavily C-, Si-, and O-doped LTG AlN (A5). (Reproduced from Ref. [7]).

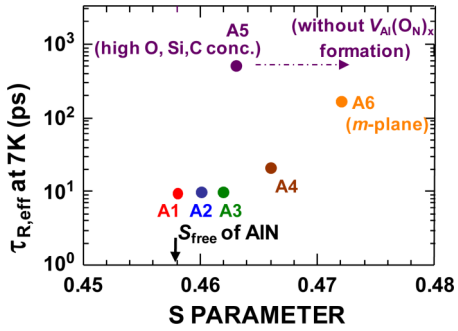

Figure 6 Low temperature $\tau_{R,eff}$ for the AlN epilayers as a function of S. The S_{free} value for AlN is 0.458. The S value for A5 is lessened in comparison with other samples due to the formation of $V_{Al}(O_N)_x$ complexes [15]. (Reproduced from Ref. [7]).

stretched exponential decay with slower lifetimes at LT. As shown in Figs. 5(a) and 5(b), $\tau_{PL(CL),eff}$ value for the NBE emission of A5 at 7 K was as long as 528 ps. This is characteristic of the emission processes in amorphous or defective semiconductors with pronounced tail states [31]. Here we note that in our weak-excitation conditions, TRCL results are quite similar to the TRPL results. The result indicates that TRCL has similar time-resolution as that of TRPL (see the signals at 300 K).

Because donor doping increases V_{Al} concentration through the Fermi-level effect [32], S of A4-A6 (>0.463) were higher than the HTG series (<0.462). Low temperature $\tau_{R,eff}$ values are plotted as a function of S in Fig. 6, in which S_{free}=0.458 [15] is marked on the horizontal axis. Considering the fact that $V_{Al}(O_N)_x$ complexes exhibit smaller characteristic S than isolated V_{Al} [15], the result shown in Fig. 6 indicates that $\tau_{R,eff}$ of excitons bound to high concentration donors (A4) and *e-h* pairs bound in band-tail states (A5 and A6) are much longer than the intrinsic $\tau_{R,eff}$ being of the order of 10 ps. We note that TD itself (N_E) has negligible influence on $\tau_{R,eff}$ (and $\tau_{NR,eff}$).

Temperature dependencies of $\tau_{R,eff}$ and $\tau_{NR,eff}$ for A1 and A5 are compared in Fig. 7. For A1, $\tau_{R,eff}$ monotonically increased according to approximately $T^{1.5}$ above 130 K, reflecting the increase in kinetic energy of quantum particles in three-dimensional (3D) free space [33]. The value of $\tau_{R,eff}$ reached 183 ps at 300 K. However, this is still the shortest among the semiconductors shown in Fig. 4. Due to the thermal activation of NRCs, $\tau_{NR,eff}$ decreased with T. On the contrary, $\tau_{R,eff}$ for the NBE emission of A5 first decreased with T up to 200 K. The result may reflect a recovery in f of *e-h* pairs, as follows: they are spatially-separated in the conduction band minima (CBM) and valence band maxima (VBM) at low-temperature, as schematically shown in Fig. 7(b), where CBM and VBM are formed due to charged impurities and counter-charged point defects. As T increases, the carriers may be released to 3D space to gain the wavefunction overlap. Above 230 K, $\tau_{R,eff}$ increases with $T^{1.5}$. The decrease in $\tau_{NR,eff}$ with T in A5 is

© 2012 WILEY-VCH Verlag GmbH & Co. KGaA, Weinheim

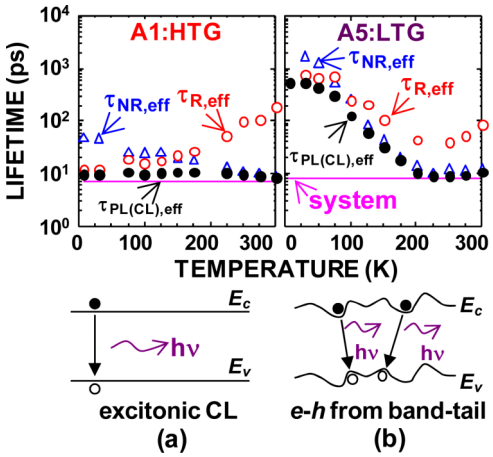

Figure 7 Temperature dependencies of measured $\tau_{PL(CL),eff}$ and calculated $\tau_{R,eff}$ and $\tau_{NR,eff}$ for the AlN epilayers (a) HTG A1 and (b) LTG A5. (Reproduced from Ref. [7].)

much remarkable than A1, reflecting enhanced carrier capture by NRCs due to the carrier release from the tail-states. Because the change in $\tau_{NR,eff}$ at 300 K was only from 10 ps to 7 ps with the increase in S and both are close to the time resolution, assertive conclusion cannot be drawn on the relation between $\tau_{NR,eff}$ and V_{Al} concentration. However, similar to the case for GaN [12] and ZnO [25], V_{Al}-complexes may act as a severe NRC in AlN.

3.2 High AlN mole fraction $Al_xGa_{1-x}N$ alloys

Steady-state PL or CL spectra at LT for the $Al_xGa_{1-x}N$ epilayers are shown in Fig.8. Their spectra exhibited a spectrally broad but reasonably intense NBE peak. Similar to the results reported previously [16, 34, 35], their peak energies are lower by approximately 200 meV than E_g. As shown, the luminescence intensities for the deep-state emission bands below 4.4 eV are two or three orders of magnitude weaker than the NBE peak. However, because these films are LTG, band-tail formation and compositional inhomogeneity are hard to avoid.

Compositional variations in the FWHM value for the NBE emission at 8 K, S parameter, $\tau_{R,eff}$(8 K), $\tau_{R,eff}$(300 K), and $\tau_{NR,eff}$(300 K) for the $Al_xGa_{1-x}N$ epilayers are shown in

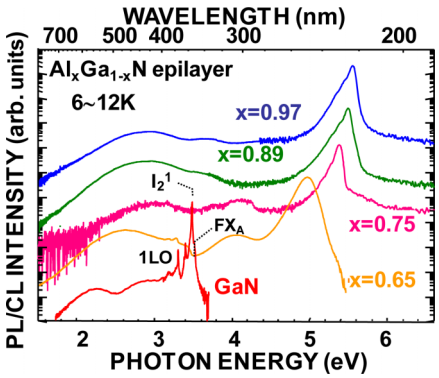

Figure 8 Steady-state PL and CL spectra at 6~12K for the $Al_xGa_{1-x}N$ alloy epilayers grown by MOVPE. (Reproduced from Ref. [8]).

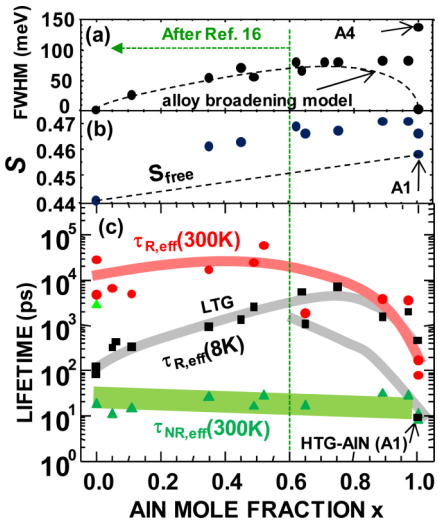

Figure 9 (a) FWHM value for the NBE emission at 8 K, (b) S parameter, and (c) $\tau_{R,eff}$ at 8 K, $\tau_{R,eff}$ at 300 K, and $\tau_{NR,eff}$ at 300 K for the NBE emission of $Al_xGa_{1-x}N$ epilayers. The samples of x<0.64 were grown at 1150 °C [16]. (Reproduced from Ref. [8].)

Fig. 9. The samples of x < 0.64 were grown at 1150 °C on a (0001) Al_2O_3 substrate [16]. The dashed curve in Fig. 9(a) shows the calculated FWHM value [16] for the NBE emission of statistically homogeneous $Al_xGa_{1-x}N$ according to alloy-broadening model [36]. The dashed line in Fig. 9(b) connects the S_{free} values of GaN [8, 12] and AlN [7, 8, 15], which represents S_{free} of $Al_xGa_{1-x}N$ alloys. From the figure, following tendency can be extracted. Because T_g was insufficient, FWHM values for the NBE emission are larger than the ideal values. In addition, S of all the epilayers are larger than S_{free}, meaning that present samples contain high concentration V_{III}-defects. As the formation energy of V_{Al} in AlN is far lower than that of Ga vacancies in GaN and even negative for n-type sample [32], major V_{III}-defect in $Al_xGa_{1-x}N$ is assigned to V_{Al}. The simultaneous increase in $\tau_{R,eff}$(8 K) and S for LTG $Al_xGa_{1-x}N$, therefore, means that certain point-defect complexes involving V_{Al} produce the band-tail to elongate $\tau_{R,eff}$(8 K), as is the case with AlN [7].

Conversely, however, $\tau_{R,eff}$(300 K) decreases with increasing x, at least for x>0.4. This is consistent with the fact that f for 3D e-h pairs (excitons) in AlN is approximately 4 to 10 times that of GaN [6-8, 37]. As a matter of fact, $\tau_{R,eff}$ values for HTG AlN are as short as 10 ps at 8 K and 180 ps at 300 K [7]. Therefore, although $\tau_{R,eff}$ values at 8 K are longer than the expected ones, room temperature $\tau_{R,eff}$ being in the order of a few ns for the $Al_xGa_{1-x}N$ alloys of high x are reasonably short, being comparable to or even shorter than that of GaN and InGaN films [12].

4 Conclusion Extremely radiative nature of AlN is revealed from the short $\tau_{R,eff}$ for the excitonic polariton emission (10 ps at 7 K and 180 ps at RT). However, the

© 2012 WILEY-VCH Verlag GmbH & Co. KGaA, Weinheim

$\tau_{R,eff}$ value increases with the increase in impurity and V_{Al} concentrations up to 530 ps at 7 K, irrespective of N_E. Continuous decrease in τ_R with temperature rise up to 200 K for LTG AlN may reflect the dominance of the emission from band-tail states formed due to impurities and point defects. For LTG high-x $Al_xGa_{1-x}N$ epilayers, τ_R is elongated due to the contribution of band-tail states. However, τ_R shows little change with temperature rise, and the value is still a few ns at 300 K. The results indicate that high-x $Al_xGa_{1-x}N$ also has an excellent radiative nature. Because point defects and impurities, rather than TDs, limit τ_R (and τ_{NR}), HT growth and appropriate defect management are necessary in extracting their radiativeperformance.

Acknowledgements The authors thank Prof. T. Sota of Waseda Univ., Prof. C. Weisbuch of Univ. California Santa Barbara, Prof. B. Gil of Univ. Montpellier II, and Dr. M. Tanaka for fruitful discussions. This work was supported in part by NEDO programs under METI, Grant-in-Aids for Scientific Research Nos. 23656206 and 18069001 under MEXT, Japan, and AFOSR/AOARD Grant Nos. FA2386-11-1-4013 and FA2386-11-1-4108 monitored by Dr. G. Jessen.

References

[1] B. Gil, Phys. Rev. B **81**, 205201 (2010).
[2] H. Ikeda, T. Okamura, K. Matsukawa, T. Sota, M. Sugawara, T. Hoshi, P. Cantu, R. Sharma, J. F. Kaeding, S. Keller, U. K. Mishra, K. Kosaka, K. Asai, S. Sumiya, T. Shibata, M. Tanaka, J. S. Speck, S. P. DenBaars, S. Nakamura, T. Koyama, T. Onuma, and S. F. Chichibu, J. Appl. Phys. **102**, 123707 (2007); Erratum in: J. Appl. Phys. **103**, 089901 (2008).
[3] Y. Taniyasu, M. Kasu, and T. Makimoto, Nature **441**, 325 (2006).
[4] Quantum efficiencies of state-of-the-art UV LEDs are described in: C. Pernot, M. Kim, S. Fukahori, T. Inazu, T. Fujita, Y. Nagasawa, A. Hirano, M. Ippommatsu, M. Iwaya, S. Kamiyama, I. Akasaki, and H. Amano, Appl. Phys. Express **3**, 061004 (2010), and references cited therein.
[5] K. B. Nam, J. Li, M. L. Nakarmi, J. Y. Lin, and H. X. Jiang, Appl. Phys. Lett. **82**, 1694 (2003).
[6] T. Onuma, K. Hazu, A. Uedono, T. Sota, and S. F. Chichibu, Appl. Phys. Lett. **96**, 061906 (2010).
[7] S. F. Chichibu, T. Onuma, K. Hazu, and A. Uedono, Appl. Phys. Lett. **97**, 201904 (2010).
[8] S. F. Chichibu, K. Hazu, T. Onuma, and A. Uedono, Appl. Phys. Lett. **99**, 051902 (2011).
[9] T. Onuma, T. Shibata, K. Kosaka, K. Asai, S. Sumiya, M. Tanaka, T. Sota, A. Uedono, and S. F. Chichibu, J. Appl. Phys. **105**, 023529 (2009).
[10] T. Onuma, Y. Kagamitani, K. Hazu, T. Ishiguro, T. Fukuda, and S. F. Chichibu, Rev. Sci. Instrum. **83**, 043905 (2012).
[11] M. Merano, S. Collin, P. Renucci, M. Gatri, S. Sonderegger, A. Crottini, J. D. Ganiere, and B. Deveaud, Rev. Sci. Instrum. **76**, 085108 (2005).
[12] S. F. Chichibu, A. Uedono, T. Onuma, B. A. Haskell, A. Chakraborty, T, Koyama, P. T. Fini, S. Keller, S. P. DenBaars, J. S. Speck, U. K. Mishra, S. Nakamura, S. Yamaguchi, S. Kamiyama, H. Amano, I. Akasaki, J. Han, and T. Sota, Nature Mater. **5**, 810 (2006); Philos. Mag. **87**, 2019 (2007).
[13] R. Krause-Rehberg and H. S. Leipner, Positron Annihilation in Semiconductors, Solid-State Sciences, Vol. 127 (Springer, Berlin, 1999).
[14] P. G. Coleman, Positron Beams and Their Application, (World Scientific, Singapore, 2000).
[15] A. Uedono, S. Ishibashi, S. Keller, C. Moe, P. Cantu, T. M. Katona, D. S. Kamber, Y. Wu, E. Letts, S. A. Newman, S. Nakamura, J. S. Speck, U. K. Mishra, S. P. DenBaars, T. Onuma, and S. F. Chichibu, J. Appl. Phys. **105**, 054501 (2009).
[16] T. Onuma, S. F. Chichibu, A. Uedono, T. Sota, P. Cantu, T. M. Katona, J. F. Keading, S. Keller, U. K. Mishra, S. Nakamura, and S. P. DenBaars, J. Appl. Phys. **95**, 2495 (2004).
[17] K. Fujito, K. Kiyomi, T. Mochizuki, H. Oota, H. Namita, S. Nagao, and I. Fujimura, Phys. Status Solidi A **205**, 1056 (2008).
[18] C. G. Dunn and E. F. Koch, Acta Metall. **5**, 548 (1957).
[19] K. Hazu, M. Kagaya, T. Hoshi, T. Onuma, and S. F. Chichibu, J. Vac. Sci. Technol. B **29**, 021208 (2011).
[20] G. A. Slack, L. J. Schowalter, D. Morelli, and J. A. Freitas, Jr., J. Cryst. Growth **246**, 287 (2002).
[21] K. B. Nam, M. L. Nakarmi, J. Y. Lin, and H. X. Jiang, Appl. Phys. Lett. **86**, 222108 (2005).
[22] A. Dadgar, A. Krost, J. Christen, B. Bastek, F. Bertram, A. Krtschil, T. Hempel, J. Blasing, U. Haboeck, and A. Hoffmann, J. Cryst. Growth **297**, 306 (2006).
[23] T. Koyama, M. Sugawara, T. Hoshi, A. Uedono, J. F. Kaeding, R. Sharma, S. Nakamura, and S. F. Chichibu, Appl. Phys. Lett. **90**, 241914 (2007).
[24] For example, see G. Pozina, J. P. Bergman, T. Paskova, and B. Monemar, Appl. Phys. Lett. **75**, 4124 (1999).
[25] S. F. Chichibu, T. Onuma, M. Kubota, A. Uedono, T. Sota, A. Tsukazaki, A. Ohtomo, and M. Kawasaki, J. Appl. Phys. **99**, 093505 (2006).
[26] G. W. 't Hooft, W. A. J. A. van der Poel, L. W. Molenkamp, and C. T. Foxon, Phys. Rev. B **35**, 8281 (1987).
[27] H. Sumi, J. Phys. Soc. Jpn. **41**, 526 (1976).
[28] C. Weisbuch, H. Benisty, and R. Houdre, J. Lumin. **85**, 271 (2000).
[29] J. Shah, Ultrafast Spectroscopy of Semiconductors and Semiconductor Nanostructures (Springer, Berlin, 1996).
[30] K. Torii, T. Deguchi, T. Sota, K. Suzuki, S. Chichibu, and S. Nakamura, Phys. Rev. B **60**, 4723 (1999).
[31] R. Kohlrausch, Ann. Phys. **12**, 393 (1847).
[32] C. Stampfl and C. G. Van de Walle, Appl. Phys. Lett. **72**, 459 (1998).
[33] J. Feldmann, G. Peter, E. O. Göbel, P. Dawson, K. Moore, C. Foxon, and R. J. Elliot, Phys. Rev. Lett. **59**, 2337 (1987).
[34] N. Teofilov, K. Thonke, R. Sauer, L. Kirste, D. G. Ebling, K. W. Benz, Diam. Relat. Mater. **11**, 892 (2002).
[35] H. Murotani, Y. Yamada, H. Miyake, and K. Hiramatsu. Appl. Phys. Lett. **98**, 021910 (2011).
[36] E. F. Schubert, E. O. Göbel, Y. Horikoshi, K. H. Ploog, and H. J. Queisser, Phys. Rev. B **30**, 813 (1984).
[37] H. Murotani, T. Kuronaka, Y. Yamada, T. Taguchi, N. Okada, and H. Amano, J. Appl. Phys. **105**, 083533 (2009).

© 2012 WILEY-VCH Verlag GmbH & Co. KGaA, Weinheim

Spatio-Time-Resolved Cathodoluminescence Studies on Freestanding GaN Substrates Grown by Hydride Vapor Phase Epitaxy

S. F. Chichibu[a], Y. Ishikawa[a], M. Tashiro[a], K. Hazu[a], K. Furusawa[a], H. Namita[b], S. Nagao[b], K. Fujito[b], and A. Uedono[c]

[a] Institute of Multidisciplinary Research for Advanced Materials, Tohoku University, 2-1-1 Katahira, Aoba, Sendai 980-8577, Japan
[b] Gallium Nitride Department, Mitsubishi Chemical Corporation, 1000 Higashi-Mamiana, Ushiku 300-1295, Japan
[c] Division of Applied Physics, University of Tsukuba, 1-1-1 Tennodai, Tsukuba, Ibaraki 305-8573, Japan

A spatio-time-resolved cathodoluminescence (STRCL) system was constructed by replacing the electron beam (*e*-beam) gun of a conventional scanning electron microscope by the in-house manufactured pulsed *e*-beam gun, which is excited using femtosecond laser pulses. By using this system, STRCL measurements were carried out on low threading dislocation density freestanding GaN substrates grown by hydride vapor phase epitaxy. High-resolution cathodoluminescence imaging allows for visualization of nonradiative recombination channels in the vicinity of accidentally formed domain boundaries. Local cathodoluminescence lifetimes (τ_{CL}) for the near-band-edge (NBE) emission are shown to be sensitively position dependent. A linear relation between the equivalent internal quantum efficiency (η_{int}^{eq}) and τ_{CL} for the NBE emission was observed at room temperature under a weak excitation condition, and spatially resolved excitation led to the observation of the highest η_{int}^{eq} of 20 % with τ_{CL} of 3.3 ns.

Introduction

As a solution to concerns about energy crisis, exploitation of high-efficiency power-switching devices using AlGaN/GaN heterostructure-field-effect-transistors and solid-state-lighting using InGaN quantum well light-emitting-diodes (LEDs) is one of the significant ways for drastically decreasing total energy consumption (1). Whilst InGaN LEDs fabricated on defective *GaN templates* grown on (0001) sapphire substrates, which have high density threading dislocations (TDs) typically 10^8~10^9 cm^{-2}, are commercially available thanks to the defect-insensitive emission probability of InGaN alloys (2-7), it becomes evident that high-purity, large-area, free-standing GaN (FS-GaN) wafers with low threading dislocation density (TDD) are necessary not only for achieving ultimate performance and/or excellent reliabilities of optical devices but also for realizing AlGaN/GaN power-switching transistors. Especially, suppression of the *efficiency-droop* phenomenon in InGaN LEDs is predicted for the devices grown on off-polar plane, heat-conducting FS-GaN substrates.

For fabricating such substrates, hydride vapor phase epitaxy (HVPE) is one of the most commonly-accepted techniques (8) despite cumulative bowing of the crystal plane that arises from the mismatch of the thermal expansion coefficients between GaN and the substrate. Indeed, both *c*-plane and off-polar plane FS-GaN wafers with significantly reduced TDD ($<10^7$ cm^{-2}) and low basal-plane stacking fault (BSF) density ($<10^3$ cm^{-1}) are distributed (8,9). From scientific point of view, fundamental influences by point defects on the electronic and optical properties can be studied using such low structural defect density, high-purity bulk crystals. For instance, equivalent internal quantum efficiency (η_{int}^{eq}) for the near-band-edge (NBE) emission is determined by the balance between the radiative and nonradiative recombination rates; $\eta_{int}^{eq}= (1+\tau_R/\tau_{NR})^{-1}$, where τ_R and τ_{NR} are the radiative and nonradiative lifetimes, respectively. As τ_{NR} for the NBE emission of GaN has been correlated with the gross concentration of point defects and complexes (10,11) rather than TDD, understanding local carrier (exciton) recombination dynamics within low structural defect density areas of a GaN substrate is of paramount importance.

Because state-of-the-art low TDD FS-GaN substrates are of high quality, the influence of a TD on the local luminescence spectrum and lifetime can be studied using a spectroscopy technique of sufficient high spatial resolution. In order to probe local carrier dynamics in wide bandgap (E_g) semiconductors, scanning near-field optical microscopy (SNOM) with a short-pulsed laser is widely used. On the other hand, the use of a scanning electron microscopy (SEM) equipped with a femtosecond electron beam (*e*-beam) gun (12-18), namely spatio-time-resolved cathodoluminescence (STRCL) technique (13,14,16,18), makes it possible to measure local time-resolved cathodoluminescence (TRCL) signals at the positions defined precisely by the secondary electron (SE) image. This becomes attractive when characterizing very wide E_g materials such as AlN and $Al_xGa_{1-x}N$ alloys of high AlN mole fraction *x*. Indeed, STRCL takes full advantage of such a pulsed *e*-beam, which enables high spatial resolution beyond the diffraction limit of light owing to the focused electronic excitation and thus makes it possible to interrogate local carrier/exciton dynamics. Unique opportunities offered by the STRCL demonstrated so far includes the investigations of the exciton dynamics around BSFs in an *a*-plane GaN (14) and the slight local variations of In incorporation in the $In_{0.05}Ga_{0.95}N$ epilayer (16) grown on an *m*-plane FS-GaN.

In this transaction, the correlation between the local cathodoluminescence (CL) intensities and lifetimes for the NBE emission of low TDD FS-GaN substrates grown by HVPE (8) is demonstrated using the STRCL technique. In the vicinity of an accidentally-formed trapezoidal dimple surrounded by domain boundaries (DBs), the spatial variations of τ_{CL} and carrier/exciton diffusion length (L_d) are clearly visualized.

Experimental

Samples

The samples investigated herein were approximately 500-μm-thick *c*-plane FS-GaN substrates named A1 and A2, which were grown using a vertical-flow HVPE apparatus (8,9). Appropriate amount of gaseous HCl was flowed on heated Ga, and NH_3 was supplied from a separate gas line. The growth temperature and pressure were 1050 °C and atmospheric pressure, respectively. The electron concentrations were 3×10^{18} and 2×10^{17} cm^{-3} for samples A1 and A2, respectively. The TDDs were estimated from the

full-width at half-maximum (FWHM) values of the x-ray rocking curves (XRCs) using the relation given in Ref. (19). Those containing edge components (N_E) were estimated to be 6.6×10^6 and 6.3×10^6 cm^{-2} for A1 and A2, respectively. The *S* parameters obtained from the positron annihilation measurement, which reflect the concentration and/or size of Ga vacancies (V_{Ga}) and V_{Ga}-complexes, of the present samples were close to (11) characteristic *S* for vacancy-free GaN (S_{free}) being 0.442, which was calculated using the first principles calculations (20). We note that V_{Ga}-defect concentration in the sample exhibiting S_{free} is lower than the detection limit for GaN ($\cong10^{15}$ cm^{-3}) (20), which corresponds to the concentration that positron trapping probability reaches zero. Details of the growth (8,9) and fundamental optical properties (11) have been given in literatures.

Prior to STRCL measurement, macroarea steady-state photoluminescence (PL) and time-resolved photoluminescence (TRPL) measurements were carried out using the 325 nm line of a cw He-Cd laser with an excitation intensity of 20 W/cm^2 and a frequency-tripled mode-locked Al_2O_3:Ti laser operating at a wavelength of 267 nm (200 nJ/cm^2), respectively. Note that for both cases, weak excitation conditions were maintained, meaning that the excited carrier concentration was lower than that of the residual carriers.

Spatio-Time-Resolved Cathodoluminescence Measurement

Schematic diagram of our STRCL equipment is shown in Fig. 1. The system (18) consists of an SEM equipped with an in-house photoelectron gun (PE-gun) (15,17), which was driven by a frequency-tripled mode-locked Al_2O_3:Ti laser pulses. The beam was focused using a fused silica lens (*f*=300 mm) with a spot diameter of 50 μm to a rear-side of a photocathode. The average power of 80 mW was used at a repetition rate of 80 MHz, corresponding to laser fluence of 32 $\mu J/cm^2$. This value was limited by the onset of optical damage of the photocathode. The output *e*-beam was launched to the SEM by focusing it to its filament position. The probe current was calibrated using a Faraday cup placed just above the temperature-controlled stage, and was typically 20 nA at an

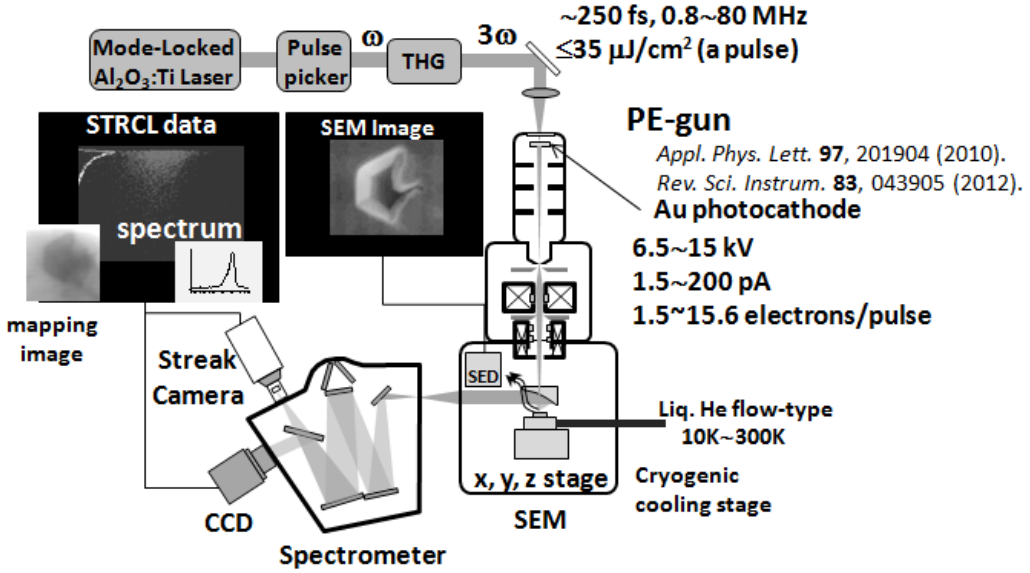

Figure 1. Schematic diagram of the STRCL measurement system. The wavelength and repetition rate of the frequency-tripled (3ω) femtosecond Al_2O_3:Ti laser are adjusted according to the purpose of the measurement.

acceleration voltage (V_{acc}) of 10 kV. Although this is smaller than what can be achieved with a conventional W filament, reasonable quality of SEM images can be obtained. The luminescence from a sample was collected using an off-axis parabolic mirror (R=12 mm) placed above the sample and then analyzed using a grating spectrometer equipped with an electronically-cooled charged-coupled device and a streak camera with a temporal resolution of approximately 10 ps.

Results and Discussion

Figure 2(a) shows a representative macroarea PL spectrum of A1 at 293 K. The sample exhibited a predominant NBE peak at 3.373 eV with the FWHM value of 73 meV and its LO phonon replica (a shoulder peak) at around 3.28 eV. The peak intensity of the broad emission band at around 2.2 eV (so-called yellow luminescence band) was more than three orders of magnitude lower than that of the NBE emission. The sample A2 showed an essentially the same spectrum, indicating that both samples are of excellent quality.

Figure 2(b) shows room temperature TRPL decay signals for the NBE emission in A1, measured at three different positions. It is found that characteristic lifetimes of the fast decay components (τ_1) were strongly position dependent, varying from 0.47 to 1.24 ns, although the overall PL spectra were almost unchanged (data not shown). The result implies that room temperature τ_{NR} varies depending on the positions.

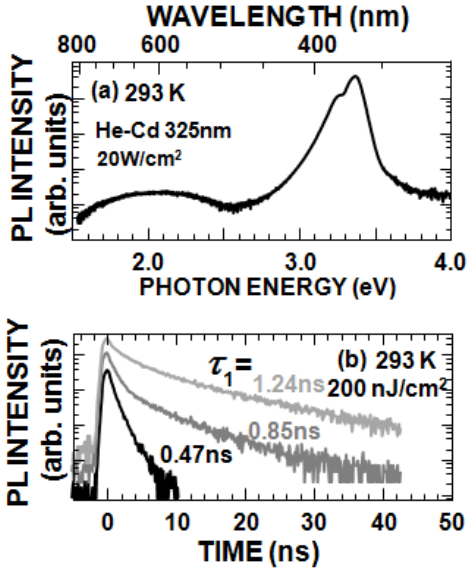

Figure 2 (a) A macroarea steady-state PL spectrum at 293 K and (b) macroarea TRPL decay signals taken at 293 K for the NBE emission of the FS-GaN substrate grown by HVPE (A1). The TRPL signals were taken from three different positions, and vertical offsets are given for better looking.

In order to visualize spatial variations of the luminescence intensity and to evaluate local τ_{NR} for the NBE emission, STRCL measurement was conducted near the region surrounded by the DBs in A1. We note that such DBs are occasionally formed by some growth perturbations. Figures 3(a), 3(b), and 3(c), respectively, illustrate SEM image and CL intensity images recorded for the NBE emission at 293 K and 20 K. These CL images

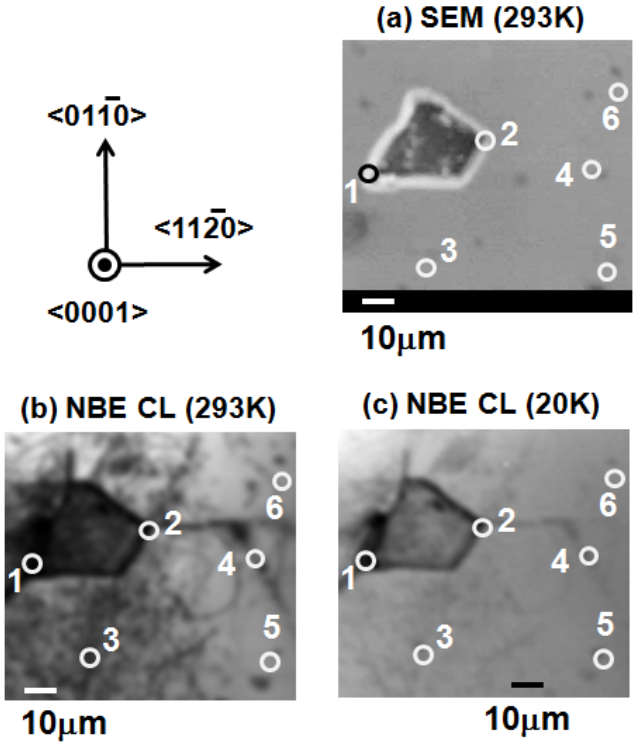

Figure 3 (a) A macroarea steady-state PL spectrum at 293 K and (b) macroarea TRPL decay signals taken at 293 K for the NBE emission of the FS-GaN substrate grown by HVPE (A1). The TRPL signals were taken from three different positions, and vertical offsets are given for better looking.

were taken with a probe current of 100 pA and a dwell time of 200 ms, corresponding to 30 minutes per image. The SEM image showed a trapezoidal dimple surrounded by the DBs. Also, several dark spots were found although their contrasts were rather faint. These spots were also observed as the dark spots in the CL image at 293 K, as shown in Fig. 3(b). The CL image at 293 K showed complex structures since its contrast reflects spatial distribution of nonradiative recombination centers (NRCs) while its spatial resolution is limited by $L_d=(D\cdot\tau)^{1/2}$ of minority carriers (21), where D and τ are their diffusivity and lifetime, respectively. The sharpness of the CL image taken at 20 K was greatly improved because D approaches to zero towards 0 K according to Einstein's relation $D=k_BT\mu/q$, where k_B is the Boltzmann constant, T the temperature, q the electric charge, and μ the mobility. Furthermore, since the NRCs are essentially frozen out at low temperatures, contributions from pure NRCs are excluded in Fig. 3(c). Therefore, the dark areas and lines that remain in Fig. 3(c) are possibly due to the absence of the material itself or the presence of extremely strong NRCs. In both Figs. 3(b) and 3(c), it can be seen that some straight line structures run from the corners of the trapezoid parallel to *m*-planes. This implies that the tensile stress accumulated around the DBs is relaxed by introducing cracks. Since there are no corresponding structures in the SEM image, it is likely that these cracks run under the surface, and which can specifically be detected in the CL images due to the finite implantation depth of the *e*-beam and the longitudinal diffusion of the minority carriers.

The virtue of STRCL is that it is readily accessible to the local recombination dynamics for a particular emission peak. Local time-integrated cathodoluminescence (TICL) and TRCL decay signals for the NBE emission of A1 measured at room

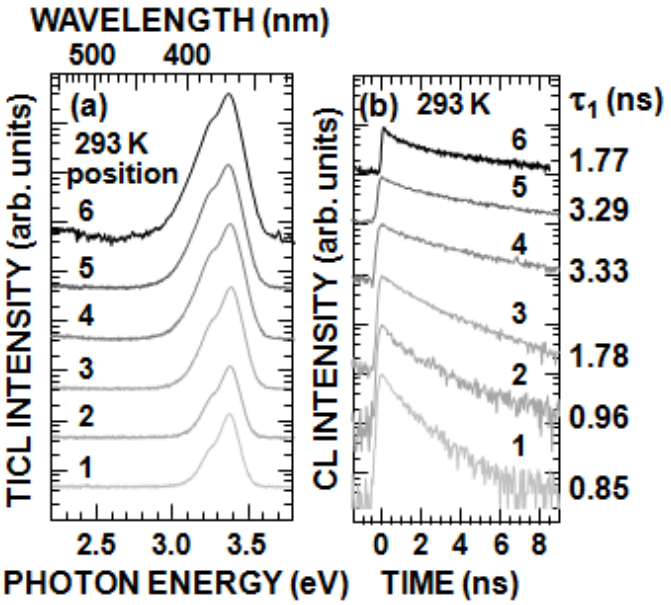

Figure 4 Position dependent TICL spectra (a) and TRCL decay signals (b) for the NBE emission of FS-GaN sample A1 measured at 293 K. The number corresponds to the position encircled in Fig. 3.

temperature at the positions encircled in Fig. 3 are shown in Figs. 4(a) and 4(b), respectively. In this instance, the probe current was decreased to 25 pA, which amounts to 2 electrons per pulse, in order to prevent any degradation in temporal resolution (17). The resultant number of excited electron-hole pairs in GaN are deduced to be less than 2000 from the empirical relation given in Ref. (22). We note that this excitation density gives the τ_1 value for the TRPL decay constant of a GaN template when excited with the laser fluence of 2 $\mu J/cm^2$ (17). This value is an order of magnitude higher than that used for the TRPL measurement. However, weak excitation conditions are still maintained. The nominal NBE peak energy was approximately 3.38 eV while the FWHM values were 90 meV, both of which are in reasonable agreement with Fig. 2(a). In these spectra, we found subtle redshifts of the NBE emission peak inside and on the peripheries of the trapezoid. This can be attributed to the local strain or increased residual electron concentration. We fit the decay curves by a double exponential function to extract τ_1, and found that τ_1 significantly varied depending on the positions. The decrease of τ_1 near the visual defects in the CL image at 293 K [see Fig. 3(b)] can be understood as enhanced recombination at NRCs because τ_1 at room temperature is generally dominated by τ_{NR}. By contrast, local τ_1 values measured at 10 K were almost independent of the positions being 180 ps. This is reasonable since τ_R dominates τ_{CL} at low temperature.

We also evaluated the local η_{int}^{eq} for the NBE emission by simply taking the ratio of the integrated spectral intensities at 293 K to that at 20 K. The results for A1 and A2 are summarized as a function of τ_1 in Fig. 5. The best data for the macroarea PL measurement on similar HVPE FS-GaN (11) and typical values observed for GaN templates are also plotted for reference. As shown, η_{int}^{eq} linearly increases with the increase in τ_1 according to $\eta_{int}^{eq}=(1+\tau_R/\tau_{NR})^{-1}$, where we assume that τ_R is an intrinsic value to a particular material (23) and that τ_{CL} is generally dominated by τ_{NR} at room temperature under the relation $\tau_{CL}^{-1}=\tau_R^{-1}+\tau_{NR}^{-1}$. Although the overall trend of higher η_{int}^{eq} in the local measurement may indicate somewhat higher excitation density used, the

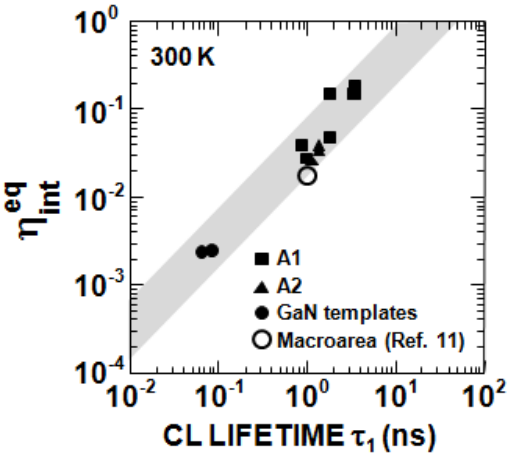

Figure 5 The values of η_{int}^{eq} for the NBE emission peak of FS-GaN samples at room temperature as a function of the fast decay constant (τ_1) obtained from the STRCL measurement. The results for the macroarea measurement for both the HVPE FS-GaN (sample C0 in Ref. (11) that exhibited the longest positron diffusion length (L_+=116 nm) and GaN templates are also included for reference.

spatially focused excitation in STRCL can selectively probe highly luminescent regions that are less affected by NRCs. As a result, a record high η_{int}^{eq} of up to 20% was obtained for position 4 in 3, where τ_1 was as long as 3.33 ns.

Conclusions

Local carrier recombination dynamics in the low TDD FS-GaN substrates grown by HVPE were studied by STRCL measurement. In addition to the visualization of defect networks originating from the DBs in the CL intensity images, the spatially resolved TICL and TRCL measurements revealed a linear correlation between η_{int}^{eq} and τ_{CL} at room temperature. The spatially focused excitation led us to observe the highest η_{int}^{eq} of 20% and the longest τ_{CL} of 3.33 ns at 293 K. We believe that our results demonstrate the potential of FS-GaN grown by HVPE and serves as a benchmark for future development.

Acknowledgments

This work was supported in part by NEDO programs by METI, Grant-in-Aids for Scientific Research (Nos. 23656206 and 24760250) from MEXT, Japan, and AOARD/AFOSR monitored by G. Jessen.

References

1. A. Nagahira, D. Probert, T. Fukuda, S. F. Chichibu, Y. Kagamitani, and A. Abe, Proceedings of the R&D Management Conference (2010), Roadmapping Session, Vol. 1, Article No.2, pp.9-23.
2. S. F. Chichibu, T. Azuhata, T. Sota, and S. Nakamura, *Appl. Phys. Lett.* **69**, 4188 (1996).

3. S. F. Chichibu, A. C. Abare, M. P. Mack, M. S. Minsky, T. Deguchi, D. Cohen, P. Kozodoy, S. B. Fleischer, S. Keller, J. S. Speck, J. E. Bowers, E. Hu, U. K. Mishra, L. A. Coldren, S. P. DenBaars, K. Wada, T. Sota, and S. Nakamura, *Mater. Sci. Eng. B* **59**, 298 (1999).
4. Y. Narukawa, Y. Kawakami, S. Fujita, S. Fujita, and S. Nakamura, *Phys. Rev.* B **55**, R1938 (1997).
5. L. Bellaiche, T. Mattila, L. -W. Wang, S. -H. Wei, and A. Zunger, A*ppl. Phys. Lett.* **74**, 1842 (1999).
6. P. R. C. Kent and A. Zunger, *Appl. Phys. Lett.* **79**, 1977 (2001).
7. S. F. Chichibu, A. Uedono, T. Onuma, B. A. Haskell, A. Chakraborty, T. Koyama, P. T. Fini, S. Keller, S. P. DenBaars, J. S. Speck, U. K. Mishra, S. Nakamura, S. Yamaguchi, S. Kamiyama, H. Amano, I. Akasaki, J. Han, and T. Sota, *Nature Mater.* **5**, 810 (2006).
8. K. Fujito, S. Kubo, H. Nagaoka, T. Mochizuki, H. Namita, and S. Nagao, *J. Cryst. Growth* **311**, 3011 (2009).
9. K. Fujito, K. Kiyomi, T. Mochizuki, H. Oota, H. Namita, S. Nagao, and I. Fujimura, *Phys. Status Solidi* A **205**, 1056 (2008).
10. S. F. Chichibu, A. Uedono, T. Onuma, T. Sota, B. A. Haskell, S. P. DenBaars, J. S. Speck, and S. Nakamura, *Appl. Phys. Lett.* **86**, 021914 (2005).
11. S. F. Chichibu, K. Hazu, Y. Ishikawa, M. Tashiro, H. Namita, S. Nagao, K. Fujito, and A. Uedono, *J. Appl. Phys.* **111**, 103518 (2012).
12. M. Merano, S. Collin, P. Renucci, M. Gatri, S. Sonderegger, A. Crottini, J. D. Ganière, and B. Deveaud, *Rev. Sci. Instrum.* **76**, 085108 (2005).
13. M. Merano, S. Sonderegger, A. Crottini, S. Collin, P. Renucci, E. Pelucchi, A. Malko, M. H. Baier, E. Kapon, B. Deveaud, J. D. Ganière, *Nature* **438**, 479 (2005).
14. P. Corfdir, P. Lefebvre, J. Levrat, A. Dussaigne, J. -D. Ganière, D Martin, J. Ristić, T. Zhu, N. Grandjean, and B. Deveaud-Plèdran, *J. Appl. Phys.* **105**, 043102 (2009).
15. S. F. Chichibu, T. Onuma, K. Hazu, and A. Uedono, *Appl. Phys. Lett.* **97**, 201904 (2010).
16. M. Kagaya, P. Corfdir, J. -D. Ganière, B. Deveaud-Plèdran, N. Grandjean, and S. F. Chichibu, *Jpn. J. Appl. Phys.* **50**, 111002 (2011).
17. T. Onuma, Y. Kagamitani, K. Hazu, T. Ishiguro, T. Fukuda, and S. F. Chichibu, *Rev. Sci. Instrum.* **83**, 043905 (2012).
18. Y. Ishikawa, M. Tashiro, K. Hazu, K. Furusawa, H. Namita, S. Nagao, K. Fujito, and S. F. Chichibu, *Appl. Phys. Lett.* **101**, 212106 (2012).
19. C. G. Dunn and E. F. Koch, *Acta Metal.* **5**, 548 (1957).
20. A. Uedono, S. Ishibashi, T. Ohdaira, and R. Suzuki, *J. Cryst. Growth* **311**, 3075 (2009).
21. K. Kumakura, T. Makimoto, N. Kobayashi, T. Hashizume, T. Fukui, and H. Hasegawa, *Appl. Phys. Lett.* **86**, 052105 (2005).
22. C. A. Klein, *J. Appl. Phys.* **39**, 2029 (1968).
23. D. Takamizu, Y. Nishimoto, S. Akasaka, H. Yuji, K. Tamura, K. Nakahara, T. Onuma, T. Tanabe, H. Takasu, M. Kawasaki, and S. F. Chichibu, *J. Appl. Phys.* **103**, 063502 (2008).

Spatio-time-resolved cathodoluminescence studies on local exciton dynamics of a freestanding GaN substrate grown by hydride vapor phase epitaxy

K. Furusawa[1], Y. Ishikawa[1], M. Tashiro[1], K. Hazu[1], S. Nagao[2], H. Ikeda[2], K. Fujito[2], and S. F. Chichibu[1]
[1]IMRAM, Tohoku University, Sendai, Japan
[2]Mitsubishi Chemical Corporation, Tsukuba, Japan
chichibulab@yahoo.co.jp

Abstract—**A novel photoelectron gun suitable for the spatio-time-resolved cathodoluminescence measurements was developed. Its increased photoelectron emission efficiency enabled to vary the acceleration voltage (mean implantation depth of electrons) over a wide range. As a result, more surface-sensitive detection became possible, allowing us to clearly visualize the area containing a basal-plane stacking fault (BSF) in a freestanding GaN substrate grown by hydride vapor phase epitaxy. Local dynamics of excitons around the BSF will be presented.**

Keywords—gallium nitride; hydride vapor phase epitaxy; cathodoluminescence

I. INTRODUCTION

Group-III nitride semiconductors have become materials of choice for low energy consumption solid-state lighting, and their applications are extending, for instance, toward power-switching devices. The use of large-area freestanding (FS-) GaN substrates with low threading dislocation density is expected to improve their device performances. Recently, *c*-plane and nonpolar plane FS-GaN wafers [1] sliced from a bulk GaN boule grown by hydride vapor phase epitaxy (HVPE) have become available. However, because the original *c*-plane boule is considerably bowed due to the residual strain caused by the use of foreign substrates, crystal mosaics are transferred to the FS-GaN wafers. Then, structural and point defects may be formed in epitaxial films grown on such substrates, and which will impede the device performance. Therefore it is important to study their spatial distributions and impacts on the electronic and optical properties by employing spectroscopic tools with sufficiently high spatial- and time-resolutions.

For this purpose, we have been developing a spatio-time-resolved cathodoluminescence (STRCL) [2] measurement system, following the development of an in-house photoelectron (PE-) gun driven by femtosecond laser pulses [3]. Based on this system, we confirmed the linear relation between the cathodoluminescence (CL) lifetime and equivalent internal quantum efficiency through local measurements at various points in a *c*-plane FS-GaN substrate [4]. In that system, the PE-gun was excited from its rear surface (opposite to the surface where the emission occurs). However, the maximum PE current was not satisfactory. Although the STRCL measurement itself requires only a small amount of current (a few tens of pA or even less), high PE current is anticipated since the focus adjustment is typically performed by observing a scanning electron microscope (SEM) image, in which spatial resolution is linked to the transmission losses of electron optics within the SEM; *i.e.* high magnification requires a large amount of losses. The limitation of the PE-gun of rear-excitation configuration arises from the absorptive losses of the excitation laser pulses. The photocathode must be sufficiently thin to decrease the light absorption. However, the optical damage threshold becomes low as the thickness decreases [5].

To avoid these trade-offs, here we introduce a novel PE-gun, with which the brightness of the PE source is increased by an order of magnitude. Furthermore, the damage issues can be avoided by employing a thick photocathode. Accordingly, we can decrease the acceleration voltage of a PE beam so that the sensitivity to the surface / sub-surface structures can be enhanced. Consequently, the spatial extent of a basal-plane stacking fault (BSF) that exists approximately 80 nm below the surface is visualized in the monochromatic CL intensity image since its emission peak energy (3.414 eV) is 58 meV lower than the near-band-edge (NBE) emission at 3.472 eV at low temperature. In addition, local time-resolved cathodoluminescence (TRCL) measurement reveals much

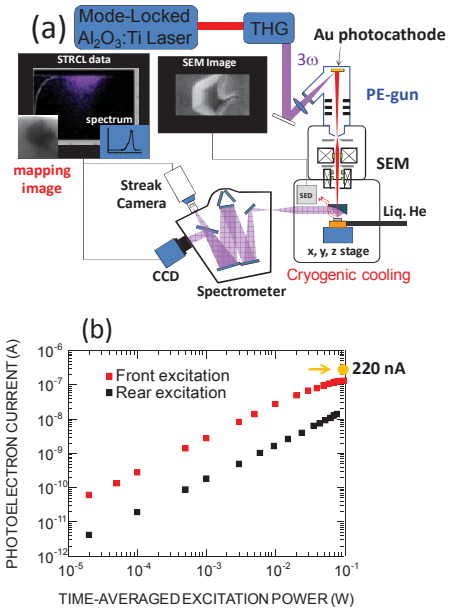

Figure 1. (a) Schematic of the STRCL measurement system equipped with the front-excitation PE-gun (THG: Third hamonic generator), and (b) comparison of PE current measured using a thin film photocathode in front- and rear-excitation configurations.

longer lifetime for the BSF peak than that for the NBE peak.

II. EXPERIMENTS AND RESULTS

A. *Front-excitation photoelectron gun*

Our front-excitation PE-gun is illustrated in Fig.1 (a). The excitation laser pulse was launched from the surface side of the photocathode at an incident angle of 45° using a lens. The beam area on the photocathode was estimated to be ~2.8×10^{-5} cm^2. To compare the PE current between the rear- and the front-excitation configurations, we mounted a 20-nm-thick Au photocathode film optimized for the rear-excitation case. Fig.1 (b) presents the PE current measured for the same Au film in both configurations using a Faraday cup, which was placed just above the sample stage. The extraction and acceleration voltages were set to 7.5 and 12 kV, respectively. A slight saturation was observed in the case of front-excitation. The result can be attributed to the gradual contamination or even damages as the net intensity at the surface is greater in the front-excitation case. This behavior was not observed for sufficiently thick Au films and we can obtain the maximum PE current up to 220 nA, as indicated in Fig.1 (b). Thus, the improvement in the PE current is approximately a factor of 10 in the entire excitation range. This value is reasonable given the strong attenuation of the excitation beam in the rear-excitation case. Note that, in this case, the excitation intensity decreased to 5.8 % at the front surface even without considering the Fresnel losses. Assuming that the beam quality of the resultant PE-gun is the same for the two cases, the brightness of the front-excitation type PE-gun is estimated to be 3.2×10^3 A/cm^2sr, which is comparable to that of the conventional W filament.

B. *Characterization of a FS-GaN substrate*

Using the front-excitation PE-gun, STRCL measurement was carried out on a FS-GaN substrate grown by a vertical-flow HVPE apparatus [1]. The details of the sample and the results obtained using the rear-excitation PE-gun have been described in Ref. [4], where the acceleration voltage of 10 kV was used. Thanks to the improved brightness of the gun, the acceleration voltage can be decreased down to 6.5 kV without compromising the lateral spatial resolution. Our simulation suggests that the projected range (RP) of the electron beam into GaN is as short as ~80 nm, as compared to ~250 nm for 10 kV. Figs. 2(a) and 2(b) show the monochromatic CL intensity images observed at 3.472 and 3.414 eV at 10K, respectively. The shadow of the slit edge of the spectrometer unfortunately made the contrast on the left upper part of the images faint. Although most of nonradiative recombination channels may be frozen, some contrasts originating from defective structures are found in Fig.2 (a). By contrast, a bright area is visualized in Fig.2 (b), and the corresponding negative contrast is noticeable in Fig.2 (a). Figs.2 (c) and (d) show the results of TRCL measurement in this area. The CL lifetime of the BSF peak was 508 ps while that of the NBE peak was 142 ps. The former is indicative of a decreased overlap between the confined electron and hole wave functions [6] around the BSF. The latter lifetime is consistent with the value for the recombination of excitons bound to a neutral donor.

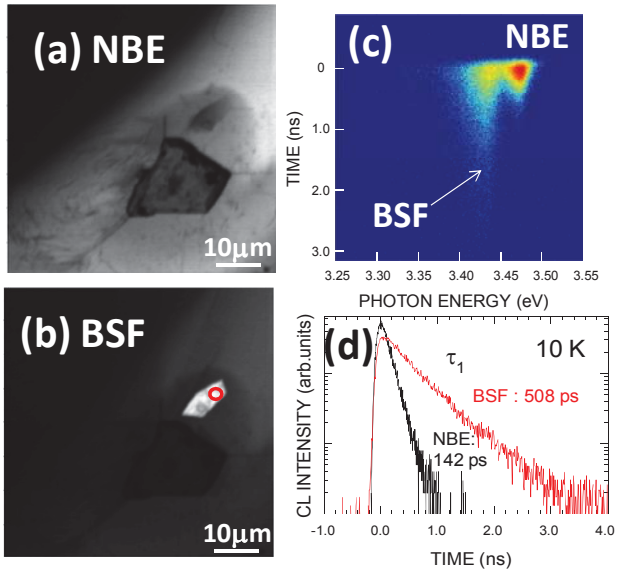

Figure 2. Monochromatic CL intensity images observed at (a) the NBE emission at 3.472 eV and (b) the BSF peak at 3.414 eV. (c) The streak-camera image measured at the point circled in (b). (d) TRCL decay signals observed at 3.472 and 3.414 eV.

III. SUMMARY

A novel front-excitation-type PE-gun was developed and applied to the STRCL system. High brightness of the gun allows for variation of the acceleration voltage over a wide range. As a result, more surface-sensitive detection became possible. This was confirmed by observing the area formed of a BSF near the surface of the FS-GaN substrate grown by HVPE. The local TRCL measurement indicates the unique emission mechanisms occurring by the presence of a BSF.

ACKNOWLEDGMENT

This work was supported in parts by NEDO programs by METI, Grant-in-Aids for Scientific Research # 23656206 from MEXT, Japan, and AOARD/AFOSR monitored by G. Jessen.

REFERENCES

[1] K. Fujito, K. Kiyomi, T. Mochizuki, H. Oota, H. Namita, S. Nagao, and I. Fujimura, "High-quality nonpolar m-plane GaN substrates grown by HVPE," Phys. Stat. Solidi A vol. 205, pp. 1056–1059, 2008.

[2] M. Merano, S. Sonderegger, A. Crottini, S. Collin, P. Renucci, E. Pelucchi, A. Malko, M. H. Baier, E. Kapon, B. Deveaud, and J.-D. Ganière, "Probing carrier dynamics in nanostructures by picosecond cathodoluminescence," Nature, vol. 438, pp.479-482, 2005.

[3] T. Onuma, Y. Kagamitani, K. Hazu, T. Ishiguro, T. Fukuda, and S. F. Chichibu, "Femtosecond-laser-driven photoelectron-gun for time-resolved cathodoluminescence measurement of GaN," Rev. Sci. Instrum. vol. 83, 043905, 2012.

[4] Y. Ishikawa, M. Tashiro, K. Hazu, K. Furusawa, H. Namita, S. Nagao, K. Fujito, and S. F. Chichibu, "Local lifetime and luminescence efficiency for the near-band-edge emission of freestanding GaN substrates determined using spatio-time-resolved cathodoluminescence," Appl.Phys.Lett. vol. 101, pp.212106 1-4, 2012.

[5] S.-S. Wellershoff, J. Hohlfeld, J. Gudde, E. Matthias, "The role of electron–phonon coupling in femtosecond laser damage of metals," Appl. Phys. A vol. 69, S99–S107, 1999.

[6] Y.T. Rebane, Y.G. Shreter, M. Albrecht, "Stacking Faults as Quantum Wells for Excitons in Wurtzite GaN," physica status solidi vol.164, pp.141-144 1997.

Impacts of Si-doping and resultant cation vacancy formation on the luminescence dynamics for the near-band-edge emission of $Al_{0.6}Ga_{0.4}N$ films grown on AlN templates by metalorganic vapor phase epitaxy

S. F. Chichibu,[1,*] H. Miyake,[2], Y. Ishikawa,[1] M. Tashiro,[1] T. Ohtomo,[1]
K. Furusawa,[1] K. Hazu,[1] K. Hiramatsu,[2] and A. Uedono[3]

[1]*Institute of Multidisciplinary Research for Advanced Materials and Department of Applied Physics, Graduate School of Engineering, Tohoku University, 2-1-1 Katahira, Aoba, Sendai 980-8577, Japan*

[2]*Depertment of Electrical and Electronic Engineering, Mie University, Tsu 514-8507, Japan*

[3]*Division of Applied Physics, Faculty of Pure and Applied Science, University of Tsukuba, Tsukuba, Ibaraki 305-8573, Japan*

(Dated: April 22, 2013)

* Author to whom correspondence should be addressed. Electronic mail:chichibulab@yahoo.co.jp

Abstract

Luminescence dynamics for the near-band-edge (NBE) emission peak at around 250 nm of c-plane Si-doped $Al_{0.6}Ga_{0.4}N$ films grown on AlN templates by low-pressure metalorganic vapor phase epitaxy were studied using deep ultraviolet time-resolved photoluminescence and time-resolved cathodoluminescence spectroscopies. For the films with the Si-doping concentration, [Si], lower than 1.9×10^{17} cm^{-3}, the doping lessened the concentration of cation vacancies, $[V_{III}]$, through the surfactant effect or the aid of the reactant doping in a form of H_3SiNH_2. The room-temperature nonradiative lifetime and consequently the equivalent value of internal quantum efficiency in the weak excitation regime steeply decreased when [Si] exceeded 10^{18} cm^{-3}. Simultaneously the intensity ratio of the deep-state emission band to the NBE emission abruptly increased. Because the increase in [Si] essentially gives rise to the increase in $[V_{III}]$ (for [Si]$\rangle 1.9 \times 10^{17}$ cm^{-3}) and the overcompensation of Si is eventually observed for the film with [Si]$=4.0\times10^{18}$ cm^{-3}, the formation of acceptor-type native-defect complexes containing Si such as V_{III}-$\mathrm{Si}_{\mathrm{III}}$ is suggested.

PACS numbers: 78.47.jd, 78.66.Fd, 78.70.Bj, 78.60.Hk

I. INTRODUCTION

High AlN mole fraction (x) $Al_xGa_{1-x}N$ alloys have attracted considerable interest for applications in UV-C (200∼280 nm) deep ultraviolet (DUV) light-emitting diodes (LEDs),[1] tubes,[2] and laser diodes. Recently, epitaxial growths of low threading dislocation (TD) density ($\sim 10^8$ cm^{-2}) $Al_xGa_{1-x}N$ films have become possible, even for x higher than 0.6, by using a variety of AlN templates on (0001) Al_2O_3 (Refs. 1-3) and freestanding AlN substrates.[4, 5] However, the external quantum efficiency (η_{ext}) of DUV LEDs is still limited at the maximum of 10%.[1]

Because η_{ext} is a product of internal quantum efficiency (η_{int}), carrier injection efficiency (η_{inj}), and light extraction efficiency, all of them must be improved. Among these, η_{int} is a fraction of radiative rate over the sum of radiative and nonradiative rates; *i.e.* $\eta_{int}=(1+\tau_R/\tau_{NR})^{-1}$, where τ_R and τ_{NR} are the radiative and nonradiative lifetimes, respectively. Obviously, the concentration of nonradiative recombination centers (NRCs) must be decreased to elongate τ_{NR}. The authors have studied the impacts of point defects on the emission dynamics in (Al,Ga,In)N compounds and alloys using a combination of time-resolved photoluminescence (TRPL) and positron annihilation spectroscopy (PAS), and the origin of NRCs in GaN has been assigned to defect complexes containing Ga vacancies (V_{Ga}) such as $V_{Ga}-X$.[6, 7] In particular for $Al_xGa_{1-x}N$ alloys, Polyakov *et al.*[8], Bradley *et al.*[9], the authors,[10] and Hashizume *et al.*[11] have independently investigated electrically and optically active native defects having midgap states using photoluminescence (PL) (Refs. 8 and 10), cathodoluminescence (CL) (Refs. 9 and 10), TRPL (Ref. 10), PAS (Ref. 10), and the combination of x-ray photoelectron spectroscopy and junction capacitance method.[11]

Meanwhile, η_{inj} to an active region can be increased by increasing conductivities of p- and n-type layers keeping a balance between the electron and hole concentrations. Accordingly, high concentration doping of donor- or acceptor-impurities with minimal defect formation is mandatory, because impurity doping is known to generate certain native defects having their counter-charge due to the Fermi-level effect[12] and such defects may diffuse into the active region. To obtain low resistivity n-type $Al_xGa_{1-x}N$ by Si-doping, extensive studies have been carried out with emphases on the growth conditions of metalorganic vapor phase epitaxy (MOVPE) (Refs. 13 and 14), exciton localization,[15] changes in the room temperature PL spectra,[16, 17] PAS,[18, 19] and estimation of η_{int} (Ref. 20). One of the additional serious

problems of heavy impurity doping is the overcompensation, which will be discussed later.

As very low TD and structural defect density AlN templates and substrates[1–5] became available, extracting intrinsic influences of point defects on the nonradiative carrier recombination and positron annihilation became possible. Consistent with the calculated results that the formation energy (E_{Form}) of Al vacancies (V_{Al}) in AlN is very low and even negative[21] in n-type materials, V_{Al} has been found to be the major vacancy defect in AlN (Ref. 22) and $Al_xGa_{1-x}N$ alloys ($x \neq 0$).[19] Therefore, impacts of point defects introduced by impurity doping on the recombination dynamics for the near-band-edge (NBE) emission in $Al_xGa_{1-x}N$ must be studied carefully, as V_{Al}-complexes may also act as NRCs. However, due to limited availability of a desirable DUV femtosecond excitation source, only a few papers[23–26] have dealt with the emission dynamics of (Al,In,Ga)N in UV-C range. The authors have been studying the recombination dynamics of excitons in unintentionally doped (UID) AlN and AlGaN alloys using DUV TRPL[24] and time-resolved cathodoluminescence (TRCL) measurements.[25, 26] According to the short τ_R being a few ns at room temperature, an excellent radiative performance of $Al_xGa_{1-x}N$ alloys of high x has been pointed out, although η_{int} values were as low as 1% due to the short τ_{NR} approximately 30 ps.[26]

Although electron concentration, n, higher than 10^{19} cm^{-3} without deactivation has been reported for Si- or Ge-doped GaN (Ref. 27), the overcompensation issue of Si is significant in $Al_xGa_{1-x}N$ alloys. Shimahara *et al.*[14] have reported that n in $Al_{0.6}Ga_{0.4}N$ films first increased with the increase in the doping concentration of Si, [Si], up to approximately 10^{18} cm^{-3}, then saturated, and eventually decreased to 5×10^{17} cm^{-3} for [Si]=4×10^{18} cm^{-3}. Uedono *et al.*[19] have studied these samples by PAS using a monoenergetic positron (e^+) beam line to detect V_{Ga}, V_{Al}, and their complexes. They observed simultaneous increase in cation vacancy (V_{III}) concentration, [V_{III}], with [Si], and also reported that the major defect species was V_{Al}.[19] Such an overcompensation phenomenon is commonly seen in III-V and II-VI semiconductors. For example, overcompensation of heavily-doped Si donors on Ga sites (Si_{Ga}) in GaAs has been attributed to the formation of a defect complex with V_{Ga}, such as V_{Ga}-Si_{Ga} (Refs. 28-30). Therefore, it is likely that V_{III}-Si_{III} defect complexes, especially on Al site (V_{Al}-Si_{III}), are formed in $Al_{0.6}Ga_{0.4}N$:Si.

In this article, the results of DUV TRPL and TRCL measurements on the NBE emission of the $Al_{0.6}Ga_{0.4}N$ alloys at various [Si] (Ref. 14) are shown to discuss the impacts of V_{III} formation on τ_{NR} and η_{int} in the weak excitation regime. Their luminescence spectra

are characterized by a predominant NBE peak at around 5 eV and a weak emission band ranging from 3 to 4 eV that originates from deep energy states. The value of τ_{NR} and consequently η_{int} for the NBE emission at room temperature steeply decreased when [Si] exceeded 10^{18} cm^{-3}, where the intensity ratio of the deep-state emission band to the NBE emission (I_{deep}/I_{NBE}) abruptly increased. As the increase in [Si] gives rise to the increase in [V_{III}] and the overcompensation of Si is eventually observed for [Si]=4×10^{18} cm^{-3}, formation of acceptor-type native defect complexes containing Si, such as V_{III}-Si$_{III}$, is suggested.

II. EXPERIMENT

Approximately 0.8-μm-thick (0001) Si-doped $Al_{0.6}Ga_{0.4}N$ epilayers ($Al_{0.6}Ga_{0.4}N$:Si) were grown at 6.7×10^3 Pa by MOVPE on a 0.8-μm-thick AlN epitaxial template,[3] which was grown on a (0001) Al_2O_3 substrate. Trimethylgallium (TMGa), trimethylaluminium (TMAl), and NH_3 were used as the precursors. Monomethylsilane (CH_3SiH_3) gas was used to control [Si] in the solid-phase from 2×10^{16} to 4×10^{18} cm^{-3}, the values being quantified by secondary-ion mass spectrometry. The growth temperature was 1180$\sim$1200 °C. All the samples were confirmed by x-ray reciprocal space mapping method to be coherently grown on the template. The TD densities having edge components (N_E) have been estimated to be about 3×10^8 cm^{-2}. Details of the growth have been given in Ref. 14.

Steady-state CL was excited using an electron beam (e-beam) operated at 3.5 kV acceleration voltage (V_{acc}) and 1.2 mA/cm^2 probe current density. Corresponding excited carrier concentration is estimated to be 2×10^{18} cm^{-3}. Approximately 200 fs pulses of a frequency-quadrupled (4ω) mode-locked Al_2O_3:Ti laser[24–26] were used for the TRPL measurement. The wavelength and power density were 200 nm and 40 nJ/cm^2 a pulse, respectively. The maximum electron-hole (e-h) pair concentration is estimated to be 4×10^{15} cm^{-3} during the pulse. The spatio-time-resolved cathodoluminescence (STRCL) system[31] equipped with a photoelectron gun driven by 200 fs pulses of a frequency-tripled (3ω) mode-locked Al_2O_3:Ti laser was used to measure the CL lifetimes for the NBE emission as a function of temperature, T. Details of our STRCL system have been described in Ref. 31. Typical V_{acc} was 6.5 kV, and approximately 1.5 electrons (about 650 e-h pairs in case of $Al_{0.6}Ga_{0.4}N$) per pulse were injected. The excitation intensities for both TRPL and TRCL were low enough to maintain weak excitation conditions. The energy-resolved TRPL and TRCL signals were

acquired using a streak-camera, of which temporal resolution was 7∼10 ps.

In order to correlate τ_R and τ_{NR} with $[V_{III}]$, PAS[32] was carried out using the monoenergetic e^+-beam line.[19, 22] Here, S parameter[6, 7, 19, 22, 24–26, 30, 32] for the Doppler-broadening spectrum of e^+-e^- annihilating γ-rays is used as the measure of concentration or size of negatively charged V_{III}-defects.[19, 22, 32] Details of the measurement and analysis are given in Refs. 19 and 22.

III. RESULTS AND DISCUSSION

Figure 1(a) shows representative temperature dependency of the CL spectra for the $Al_{0.6}Ga_{0.4}N$:Si film with [Si] of 1.9×10^{17} cm^{-3}. The spectra are characterized by a predominant NBE peak at around 5 eV and very weak deep-state emission band ranging from 3 to 4 eV. In contrast, as shown in Fig. 1(b), CL spectra at elevated temperatures of heavily Si-doped ([Si]=4×10^{18} cm^{-3}), overcompensated film exhibited a predominant deep-state emission band in the green color region at around 2.4 eV, in addition to the NBE emission peak. The result implies that the heavily doped sample contains high density V_{III}, because these deep-state emission centers have been ascribed to contain V_{III} with deferent charge states.[6, 8–10, 16–18, 22]

Figures 1(c) and 1(d) show the temperature dependencies for the ratios of spectrally-integrated CL intensities at given T $[I_{CL}(T)]$ to those at 12 K $[I_{CL}(12\text{K})]$ for the NBE emission, which are used as the equivalent values for $\eta_{int}(T)$ $[\eta_{int}^{eq}(T)]$ in this article. For the films with [Si]=1.9×10^{17} and 4.0×10^{18} cm^{-3}, $\eta_{int}^{eq}(300\text{K})$ were 11 and 0.015%, respectively. The former value was the highest among the present samples.

Room-temperature PL spectra and the PL decay signals for the NBE emission of the $Al_{0.6}Ga_{0.4}N$ films are shown as a function of [Si] in Figs. 2(a) and 2(b), respectively. The signal decay is seen to be abruptly shortened when [Si] exceeds 10^{18} cm^{-3}, at which concentration the relative intensity of the green CL band increases. We fit the decay curves by a double exponential function to extract the characteristic lifetimes of the fast decay components (τ_1), because this value essentially determines the NBE emission intensity at elevated temperatures. The results are shown in Fig. 3(d).

Figures 3(a)-3(c) summarize room-temperature values of n, S, and I_{deep}/I_{NBE} for the $Al_{0.6}Ga_{0.4}N$:Si films, respectively, as a function of [Si]. The values of τ_1 and η_{int}^{eq} for the NBE

emission are plotted in Figs. 3(d) and 3(e), respectively. The values of n and S are taken from Refs. 14 and 19, respectively. As shown in Fig. 3(b), S for the films of [Si]$\langle 10^{17}$ cm^{-3} were larger than that for the smallest S being 0.457 at [Si]=1.9×10^{17} cm^{-3}. The result means that the presence of certain amount of Si suppresses the introduction of excess vacancy-type defects, possibly at the growing surface. There are several plausible explanations for this. One is that Si acts as a surfactant and provides wetting conditions to improve the surface morphology of the epilayer,[33] which reduces $[V_{III}]$ although n-type doping decreases E_{Form} of V_{Ga} and V_{Al} in the bulk. Another explanation is the presence of doping reactants that give lower surface and internal energies when incorporated on the growing surface. It is well known for MOVPE of GaAs:Si using TMGa-AsH_3-SiH_4 and TMGa-$C_4H_9AsH_2$-SiH_4 systems that the reaction between SiH_4 and AsH_3 or $C_4H_9AsH_2$ forms H_3SiAsH_2 in the gas-phase (boundary layer), and H_3SiAsH_2 acts as the major doping reactant.[34, 35] In the present TMGa-TMAl-NH_3-CH_3SiH_3 system, H_3SiNH_2 is most likely effective on Si-doping, because CH_3SiH_3 decomposes into SiH_3 faster than SiH_4 does and reacts with NH_3 to form H_3SiNH_2.[36] Then, Si is expected to be incorporated in a form of metastable N-Si bond, which decreases the internal energy of isolated Si_{III} donor[30] forming $Si_{Ga}^{(+)}$-$N_N^{(0)}$ (or $Si_{Al}^{(+)}$-$N_N^{(0)}$) and a free e^- at the surface and in the bulk. We note that the N-Si bond would give less chance for Si to occupy N sites forming a Si_N acceptor. Under the presence of N-Si bond, $[V_{III}]$ could be lower than the UID case, although E_{Form} of isolated V_{Al} in AlN is very low and even negative in n-type materials.[21] On the other hand, the increase in S with further increase in [Si] ($\rangle 10^{17}$ cm^{-3}) is most likely due to the decrease in E_{Form} of V_{III} due to the Fermi-level effect.[12, 21]

As shown in Fig. 3(a), n increased linearly with [Si] up to approximately 10^{18} cm^{-3}. However, n saturated to increase for higher [Si] and then decreased to 5×10^{17} cm^{-3} for further increase in [Si] to 4.0×10^{18} cm^{-3}; *i. e.* electrical overcompensation is significant. The results shown in Figs. 3(a) and 3(b) are similar to what were observed for MOVPE of heavily Si-doped GaAs,[30] in which the overcompensation of Si and steep increase in S were significant for [Si]$\rangle 10^{19}$ cm^{-3}. It is apparent that I_{deep}/I_{NBE} abruptly increased while τ_1 and η_{int}^{eq} rapidly decreased for [Si]$\rangle 10^{18}$ cm^{-3} in the present case, as shown in Figs. 3(c), 3(d), and 3(e), respectively. Because N_E for all the $Al_{0.6}Ga_{0.4}N$ films have been confirmed to be nearly the same,[14, 19] the changes in I_{deep}/I_{NBE}, τ_1, and η_{int}^{eq} are purely correlated with the increase in S, namely the increase in $[V_{III}]$ and the concentration of V_{III}-complexes.

Consistently, deep-state emission bands commonly observed in GaN (2.2 eV), AlN (3.1 eV), and AlGaN (between 2.2 and 3.1 eV) have been assigned to originate from V_{III} or V_{III}-O_N complexes.[6, 19, 22] In the case of GaAs:Si, such an overcompensation due to heavy doping has been attributed to the formation of defect complexes such as V_{Ga}-Si_{Ga} (Refs. 28-30). By analogy, complex defects such as V_{III}-Si_{III} (V_{Al}-Si_{Al}, V_{Al}-Si_{Ga}, etc) are major culprits for the present $Al_{0.6}Ga_{0.4}N$:Si films.

It is noteworthy that significant correlations between τ_1 and S ($\tau_1 - S$ relation) and between $I_{CL}(300\text{K})/I_{CL}(12\text{K})$ and τ_1 ($\eta_{int}^{eq} - \tau_1$ relation) seen in GaN[6, 7, 31, 37] are also remarkable in the $Al_{0.6}Ga_{0.4}N$:Si films, as shown in Figs. 4(a) and 4(b), respectively. Almost linear $\tau_1 - S$ relation indicates that the major NRCs in the $Al_{0.6}Ga_{0.4}N$:Si films are most likely[6, 7, 31, 37] composed of defect complexes incorporated with V_{III}, such as $V_{Al} - X$ (and $V_{Ga} - X$), because τ_1 at room temperature is generally dominated by τ_{NR} that decreases with increasing the concentration of NRCs. As shown in Fig. 4(b), η_{int}^{eq} increases linearly with increasing τ_1. The result is quite reasonable because $\eta_{int}^{eq} = (1 + \tau_R/\tau_{NR})^{-1}$, τ_R is an intrinsic value to a particular material, and τ_1 is dominated by τ_{NR} at room temperature with the relation $\tau_1^{-1} = \tau_R^{-1} + \tau_{NR}^{-1}$. Very similar trends have been found in GaN and ZnO.[6, 7, 31, 37–39]

By measuring τ_1 and η_{int}^{eq} for the NBE emission of the $Al_{0.6}Ga_{0.4}N$:Si films as a function of T, τ_R and τ_{NR} are derived. Representative data for the films of [Si]=1.9×10^{17} and 1.5×10^{18} cm^{-3} are plotted in Figs. 5(a) and 5(b), respectively. Corresponding $\eta_{int}^{eq}(300\text{K})$ were 11 and 0.07%, respectively. The value of τ_1 at low T, which mostly represents τ_R, for the former lightly-doped sample (150 ps) was shorter than that for the latter highly-doped sample ($\sim$300 ps), reflecting better overlapping of electron and hole wavefunctions due most likely to the small potential inhomogeneity; *i. e.* shallower band-tail.[26] The values of τ_R increase with T for both the samples, reflecting the decrease in the oscillator strengths of excitons. Because of the larger potential inhomogeneity (deeper band-tail), τ_R of the latter highly-doped sample shows small change with T, being about 1 ns at 300 K. However, absolute τ_R values for both the samples are similar, and distinct difference between the two is the change in τ_{NR} with the increase in T: *i. e.* τ_{NR} of the latter sample decreases really rapidly than the former does due to the presence of high concentration NRCs (V_{III}-complexes).

IV. CONCLUSION

The luminescence dynamics for the NBE emission peak at around 250 nm of c-plane Si-doped $Al_{0.6}Ga_{0.4}N$ films were studied using DUV TRPL and TRCL in the weak excitation regime. For the films with [Si]$\langle 1.9 \times 10^{17}$ cm^{-3}, the Si-doping lessened $[V_{III}]$ through the surfactant effect or the aid of the reactant doping scheme of H_3SiNH_2. The room-temperature values of τ_{NR} and η_{int}^{eq} for the NBE emission steeply decreased when [Si] exceeded 10^{18} cm^{-3}, where I_{deep}/I_{NBE} abruptly increased. Because the increase in [Si] essentially gives rise to the increase in $[V_{III}]$ (for [Si]$\rangle 1.9 \times 10^{17}$ cm^{-3}) and the overcompensation of Si was observed for the sample with [Si]$=4.0 \times 10^{18}$ cm^{-3}, the formation of acceptor-type native-defect complexes containing Si such as $V_{\rm III}$-$Si_{\rm III}$ is suggested.

Acknowledgments

This work was supported in part by Grant-in-Aids for Scientific Research Nos. 23656206, 24760250, and 18069001 under MEXT, Japan, and AFOSR/AOARD Grant No. FA2386-11-1-4013 monitored by Dr. G. Jessen.

[1] Quantum efficiencies of state-of-the-art UV LEDs are described in C. Pernot, M. Kim, S. Fukahori, T. Inazu, T. Fujita, Y. Nagasawa, A. Hirano, M. Ippommatsu, M. Iwaya, S. Kamiyama, I. Akasaki, and H. Amano, Appl. Phys. Express **3**, 061004 (2010); M. Shatalov, W. Sun, A. Lunev, X. Hu, A. Dobrinsky, Y. Bilenko, J. Yang, M. Shur, R. Gaska, C. Moe, G. Garrett, and M. Wraback, *ibid* **5**, 082101 (2012) and references cited therein.

[2] Y. Shimahara, H. Miyake, K. Hiramatsu, F. Fukuyo, T. Okada, H. Takaoka, and H. Yoshida, Appl. Phys. Express **4**, 042103 (2011).

[3] T. Shibata, K. Asai, S. Sumiya, M. Mouri, M. Tanaka, O. Oda, H. Katsukawa, H. Miyake, and K. Hiramatsu, Phys. Status Solidi C **0**, 2023 (2003).

[4] A. Rice, R. Collazo, J. Tweedie, R. Dalmau, S. Mita, J. Xie, and Z. Sitar, J. Appl. Phys. **108**, 043510 (2010).

[5] J. R. Grandusky, Z. Zhong, J. Chen, C. Leung, and L. J. Schowalter, Solid-State Electron. **78**, 127 (2012).

[6] S. F. Chichibu, A. Uedono, T. Onuma, T. Sota, B. A. Haskell, S. P. DenBaars, J. S. Speck, and S. Nakamura, Appl. Phys. Lett. **86**, 021914 (2005).

[7] S. F. Chichibu, A. Uedono, T. Onuma, B. A. Haskell, A. Chakraborty, T, Koyama, P. T. Fini, S. Keller, S. P. DenBaars, J. S. Speck, U. K. Mishra, S. Nakamura, S. Yamaguchi, S. Kamiyama, H. Amano, I. Akasaki, J. Han, and T. Sota, Nature Mater. **5**, 810 (2006); Philos. Mag. **87**, 2019 (2007).

[8] A. Y. Polyakov, M. Shin, J. A. Freitas, M. Skowronski, D. W. Greve, and R. G. Wilson, J. Appl. Phys. **80**, 6349 (1996).

[9] S. T. Bradley, S. H. Goss, L. J. Brillson, J. Hwang, and W. J. Schaff, J. Vac. Sci. Technol. B **21**, 2558 (2003).

[10] T. Onuma, S. F. Chichibu, A. Uedono, T. Sota, P. Cantu, T. M. Katona, J. F. Keading, S. Keller, U. K. Mishra, S. Nakamura, and S. P. DenBaars, J. Appl. Phys. **95**, 2495 (2004).

[11] T. Kubo, H. Taketomi, H. Miyake, K. Hiramatsu, and T. Hashizume, Appl. Phys. Express **3**, 021004 (2010); K. Ooyama, K. Sugawara, S. Okuzaki, H. Taketomi, H. Miyake, K. Hiramatsu, and T. Hashizume, Jpn. J. Appl. Phys. **49**, 101001 (2010).

[12] J. Neugebauer and C. G. Van de Walle, Phys. Rev. B **50**, 8067 (1994); Appl. Phys. Lett. **69**,

503 (1996); C. Stampfl and C. G. Van de Walle, Appl. Phys. Lett. **72**, 459 (1998); C. G. Van de Walle and J. Neugebauer, J. Appl. Phys. **95**, 3851 (2004); A. F. Wright and U. Grossner, Appl. Phys. Lett. **73**, 2751 (1998); K. Leung, A. F. Wright, and E. B. Stechel, Appl. Phys. Lett. **74**, 2495 (1999); A. F. Wright, J. Appl. Phys. **90**, 1164 (2001).

[13] St. Keller, P. Cantu, C. Moe, Y.Wu, Sa. Keller, U. K. Mishra, J. S. Speck, and S. P. DenBaars, Jpn. J. Appl. Phys. **44**, 7227 (2005).

[14] Y. Shimahara, H. Miyake, K. Hiramatsu, F. Fukuyo, T. Okada, H. Takaoka, and H. Yoshida, Jpn. J. Appl. Phys. **50**, 095502 (2011).

[15] G. R. James, A. W. R Leitch, F. Omnes, and M. Leroux, Semicond. Sci. Technol. **21**, 744 (2006).

[16] N. Nepal, M. L. Nakarmi, J. Y. Lin, and H. X. Jiang, Appl. Phys. Lett. **89**, 092107 (2006).

[17] K. X. Chen, Q. Dai, W. Lee, J. K. Kim, E. F. Schubert, W. Liu, S. Wu, X. Li, and J. A. Smart, Appl. Phys. Lett. **91**, 121110 (2007).

[18] J. Slotte, F. Tuomisto, K. Saarinen, C. G. Moe, S. Keller, and S. P. DenBaars, Appl. Phys. Lett. **90**, 151908 (2007).

[19] A. Uedono, K. Tenjinbayashi, T. Tsutsui, Y. Shimahara, H. Miyake, K. Hiramatsu, N. Oshima, R. Suzuki, and S. Ishibashi, J. Appl. Phys. **111**, 013512 (2011).

[20] H. Murotani, D. Akase, K. Anai, Y. Yamada, H. Miyake, and K. Hiramatsu, Appl. Phys. Lett. **101**, 042110 (2012).

[21] C. Stampfl and C. G. Van de Walle, Phys. Rev. B **65**, 155212 (2002).

[22] A. Uedono, S. Ishibashi, S. Keller, C. Moe, P. Cantu, T. M. Katona, D. S. Kamber, Y. Wu, E. Letts, S. A. Newman, S. Nakamura, J. S. Speck, U. K. Mishra, S. P. DenBaars, T. Onuma, and S. F. Chichibu, J. Appl. Phys. **105**, 054501 (2009).

[23] K. B. Nam, J. Li, M. L. Nakarmi, J. Y. Lin, and H. X. Jiang, Appl. Phys. Lett. **82**, 1694 (2003).

[24] T. Onuma, K. Hazu, A. Uedono, T. Sota, and S. F. Chichibu, Appl. Phys. Lett. **96**, 061906 (2010).

[25] S. F. Chichibu, T. Onuma, K. Hazu, and A. Uedono, Appl. Phys. Lett. **97**, 201904 (2010).

[26] S. F. Chichibu, K. Hazu, T. Onuma, and A. Uedono, Appl. Phys. Lett. **99**, 051902 (2011).

[27] S. Nakamura, T. Mukai, and M. Senoh, Jpn. J. Appl. Phys., Part 1 **31**, 2883 (1992).

[28] R. T. Chen, V. Rana, and W. G. Spitzer, Appl. Phys. Lett. **51**, 1531(1980).

[29] N. Furuhata, K. Kakimoto, M. Yoshida, and T. Kamejima, J. Appl. Phys. **64**, 4692 (1988).

[30] S. Chichibu, A. Iwai, Y. Nakahara, S. Matsumoto, H. Higuchi, L. Wei, and S. Tanigawa, J. Appl. Phys. **73**, 3880 (1993).

[31] Y. Ishikawa, M. Tashiro, K. Hazu, K. Furusawa, H. Namita, S. Nagao, K. Fujito, and S. F. Chichibu, Appl. Phys. Lett. **101**, 212106 (2012).

[32] R. Krause-Rehberg and H. S. Leipner, *Positron Annihilation in Semiconductors, Solid-State Sciences* (Springer, Berlin, 1999) Vol. 127; P. G. Coleman, *Positron Beams and Their Application* (World Scientific, Singapore, 2000).

[33] V. Lebedev, F. M. Morales, H. Romanus, S. Krischok, G. Ecke, V. Cimalla, M. Himmerlich, T. Stauden, D. Cengher, and O. Ambacher, J. Appl. Phys. **98**, 093508 (2005).

[34] M. Mashita, Jpn. J. Appl. Phys. **28**, 1298 (1989).

[35] S. Chichibu, A. Iwai, S. Matsumoto, and H. Higuchi, Appl. Phys. Lett. **60**, 489 (1992); erratum **60**, 2439 (1992).

[36] B. T. Luke, J. A. Pople, M. K. Jespersen, Y. Apeloig, J. Chandrasekhar, and P. R. Schleyer, J. Am. Chem. Soc. **108**, 260 (1986).

[37] S. F. Chichibu, K. Hazu, Y. Ishikawa, M. Tashiro, H. Namita, S. Nagao, K. Fujito, and A. Uedono, J. Appl. Phys. **111**, 103518 (2012).

[38] S. F. Chichibu, A. Uedono, A. Tsukazaki, T. Onuma, M. Zamfirescu, A. Ohtomo, A. Kavokin, G. Cantwell, C. W. Litton, T. Sota, and M. Kawasaki, Semicond. Sci. Technol. **20**, S67, (2005); S. F. Chichibu, T. Onuma, M. Kubota, A. Uedono, T. Sota, A. Tsukazaki, A. Ohtomo, and M. Kawasaki, J. Appl. Phys. **99**, 093505 (2006).

[39] D. Takamizu, Y. Nishimoto, S. Akasaka, H. Yuji, K. Tamura, K. Nakahara, T. Onuma, T. Tanabe, H. Takasu, M. Kawasaki, and S. F. Chichibu, J. Appl. Phys. **103**, 063502 (2008).

FIG. 1: Representative CL spectra of the $Al_{0.6}Ga_{0.4}N$:Si films for (a) [Si]=1.9×10^{17} cm^{-3} and (b) [Si]=4.0×10^{18} cm^{-3} as a function of T. Temperature dependencies for the ratios of spectrally-integrated CL intensities at given T [$I_{CL}(T)$] to those at 12 K [I_{CL}(12K)] for the NBE emission at around 5 eV, which are used as the equivalent value of $\eta_{int}(T)$ [$\eta_{int}^{eq}(T)$], for the $Al_{0.6}Ga_{0.4}N$:Si films of (c) [Si]=1.9×10^{17} cm^{-3} and (d) [Si]=4.0×10^{18} cm^{-3}.

FIG. 2: (a) Room-temperature PL spectra and (b) PL decay signals for the NBE emission of the $Al_{0.6}Ga_{0.4}N$:Si films at various [Si].

FIG. 3: Room-temperature values of (a) electron concentration, n, (b) S parameter, (c) I_{deep}/I_{NBE}, and (d) τ_1 and (e) η_{int}^{eq} for the NBE emission, of the $Al_{0.6}Ga_{0.4}N$:Si films plotted as a function of [Si]. The values of n and S are taken from Refs. 14 and 19, respectively.

FIG. 4: (a) $\tau_1 - S$ and (b) $\eta_{int}^{eq} - \tau_1$ relations for the $Al_{0.6}Ga_{0.4}N$:Si films at various [Si], which are derived from Fig. 3.

FIG. 5: Measured τ_1 (squares), derived τ_R (circes), and derived τ_{NR} (triangles) values as a function of T for the $Al_{0.6}Ga_{0.4}N$:Si films with [Si] of (a) 1.9×10^{17} and (b) 1.5×10^{18} cm^{-3}. Corresponding η_{int}^{eq}(300K) were 11 and 0.07%, respectively.

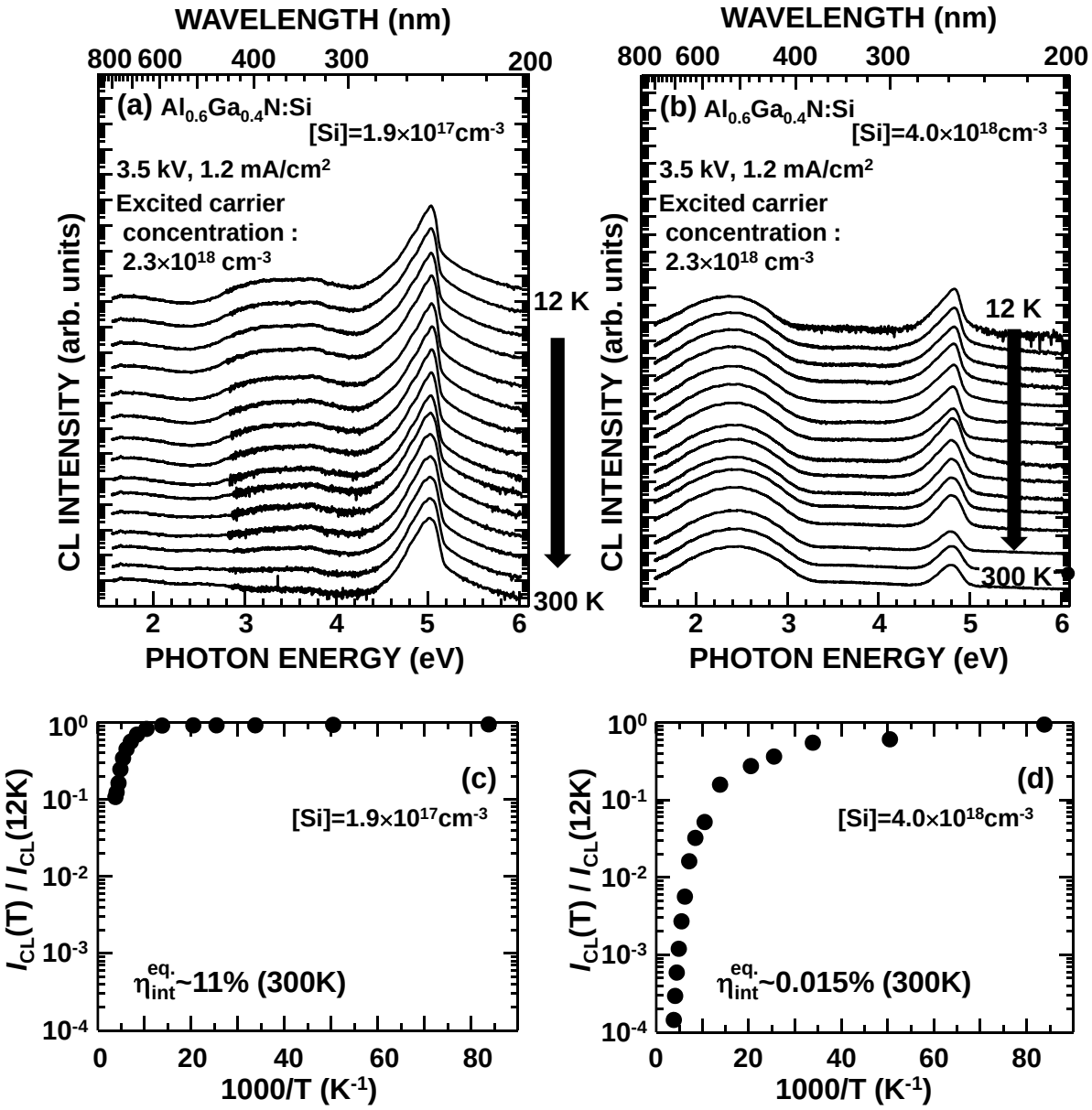
WAVELENGTH (nm)
800 600 400 300 200
(a) Al0.6Ga0.4N:Si
[Si]=1.9×10^17cm^-3
3.5 kV, 1.2 mA/cm^2
Excited carrier concentration : 2.3×10^18 cm^-3
12 K
300 K
CL INTENSITY (arb. units)
PHOTON ENERGY (eV)
(b) Al0.6Ga0.4N:Si
[Si]=4.0×10^18cm^-3
3.5 kV, 1.2 mA/cm^2
Excited carrier concentration : 2.3×10^18 cm^-3
12 K
300 K
(c)
[Si]=1.9×10^17cm^-3
η_int^eq.~11% (300K)
I_CL(T) / I_CL(12K)
1000/T (K^-1)
(d)
[Si]=4.0×10^18cm^-3
η_int^eq.~0.015% (300K)

Fig. 1

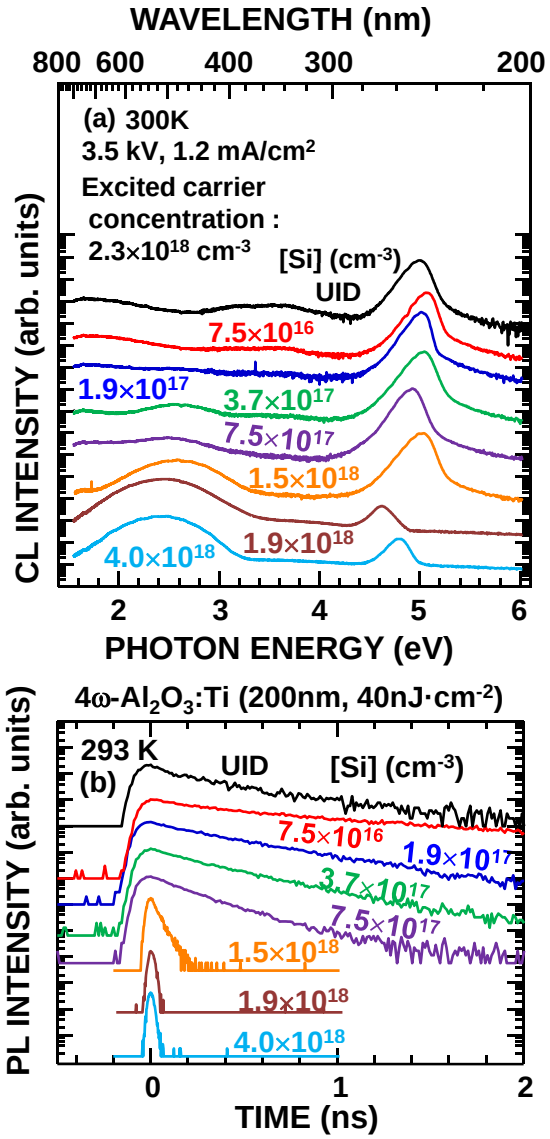
WAVELENGTH (nm)
800 600 400 300 200
(a) 300K
3.5 kV, 1.2 mA/cm2
Excited carrier
concentration :
2.3×10^18 cm^-3
[Si] (cm^-3)
UID
7.5×10^16
1.9×10^17
3.7×10^17
7.5×10^17
1.5×10^18
1.9×10^18
4.0×10^18
CL INTENSITY (arb. units)
2 3 4 5 6
PHOTON ENERGY (eV)
4ω-Al2O3:Ti (200nm, 40nJ·cm^-2)
293 K
(b)
UID
[Si] (cm^-3)
7.5×10^16
1.9×10^17
3.7×10^17
7.5×10^17
1.5×10^18
1.9×10^18
4.0×10^18
PL INTENSITY (arb. units)
0 1 2
TIME (ns)

Fig. 2

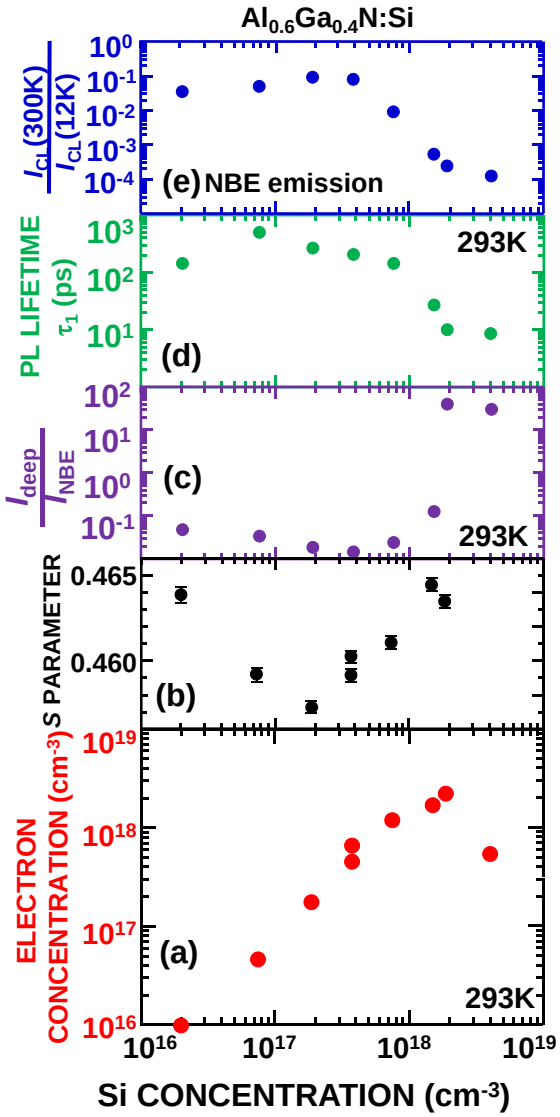
Al0.6Ga0.4N:Si
ICL(300K) / ICL(12K)
(e) NBE emission
PL LIFETIME τ1 (ps)
293K
(d)
Ideep / INBE
(c)
293K
S PARAMETER
(b)
ELECTRON CONCENTRATION (cm-3)
(a)
293K
Si CONCENTRATION (cm-3)

Fig. 3

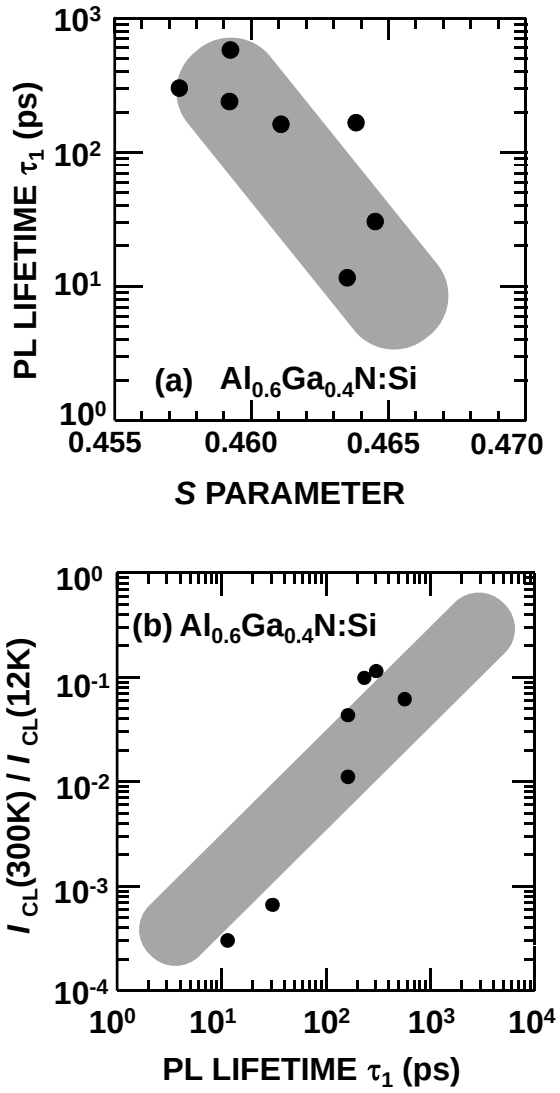
PL LIFETIME τ_1 (ps)
10^3
10^2
10^1
10^0
(a) $Al_{0.6}Ga_{0.4}N$:Si
0.455
0.460
0.465
0.470
S PARAMETER
$I_{CL}(300K) / I_{CL}(12K)$
10^0
10^{-1}
10^{-2}
10^{-3}
10^{-4}
(b) $Al_{0.6}Ga_{0.4}N$:Si
10^0
10^1
10^2
10^3
10^4
PL LIFETIME τ_1 (ps)

Fig. 4

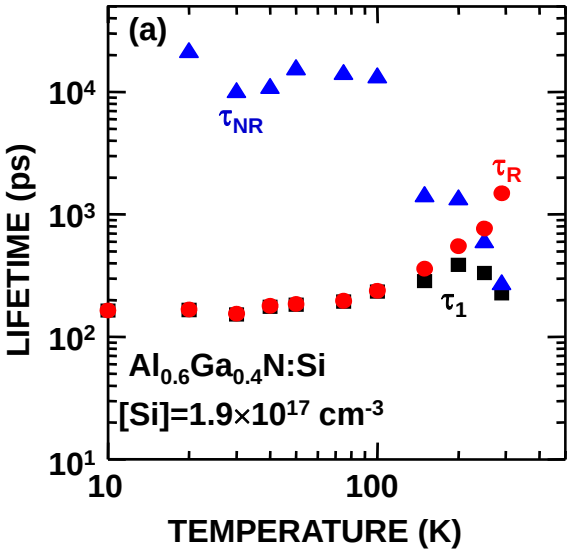
(a)
τ_{NR}
τ_R
τ_1
$Al_{0.6}Ga_{0.4}N$:Si
[Si]=1.9×10^{17} cm^{-3}
LIFETIME (ps)
TEMPERATURE (K)
10^4
10^3
10^2
10^1
10
100

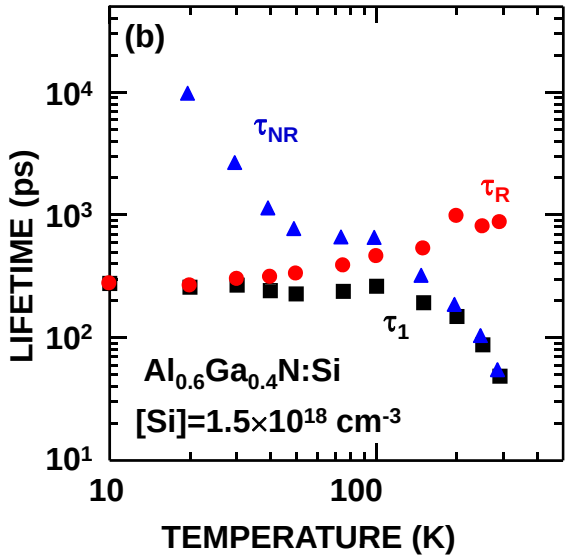
(b)
τ_{NR}
τ_R
τ_1
$Al_{0.6}Ga_{0.4}N$:Si
[Si]=1.5×10^{18} cm^{-3}
LIFETIME (ps)
TEMPERATURE (K)
10^4
10^3
10^2
10^1
10
100

Fig.5

ISSN 1610-1642
Phys. Status Solidi C
10 · No. 3 March
273–548 (2013)

physica status solidi pss c

www.pss-c.com

current topics in solid state physics

3
2013

Deep ultraviolet time-resolved luminescence studies on AlN and high AlN mole fraction AlGaN alloys

Shigefusa F. Chichibu, Takeyoshi Onuma, Kouji Hazu, and Akira Uedono

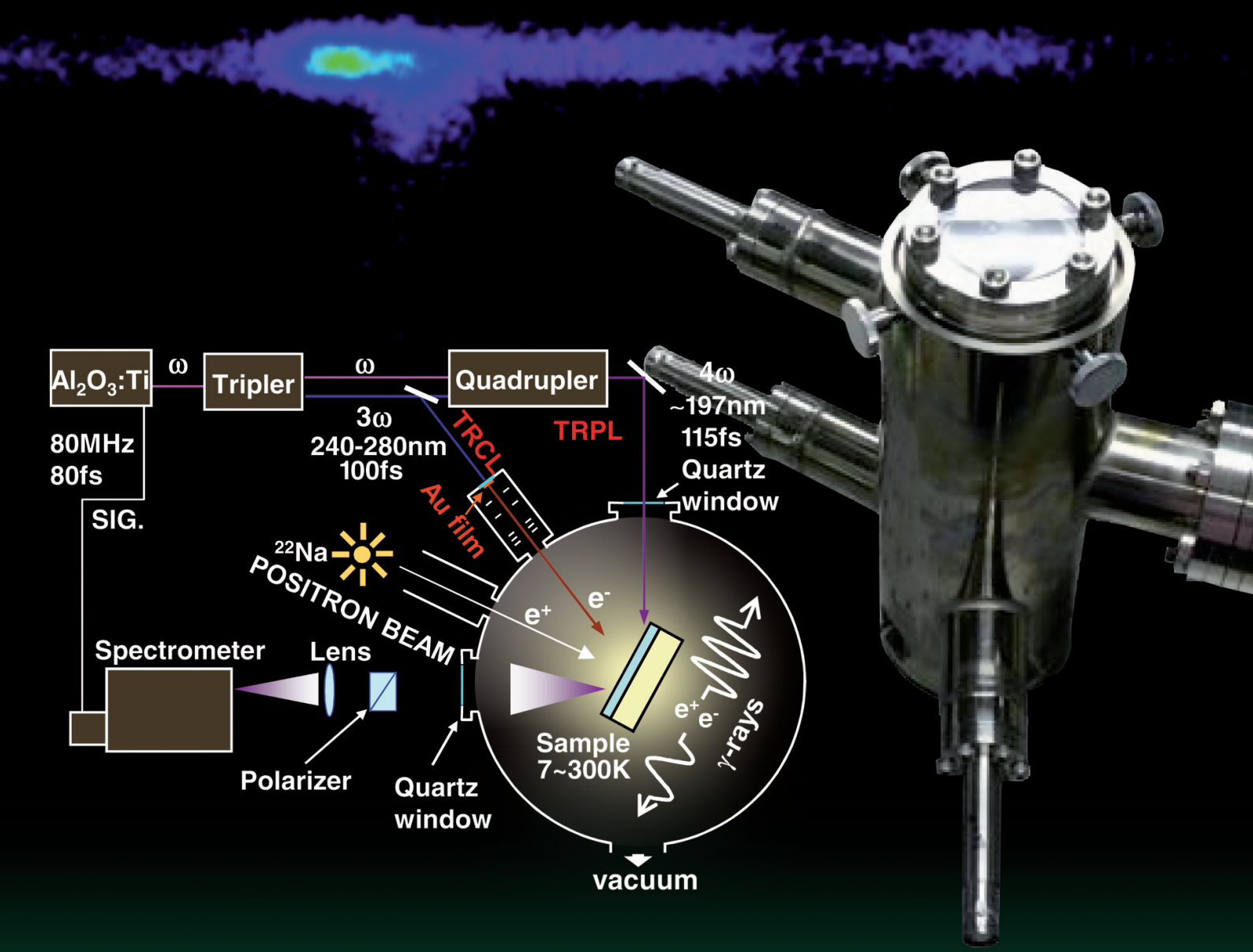

WILEY-VCH